Republic of Iraq
Ministry of Higher Education
and Scientific Research
University of Babylon
College of Engineering
Department of Mechanical Engineering

Experimental Study of Droplet Evaporation of Different Liquid Hydrocarbon Fuels and Water

A Thesis Submitted to the Mechanical Engineering Department
College of Engineering/University of Babylon in
Partial Fulfillment of the Requirements for the Degree of
Master in Engineering/ Mechanical Engineering/ Power.

By

Wissam Yassin Jabr Giyad

Supervised by

Prof. Dr. Haroun A.K. Shahad

2023 A.D. **1445 A.H.**

بِسْمِ اللَّهِ الرَّحمن الرَّحيم

﴿ فَتَعَالَى اللَّهُ الْمَلِكُ الْحَقُّ وَلَا تَعْجَلْ

بِالْقُرْآنِ مِنْ قَبْلِ أَنْ يُقْضَى إِلَيْكَ وَحْيُهُ

وَقُلْ رَبِّ زِدْنِي عِلْمًا ﴾

صدق الله العلي العظيم

[طه: 114]

Certification

I certify that this thesis entitled ***"Experimental Study of Droplet Evaporation of Different Hydrocarbon Fuels"*** was prepared by ***Wissam Yassin Jabr Giyad*** under my supervision at the University of Babylon in a partial fulfilment of the requirements for the degree of Master science(M.Sc.) in Mechanical Engineering/ Power.

I recommend that this thesis be forwarded for examination in accordance with the regulation of the University of Babylon.

Signature:

Name: ***Prof. Dr. Haroun A.K. Shahad***

Title: Supervisor

Date: / /

Dedication

I would like to express my gratefulness to my biggest supporters, to the reason of where I am and where I will be my father, and mother.

Wisam 2023

Acknowledgments

Deepest appreciation for the almighty Allah for the modest assistance in all aspects of my preparation of this work. My sincere thanks and respect to my supervisor ***Prof. Dr. Haroun A.K. Shahad*** who never hesitated in helping to achieve this work.

I also thank all staff of The Department of Mechanical Engineering at the University of Babylon for being the greatest cooperators with special thanks to ***Mr. Hussain H. Rashid ,***the technician in the P.G laboratory for his unlimited help in the construction of the experimental rig.

Wisam 2023

Abstract

The process of fuel droplet evaporating is one of the most important factors that directly affect the efficiency of the combustion process. The current work is an experimental study on the evaporation process of five different hydrocarbon fuels, kerosene, gasoline, ethanol, and acetone, in addition to water. The temperature of the evaporation chamber ranged from 25 to 100 °C. The effect of temperature and fuel type on evaporation rate and evaporation constant as well as the droplet lifetime will be investigated. The experimental rig was built to study the evaporation process of the free flying droplet into a cylindrical evaporation chamber. Diffusion controller evaporation mode is the only considered mode in this study. The droplet was photographed during the evaporation process using a high-speed camera for the purpose of calculating the droplet evaporation rate. The image extracted from the camera is analyzed using MATLAB code. The results showed that the evaporation rate increases logarithmically with the increase in the temperature of the evaporation chamber. The lifetime of a droplet of acetone decreases by 63% when the temperature is raised to 45 °C. Lifetime of droplet ethanol decreases by 66.7% when the temperature is increased from 25 ^{o}C to 45^{o}C. The lifetime of the gasoline droplet decreases by 59.1% when the temperature is raised from 25 ^{o}C to 45^{o}C. The lifetime decreases by 70.5% for water. The lifetime of the kerosene droplet decreases by 67.7% when the temperature is raised from 25 ^{o}C to 45^{o}C. Increasing the temperature leads to an increase in the rate of evaporation and thus decreases the lifetime of the droplet. The evaporation constant rises by 0.007, 0.021, 0.006, 0.02, 0.015 mm^{2}/s for every one centigrade temperature for kerosene, acetone, water, ethanol, and gasoline, respectively

Nomenclature

Notation	Description
A	area (m^2)
D	diameter (m)
K	evaporation constant (m^2/s)
r	radius (m)
t	time (s)
T	temperature (^oC)
t_d	droplet lifetime (s)
$\dot{m}$	evaporation rate (kg/s)
V	volume (m^3)
D_{AB}	Diffusion coefficient (mm^2/s)
h_{fg}	Heat of vaporization (KJ/kg)
$R_\circ$	Universal gas constant
X	Mole fraction
MW	Molecular weight (kg/kmol)
B_Y	Dimensionless transfer number or spalding number
R	Specific gas constant (J/kmol.k)
$Y_{A,\infty}$	Mass fraction of A in the free stream flow
$Y_{A,i}$	Interface mass fraction
Greek symbols	
ρ	density (kg/m^3)
Abbreviations	
SU	standard uncertainty

SD	standard deviation
Subscripts	
l	liquid
v	vapor
1,2	droplet location
o	initial
mix	Mixture
sat	Saturation state
i	ith species or inlet
A	Species *A*
B	Species *B*
boil	Boiling point
MD	Molecular dynamic
HFO	Heavy fuel oil
DCM	Discrete component model
IBM	Immersed boundary method
WTO	Waste transformer oil
TWTO	Trans-esterification waste transformer oil
CWSP	Coal-water slurry petrochemicals
GTL	Gas to liquid
DNS	Direct numerical simulations
GC	Gas chromatography
SDD	Single droplet drying

Contents

Contents ***Page No.***

Chapter One

Introduction

Chapter One: Introduction

1.1 General.

The evaporation and combustion of liquid fuel droplets play a significant role in various fields of science and technology, such as power and process industries, chemistry, medicine, and environmental processes. The research work in the area of droplet evaporation is going on for decades. A phenomenal progress has already taken place in the theory of evaporation and combustion of liquid fuel droplets and sprays. The theoretical progress includes the development of physical models and computer codes capable of solving model equations. The experimental advances, on the other hand, involve the development of improved instruments for calibrating the model predictions and for investigations of several complex phenomena occurring in the process of droplet evaporation and combustion. A large number of investigations carried out in the field have contributed well to the scientific understanding of the subject. A liquid droplet (in the context of evaporation/ combustion study) can be classified into three categories based on its constituents. The first one is a pure component droplet which comprises a single component liquid. The second one is a multi-component droplet which consists of two or more liquids (miscible or immiscible), and the third one is a Nano fuel droplet where solid nanoparticles are suspended in the liquid droplet. The understanding of physical processes and their consequences in the combustion of pure component fuel droplet is well established.

1.2 Droplet Evaporation Techniques

There are four famous techniques for droplet evaporation which are:

1.2.1 Levitated droplet technique

The Levitated droplet technique involves levitating a droplet in a controlled environment to study its evaporation behavior. In this technique, a droplet is suspended in mid-air using acoustic or electromagnetic forces, and its evaporation is monitored over time. It depends on the balances between the gravity force and magnetic, acoustic, fuel vapor bounce force as shows in Figure (1-1), the schematic diagram of this methods. In this technique the droplet shape is stable (spherical) without any deformation. The droplet can be observed for a long time as investigated by Grosshans et al. [1]. The levitation force by acoustic or magnetic field affects the evaporation process. The levitation technique can be used only with low ambient temperature and atmospheric pressure.

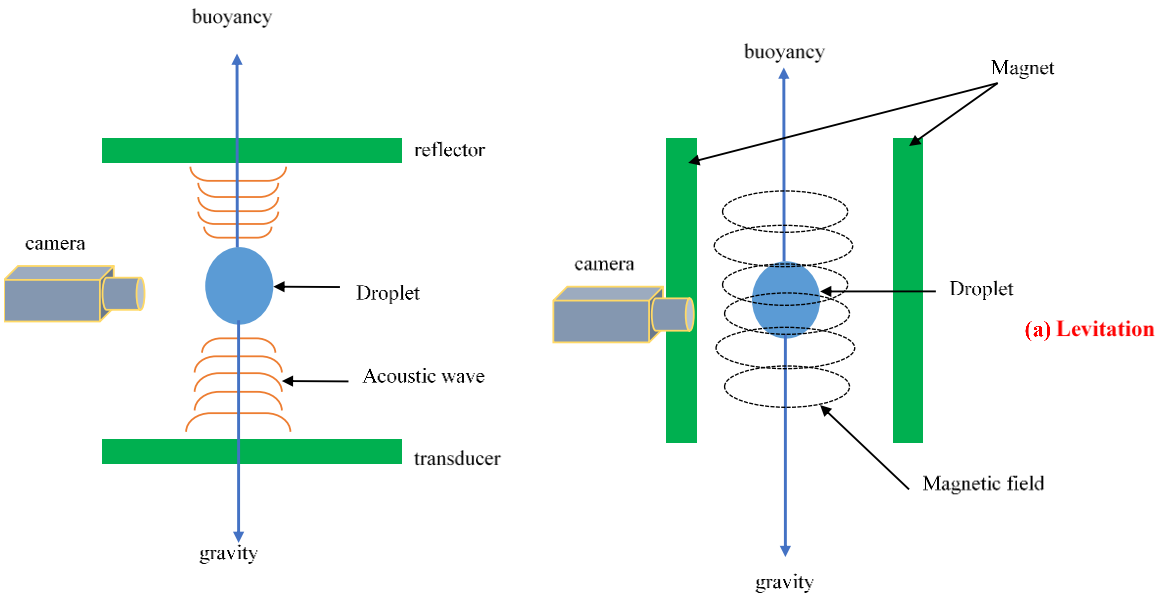

Figure (1- 1) Levitated Droplet Technique. [2]

The Levitated droplet method has applications in a wide range of research fields, including materials science, environmental science, and biophysics. For example, it can be used to study the evaporation behavior of liquid aerosols, which are important in atmospheric science and air

quality monitoring. It can also be used to study the behavior of biological fluids, such as saliva or tears, which can provide insights into disease diagnosis and drug delivery.

The evaporation rate was not taken into consideration in the reports by Mondragon and coworkers [3] [4]]; instead, the droplet drying behavior in the acoustic field was simply assessed by the size changes, with the effects of drying conditions and initial droplet conditions on the final particle properties being investigated. The single droplet drying (SDD) was used to measure the rate of droplet evaporation in sonic levitation technique. For the purpose of accomplishing a continuous, on-line measurement of the droplet moisture content while drying progressed, Groenewold et al. [5] included a dew point hygrometer to the system. Calculating the partial vapor pressure of outflow air converted the experimental data into droplet drying curves.

The acoustically levitated droplets is shown in Figure (1-2). The results showed that the droplet aspect ratio, as shown in Figure (1-3) affects the rate of evaporation. Also many studies used acoustic levitation such as [6-8] where they investigated the effect of an acoustic stream on the mass and heat transfer around the droplet.

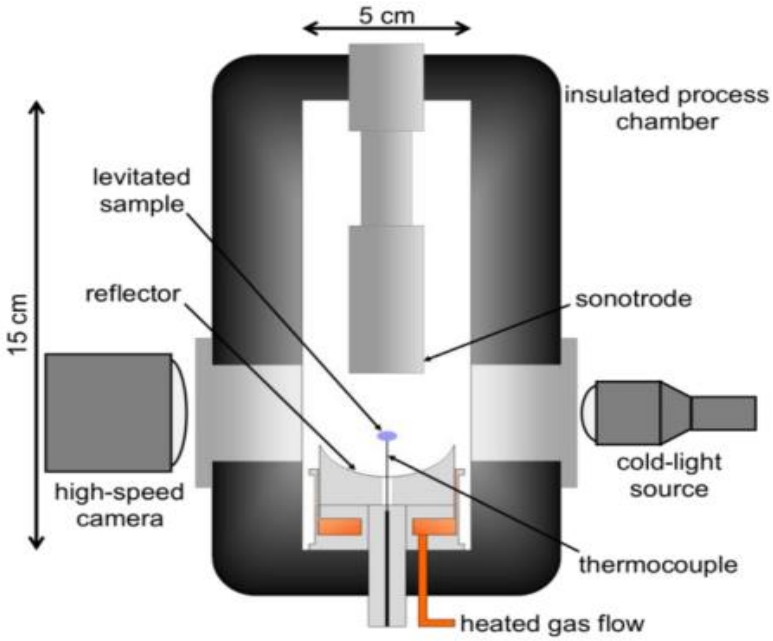

Figure (1- 2) Experimental Setup of Single Droplet Levitation by Acoustic [9]

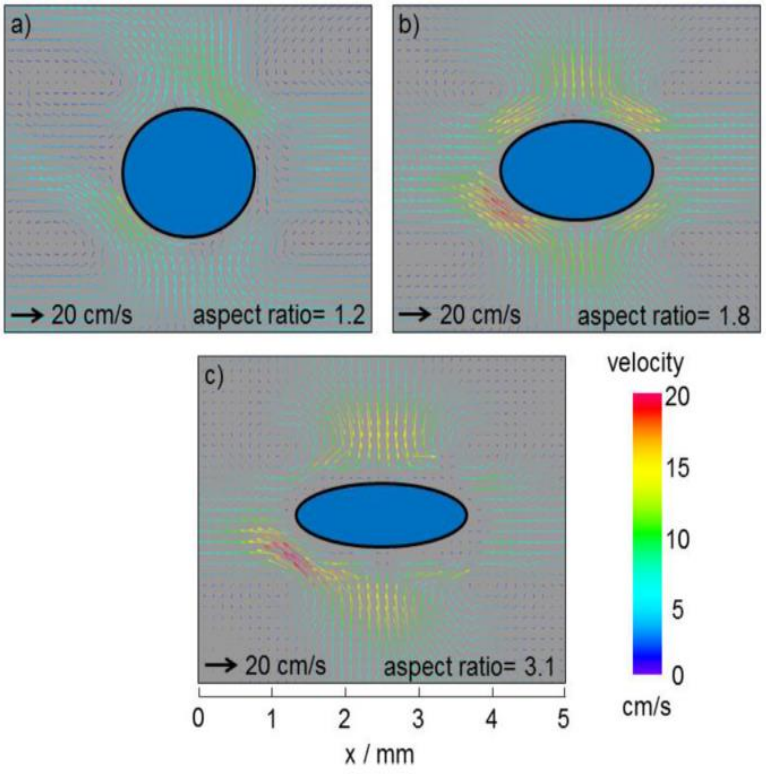

Figure (1- 3) Acoustic Flow Velocity with Different Aspect Ratio [9]

1.2.2 Free-flying droplet technique.

The Free-flying droplet technique is a droplet evaporation technique that involves tracking the motion of droplets as they evaporate in a controlled environment. In this technique, droplets are typically released from a nozzle or a pipette and allowed to freely fall or rise under the influence of gravity. The motion of the droplets is tracked using high-speed cameras or other imaging techniques, and the evaporation behavior is analyzed from the changes in the droplet size and shape over time.

In this method the droplet falling freely under gravity force in the evaporation chamber. The evaporation process is captured by high speed camera. The camera may be a wide angle fixed or moving camera as shown in Figure (1-4). In this method it is easy to control the droplet evaporation and easy to produce a small droplet as in real engine. The droplet evaporation in this method is not effected by any external force. This method involves creating one homogeneous free-falling droplet or a chain of droplets at the top of chamber. [10, 11]**.**

A non-contact optical sensor for the detection of single droplets in flight was described by Tröndle et al. [12]. The sensor enables non-contact dispensing systems that deliver droplets in the nanoliter range to have online process control. Bae and Avedisian [13] studied the evaporation and combustion of JP8 fuel droplets mixed with hexanol ($C_6H_{14}O$) additives in a low gravity environment. They used two types of evaporation technique free flying and supported droplet to examine the effect of convection on the evaporation rate under the low gravity environment The initial droplet diameters ranged from 0.40 to 0.52 mm. The results of the evaporation rate of JP8 with additives and pure JP8 are shown in Figure (1-5).

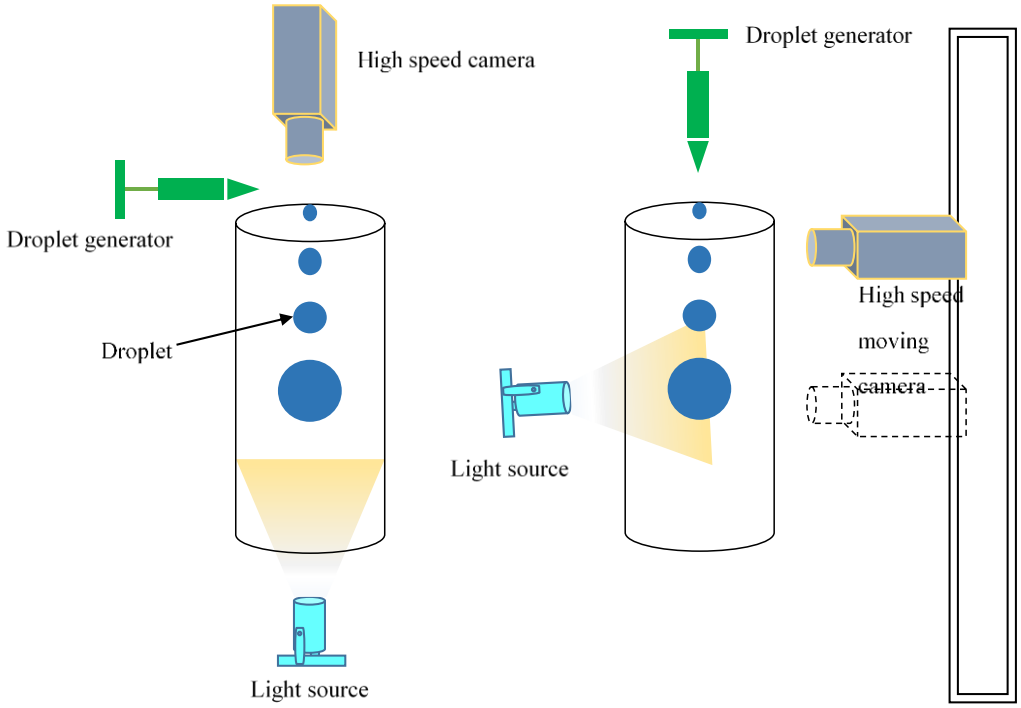

Figure (1- 4) Flying Droplet Method .[14]

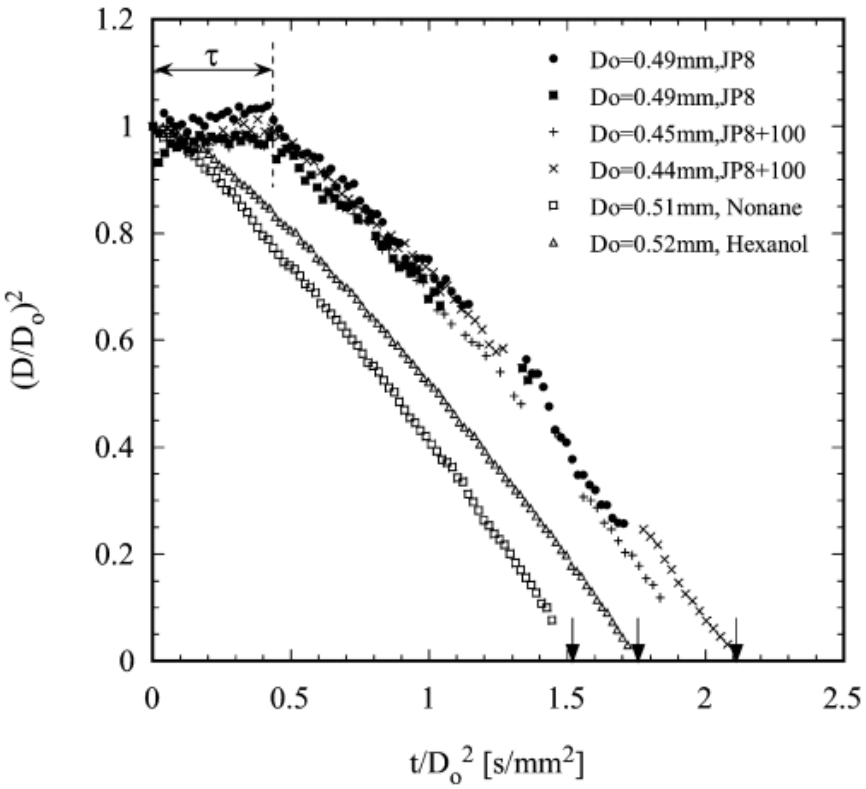

Figure (1- 5) Evolution of Droplet Diameter in The Coordinates of The Classical D^2 Law for Free Flying Droplet. Droplet Heating Period Is Indicated as τ. [13]

1.2.3 The suspended droplet technique

The Suspension droplet method is a droplet evaporation technique that involves suspending a droplet in a surrounding fluid, such as air or a gas, using a support structure or a carrier particle. The droplet is typically released onto the support structure, and the evaporation behavior is monitored over time using various techniques, such as microscopy or interferometry. The advantage of the suspension droplet method is that it allows for the study of droplet evaporation under controlled environmental conditions, such as temperature and humidity. It can also be used to study the behavior of droplets with different compositions, such as suspensions or emulsions. The suspened droplet method has applications in a wide range of research fields, including materials science, chemical engineering, and environmental science. For example, it can be used to study the evaporation behavior of liquid fuels in combustion engines, or the drying behavior of coatings and paints. One of the challenges of this technique is that the presence of the support structure or carrier particle can affect the evaporation behavior of the droplet. This can make it difficult to accurately measure the evaporation rates or to compare the behavior of different droplets. However, by carefully controlling the experimental conditions and choosing an appropriate support structure, it is possible to minimize these effects.

The suspension structure can be a thermocouple wire [15-17], Ceramic wire [18, 19], or quartz wire [19, 20]. The suspension technique is shown in Figure (1-6). The supported shape may be crossed, ring shape, or by using capillary tube. This method is used for only large droplet evaporation. In this technique it is easy to observe and measure the temperature and evaporation rate of droplet for a long time. The supported material greatly affect the evaporation process.

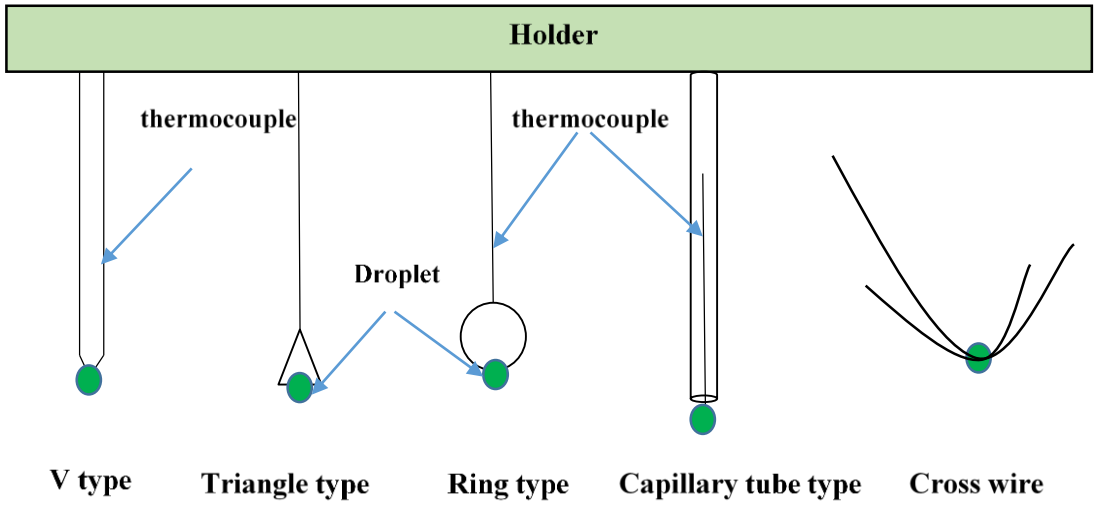

Figure (1- 6) The Suspension Droplet Technique. [21, 22]

1.2.4 Sessile droplet technique

The Sessile droplet technique is a droplet evaporation technique that involves studying the behavior of a droplet that is placed on a solid substrate, such as a glass slide or a metal surface. In this technique, the droplet is typically deposited onto the substrate using a pipette or a microsyringe, and the evaporation behavior is monitored over time using various techniques, such as optical microscopy or interferometry (see Figure (1-7)). Similar to the suspension technique the sessile droplet technique has advantages that it allows for the study of droplet evaporation under controlled environmental conditions, such as temperature and humidity. It can also be used to study the behavior of droplets with different compositions, such as suspensions or emulsions.

The Sessile droplet technique has applications in a wide range of research fields, including materials science, chemical engineering, and biophysics. For example, it can be used to study the drying behavior of coatings and films, the evaporation of aerosol droplets, or the behavior of biological fluids, such as blood or saliva. One of the challenges of this technique is that the evaporation behavior of the droplet can be influenced

by a number of factors, such as the properties of the substrate, the surrounding gas composition and flow, and the size and composition of the droplet. These factors can make it difficult to accurately measure the evaporation rates or to compare the behavior of different droplets. However, by carefully controlling the experimental conditions and choosing an appropriate substrate, it is possible to minimize these effects. Overall, the Sessile droplet technique is a valuable tool for studying the fundamental physics and chemistry of droplet evaporation, especially under controlled environmental conditions. It provides a way to investigate the behavior of droplets in a variety of systems and can be used to gain insights into the underlying mechanisms of the process.

This method involves properly placing a droplet with size ranged from nanometer to millimeter on a hydrophobic surface inside a dry well with regulated environmental conditions. Xu et al. [23-27] covered the latest recent findings from research on liquid droplet evaporation on solid substrates.

The Spreading stage. During this stage, the initial droplet diameter is as large as possible and the contact angle is advanced. Therefore, the rate of evaporation during this stage is very low for single component fluids. Therefore, most studies neglected the evaporation during this stage, only the remaining three stages are focused on [28-30]. The drop base radius remains constant throughout the first stage of evaporation, but the contact angle decrease. As a result, the first step of evaporation is an example of angle hysteresis. The second stage sees no change in the angle., but the droplet base radius decreases. In the third and last stage of evaporation, the angle and droplet base radius both decrease until the droplet disappears, as seen in Figure (1-8).

In the Sessile droplet technique, several parameters can affect the evaporation behavior of the droplet. Some of the key parameters include:

- Substrate properties: The substrate material, roughness, and wettability can influence the contact angle and the evaporation rate of the droplet.
- Droplet properties: The composition, size, and initial volume of the droplet can affect the evaporation rate and the time taken for the droplet to completely dry.
- Environmental conditions: The temperature, humidity, and gas flow around the droplet can affect the evaporation rate and the drying behavior of the droplet.
- Experimental conditions: The experimental setup, such as the imaging and analysis techniques used, can affect the accuracy and reproducibility of the results.

The evaporation profile for a sessile droplet is described in Figure (1-8). The evaporation of a Sessile droplet typically occurs in several stages, which can be characterized by changes in the droplet's size, shape, and composition. The specific stages and their order can vary depending on the droplet properties, environmental conditions, and substrate properties. However, in general, the stages of Sessile droplet evaporation can be described as follows:

1. Initial spreading stage: At the beginning of the evaporation process, the droplet spreads out on the substrate to form a thin film. During this stage, the contact angle between the droplet and the substrate decreases, and the droplet begins to wet the substrate.
2. Constant contact angle stage: After the droplet has spread out, it enters a stage in which the contact angle remains constant. During this stage,

the droplet continues to evaporate, but the rate of evaporation is approximately constant, and the shape of the droplet remains roughly the same.

3. Contact line pinning stage: As the droplet continues to evaporate, it can enter a stage in which the contact line of the droplet becomes pinned at the edge of the droplet. During this stage, the droplet volume decreases rapidly, and the shape of the droplet becomes distorted.
4. Contact line depinning stage: After the contact line has been pinned for some time, it can suddenly depin and move inward towards the center of the droplet. This stage is associated with a sudden increase in the evaporation rate, and it can lead to the formation of various structures, such as a coffee ring or a uniform deposit.
5. Final drying stage: In the final stage of evaporation, the droplet volume decreases further, and the droplet can form a solid deposit or a ring-like structure. The specific structure that forms depends on the droplet properties and the environmental conditions.

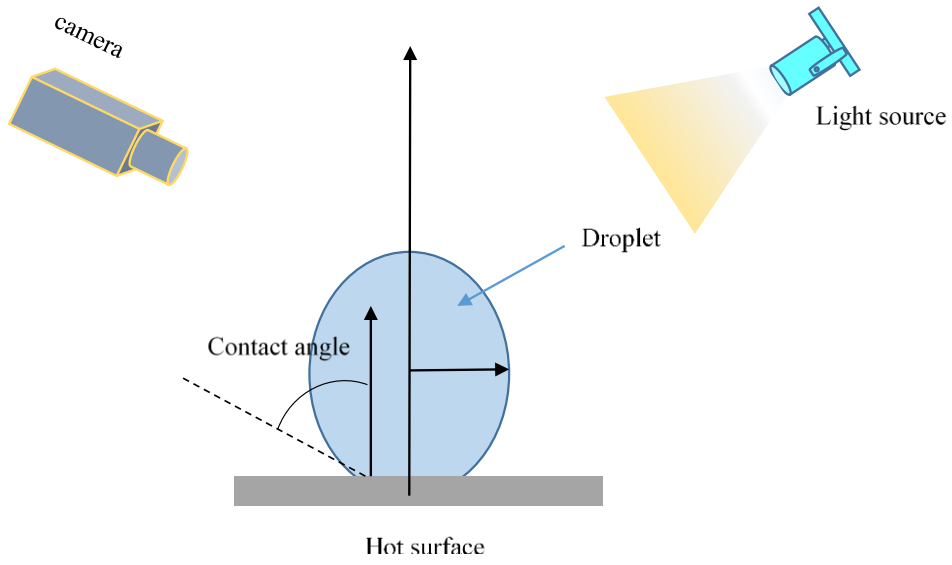

Figure (1- 7) Sessile Droplet Technique.[31]

Due to the larger droplets and the fact that their drying behavior might be affected by the experimental drying equipment, their static state, and the

experimental environment, single-droplet investigations are not recommended **[32]**. Heat conduction between the solid support and the droplet can impact the transmission of mass and heat [33].

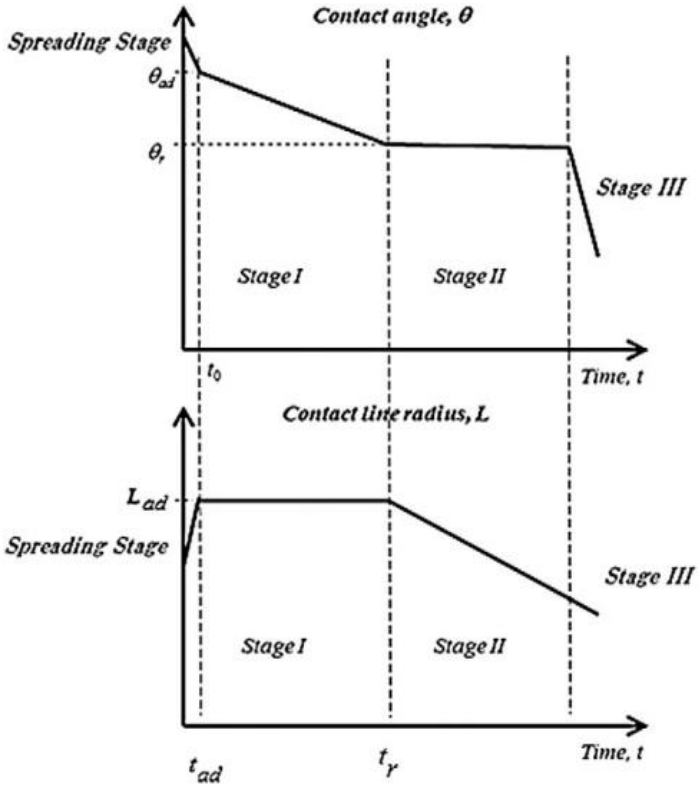

Figure (1- 8) The Stages of Evaporation of Sessile Droplet.[27]

The four methods mentioned earlier are the most famous methods through which the process of evaporation of the fuel drop was studied. A comparison between the previously mentioned methods is shown in Table (1-1). Some methods are easy to measure, while other methods require more advanced techniques.

Table (1- 1) Comparison of Evaporation Techniques

Suspension droplet	**levitation droplet**	**free flying droplet**	**sessile droplet**
the droplet size larger than droplet in real engine	may be produced small or large droplet	Droplet size can be controlled	Large droplet
the supporting wire affects the evaporation rate	the levitation force (acoustic or magnetic) affects evaporation rate	no external force but the air liquid interface affects the evaporation rate	the surface material affects greatly the evaporation rate
shape of droplet unstable because the support wire	shape of droplet approximately spherical (stable)	the shape of droplet is deformed by the interaction between air and droplet	the shape of droplet depends on the contact angle between the surface and droplet
easy to generate droplet	takes time for levitation droplet to stable	easy to generate droplet	easy to generated droplet
easy to measure the surface temperature and evaporation time.	easy to measure the evaporation rate for long time	difficult to measure the evaporation rate.	easy to measure the evaporation rate for long time.

1.3 Objective of the present work:

As mentioned earlier the aim of the research is to study the effect of environmental temperature and liquid type of evaporation characteristic of a single droplet. The technique that shall be used in the free flying droplet and technique with high speed photography. To achieve this, aim a special experimental rig will be fabricated as shall be described in chapter three of this work. The generation and evaporation of liquid droplet need further research to study the effect of surrounding condition and liquid type of this phenomena is the aim of research.

1.4. Properties of materials used in the experiment

We list below some of the physical properties of the materials used in the experiment, as shown in the Table (1-2)

Table (1-2) show the physical properties of the materials used.

substance	Chemical formula	Boiling point °C	Molecular weight(g/mol)	Latent heat of vaporization (KJ/Kg)
Acetone	C_3H_5OH	56.5	58	518
Ethanol	C_2H_5OH	78.2	46	846
Kerosene	$C_{12}H_{26}$	215	170	251
Gasoline	C_8H_{18}	125	104	356
Water	H_2O	100	18	2256

1.5. Thesis Layout

This thesis is divided into five chapters:

1) The first chapter states the research problem and the technique used to solve it.

2) The second chapter provides a comprehensive and thorough review of the literature related to the research problem.

3) The experimental rig construction and measuring instruments are described in the third chapter.

4) In chapter four, the study's findings are presented and debated.

5) The fifth chapter summarizes the conclusions and recommendations

CHAPTER TWO

LITERATURES

REVIEW

Chapter Two: Literatures Review

2.1 Introduction

In this chapter a review of previous literature related to the subject of droplet formation and evaporation are presented. It includes an explanation of different hydrocarbon fuel droplet generation, droplet evaporation. Finally, a summary of detailed aims of the study are provided.

2.2 Experimental Literatures.

Ma et al. [34] studied an experimental study on the evaporation and combustion of single hydrocarbon droplets under sub- and super-critical pressure conditions in a normal gravity environment. They measured droplet temperature using embedded thermocouples and captured photographs using a high-speed video camera. The results showed that as ambient pressure increased in sub-critical conditions, droplet combustion time decreased rapidly and the droplet burning rate was controlled by phase equilibrium. In super-critical conditions, the interface between the droplet and ambient gas became ambiguous, and the droplet combustion time did not decrease significantly and approached a stable value. Phase change disappeared and the diffusion coefficient started to affect the droplet burning rate. The change in trend of the combustion time variation at the critical pressure point indicated that it was important in determining whether the droplet entered super-critical combustion or not. The ratio of droplet evaporation time to droplet combustion time remained largely constant in sub-critical pressure environments, but it decreased rapidly in super-critical pressure environments, indicating that droplet evaporation was completed earlier in super-critical pressure environments.

Patel and Sahu [35] conducted an experiment to investigate how the composition of fuel and air turbulence affect the evaporation of bi-component fuel droplets. They suspended a single droplet, made of a

mixture of n-heptane and ethanol, using the cross-wire technique in a turbulence box that can generate near-zero-mean homogeneous and isotropic turbulence. They used back-light illumination to capture images of the evaporating droplet. The initial size of the droplet was much smaller than the integral length scale of air turbulence, but much larger than the Kolmogorov length scale. They considered five different turbulent conditions for each fuel composition. The results showed that turbulence had a positive effect on the evaporation rate of droplets, but the extent of its influence depended on the fuel vapor mass diffusivity in air and the initial fuel composition of the binary mixtures. The first stage of evaporation was found to be sensitive to both air turbulence level and composition, while the second stage of evaporation showed a specific trend with fuel composition for all cases of turbulent intensity.

Dai et al. [36] performed experimental study to investigate the evaporation behavior of diesel/cerium oxide nanofluid fuel droplets. The droplet suspension technique was used to conduct experiments under ambient temperatures of 673 K and 873 K, normal gravity, and atmospheric pressure to ensure the accuracy of the data. The results indicated that diesel/cerium oxide nanofluid fuel and diesel exhibited similar evaporation behavior at 673 K. Butμ at 873 K, both the nanofluid fuel and diesel droplets expanded and exploded, but the nanofluid fuel droplets were easier to explode and had a shorter evaporation duration. This was because ceria nanoparticles and their aggregation had a greater attraction near the surface of the droplet, which resulted in a decrease in partial surface tension. This caused the expansion ratio of the nanofluid fuel droplet to be less than that of the diesel droplet. In summary, the presence of nanoparticles in the droplet film reduced the partial surface tension, promoted microexplosion, and greatly reduced the evaporation time.

Wang et al. [37] conducted a study on the evaporation characteristics of a nanofluid fuel containing different concentrations (0.05%, 0.25%, 1.25%, and 5% by weight) of ceria nanoparticles. The experiments were carried out at ambient temperatures of 673 K and 873 K under normal gravity. Their findings revealed that the ambient temperature had a significant impact on the evaporation rate of the nanofluid fuel droplet. The addition of ceria nanoparticles led to repeated and intense micro-explosions of the fuel droplet at 873 K, which was the main factor responsible for the increased evaporation rate compared to pure diesel. The evaporation enhancement of the nanofluid fuel droplets was highest at ceria concentrations of 0.25% to 1.25%, but decreased from 1.25% to 5% at 873 K. The accumulation of nanoparticles at the edge of the droplet led to the formation of a porous spherical shell on the surface at 673 K, which inhibited evaporation compared to pure diesel. The researchers proposed a conceptual model of the evaporation mechanism for nanofluid fuel at ambient temperatures of 673 K and 873 K based on their findings.

Hinrichs et al. [38] utilized a discrete continuous multicomponent (DCMC) evaporation model to investigate the evaporation behavior of diesel fuel. The model incorporated detailed composition data obtained from 2D gas chromatography (GCxGC) analysis, which identified 180 individual species from 11 different hydrocarbon families in the diesel fuel. To use this composition data, four continuous distribution functions were derived for normal paraffins, mono-naphthenics, mono-aromatics, and naphthenic-mono-aromatics. The model was able to accurately capture the preferential evaporation behavior of diesel fuel at gas temperatures up to 200°C, which was due to the presence of very long-chain compounds with low volatilities. Additionally, the study showed that using the DCMC model with experimentally-based fuel composition data is important for

accurately predicting the evaporation behavior of diesel fuel in engine conditions, as a diesel droplet exhibited a longer lifetime than dodecane, which is commonly used in diesel surrogate mixtures.

Yadav et al. [39] investigated the potential of using waste transformer oil (WTO) as a replacement for diesel to reduce fuel costs. They refined the WTO through a two-stage trans-esterification process using acid and alkali catalysts to produce trans-esterified waste transformer oil (TWTO) with suitable physical and thermal properties for use in a diesel engine. Before testing TWTO-diesel blends in a diesel engine, they conducted a fundamental study on droplet evaporation using a suspended droplet experimental facility to evaluate their evaporation characteristics. The results showed that B50 (50% TWTO and 50% diesel) had superior droplet regression, evaporation constant, and droplet lifetime compared to B100 (100% TWTO). In the application study, the TWTO-diesel blends operated in a diesel engine showed comparable performance and combustion for B25 with that of diesel. Additionally, gaseous emissions, such as CO, smoke, and NOX, were found to be similar for B25 and diesel, making it the optimal blend for an unmodified diesel engine.

Valiullin et al. [40] conducted simulations to examine the ignition and combustion characteristics of coal-water slurry containing petrochemicals (CWSP) and oil droplet groups surrounded by water droplets in a combustion chamber. They aimed to investigate the behavior of a heterogeneous fuel aerosol that can occur due to multi-component flows delamination or the intersection of different liquid jets. Their findings showed that decreasing the distance between droplets from 10 mm to 2 mm, which is typical for fuel droplet size, reduced the gas-phase and heterogeneous ignition delay times of oil and CWSP by an average of 30%. Additionally, increasing the distance between water droplets in the

combustion chamber led to approximately 25% reduction in their evaporation times. Moreover, when a combustible liquid droplet was positioned in the center with six water droplets around it, the ignition delay times of oil and CWSP increased by 20-40% and 40-70%, respectively.

Luo et al. [41] conducted an experimental study to investigate the impact of an electric field on the combustion process of droplets. The results demonstrated that the electric field had a significant effect on the droplet's shape, flame temperature, and combustion time. Specifically, when an electric field was applied, the droplet's initial shape became elongated, the flame became brighter, the droplet shape became more stable, and the flame height decreased significantly. Additionally, the combustion time was reduced by 14.9% compared to the condition without an electric field. The flame temperature initially increased and then decreased with increasing electric field intensity, while the droplet and evaporation temperatures decreased. Moreover, the maximum temperature of the flame increased by 17.6%, the maximum temperature of the droplet decreased by 12.9%, and the evaporation temperature decreased by 4.2% compared to the condition without an electric field. However, the electric field did not have a significant effect on the combustion rate.

Rosli et al. [42] investigated the evaporation behavior of gas to liquid (GTL) diesel fuel blends with varying percentages of GTL fuel. They prepared four different fuel blends, G20, G50, G80, and G100, where the number represents the percentage of GTL fuel in the blend. They used the suspended droplet method in a controlled heating chamber to visualize the evaporation behavior of the fuel blends using a high-speed camera connected to a long-distance microscope. The study revealed that puffing was not observed for G100, while micro-explosions were absent for G20. The remaining fuel blends experienced both phenomena. The highest

enlargement factor was observed for G20, followed by G50 and G80. G50 had the highest micro-explosion intensity, followed by G80 and G100. The study also found that adjusting the detection threshold determined the numbers and sizes of the child droplets, and G50 had the highest number of child droplets, followed by G80, G100, and G20. The study suggested that the presence of 50% GTL fuel in a GTL-diesel fuel blend could lead to the best droplet micro-explosions compared to the other fuel blends.

Kastner et al. [43] observed the diameter variations of single droplets dried in an acoustic field. However, determining the rate of evaporation was more difficult than determining the rate of size change. According to changes in droplet volume, they separated each droplet drying procedure into two stages. In the first drying stage, the droplet volume was used to estimate the evaporation rate; however, in the second drying stage, when the volume reduction becomes minimal, the evaporation rate was measured by changes in the position of the droplet particles in the acoustic field.

Brenn et al.[44] estimated the rate of evaporation using changes in droplet diameter. The evaporation rate was not taken into consideration in the reports by Mondragon and coworkers **[3, 4]**; instead, the droplet drying behavior in the acoustic field was simply assessed by the size changes, with the effects of drying conditions and initial droplet conditions on the final particle properties being investigated. to make it easier to measure the rate of droplet evaporation in the SDD processes that use sonic levitation. For the purpose of accomplishing a continuous, on-line measurement of the droplet moisture content while drying progressed, **Groenewold et al. [5]** included a dew point hygrometer to the system. Calculating the partial vapor pressure of outflow air converted the experimental data into droplet drying curves **[45, 46]**. A droplet with a diameter of 1μm is suspended

from the end of a thin glass or glass capillary tube and placed in a regulated air stream in a contact levitation experiment. A camera and a thermocouple (one placed in the core of the droplet and the other in the tube) are used to evaluate drying variables such the droplet's mass as well as diameter reductions **[46]**.

2.3. Theoretical Literature

Many studied analyzed the discrete component model or individual component to simulate fuel droplet heating and evaporation such as **[47-51]**. They found that discrete component model gives highest accuracy. A multi-dimensional quasi-discrete model was utilized in several investigations **[52, 53]**. A modest number of representative components were used in place of a huge number of other components in this modeling.

Rybdylova et al. [54] modeled the analytical approximations to the heat conduction and species diffusion equations in the liquid phase, the multi-component droplet heating and evaporation was using ANSYS Fluent software. They used three droplets (25% ethanol/75% acetone), (50% ethanol/50% acetone), (75% ethanol/25% acetone). The results indicated that the highest variation between estimated temperatures did not exceed 0.16% for t = 4 ms, 0.14% for t = 5 ms, and 0.13% for t = 6 ms. This indicates that the consistency between ANSYS Fluent's predictions and the in-house code is reasonably excellent. In practically all practical applications, this disparity between the findings can be disregarded.

Sazhin et al. [55] introduce novel method for simulating the evaporation of fuel droplet. They used gasoline fuel with specific condition as in real condition in internal combustion engine. The numerical model used to simulate the number of components of gasoline with identical chemical formulae and similar thermodynamic and transport properties.

The modeling process used to replace the 83 components of original composition of gasoline fuel with 20 components only. In a subsequent study by the same researcher with **Al Qubeissi et al. [52]** the blended Diesel and biodiesel fuel was used. They found that Multi-component model gives longer evaporation time and higher surface temperature than single component model for both gasoline and diesel fuel droplet.

Sazhin et al. [56] developed a quasi-discrete model to analyze the heating and evaporation of multicomponent hydrocarbon fuel droplets in Diesel engine-like conditions. The model was developed based on the assumption that the properties of components were weakly dependent on the number of carbon atoms (n) in the components. Quasi-components with average properties were calculated for groups of actual components with relatively close n. The model was then applied to Diesel fuel droplets, approximated as a mixture of 21 components C_nH_{2n+2} for $5 \leqslant n \leqslant 25$. This resulted in a maximum of 20 quasi-components with average properties for $n = n_j$ and $n = n_{j+1}$, where j varied from 5 to 24. The study showed that the droplet surface temperatures and radii predicted by the quasi-discrete model using only five quasi-components were very close to those predicted by a rigorous model considering all 20 quasi-components. However, it was noted that errors due to the assumption that droplet thermal conductivity and species diffusivities were infinitely large could not be disregarded in the general case.

Elwardany and Sazhin [57] examined a quasi-discrete model to analyze droplet heating and evaporation, using gasoline fuels in a diesel engine. They found that the simplified version of the model, which assumed that the density, viscosity, heat capacity, and thermal conductivity of all liquid components were the same as for n-dodecane, produced results consistent with the predictions of the more complex model. However, the

difference in predictions between the 13 and 1 component models was significant when droplets evaporated in gas at a relatively low temperature (450 K) and low pressure (0.3 MPa). In such cases, the evaporation time predicted by the 1 component model was less than half of the time predicted by the 13 component model. The study also revealed that the surface mass fraction of the lightest quasi-component in gasoline fuel steadily decreased over time, while the surface mass fraction of the heaviest component steadily increased. The surface mass fractions of intermediate components initially increased with time but then rapidly decreased at later times.

Dgheim et al. [58] conducted a numerical study of heat and mass transfer from an evaporating fuel droplet that was rotating around its vertical axis under forced convection, which only occurred on the side opposite to the flow. The researchers assumed that the flow was laminar and that the droplet retained its spherical shape throughout its lifetime. Based on these assumptions, they numerically solved the conservation equations in a general curvilinear coordinate. They analyzed the effects of droplet rotation on the evaporation process of multi-component hydrocarbon droplets by simulating the droplet as a hard sphere. They discretized the transfer equations using an implicit finite difference method and used the Thomas algorithm to solve the system of algebraic equations. The study also determined dimensionless parameters for heat and mass transfer phenomena around a rotating hydrocarbon droplet, which considered the rotation phenomenon and the variation of thermophysical and transport properties in the vapor phase of multi-component blends.

Xiao et al. [59] employed molecular dynamics (MD) simulations to investigate the evaporation of suspended n-dodecane droplets of various initial diameters into a nitrogen environment under sub- and supercritical

ambient conditions. They varied both ambient pressure and temperature from sub- to supercritical values, crossing the critical condition of the fuel. The researchers obtained the temporal variation in droplet diameter and recorded the droplet lifetime. They determined the time of supercritical transition by analyzing the temperature and concentration distributions of the system and comparing them with the critical mixing point of the n-dodecane/nitrogen binary system. The study quantified the dependence of evaporation characteristics on ambient conditions and droplet size and found that the droplet lifetime decreases with increasing ambient pressure and/or temperature. Additionally, the supercritical transition time decreases with increasing ambient pressure and temperature. The researchers observed that the droplet heat-up time as well as the subcritical to supercritical transition time increases linearly with the initial droplet size d0, while the droplet lifetime increases linearly as well. They generated a regime diagram that shows the subcritical and supercritical regions as a function of ambient temperature and pressure as well as the initial droplet size.

Azimi et al. [60] conducted a numerical investigation of the evaporation process of heavy fuel oil (HFO) droplets under atmospheric pressure using a fully transient approach. The HFO is considered to be a multi-component liquid with temperature-dependent properties. The accuracy of this approach was evaluated for various fuels and the results were compared with available experimental data for gasoline and diesel fuel. The composition was divided into several pseudo-components and the effects of the number of components and their selection method were studied. It was discovered that even though heavy fuels have a wide range of compositions, a compound consisting of a few pseudo-components can be an appropriate representation for them. Additionally, the pseudo-

components should be selected based on equal interval temperature and narrow boiling temperature range. The study also explored the effects of environmental temperature on droplet evaporation through a parametric analysis. The findings showed that the internal temperature distribution of the droplet is not highly sensitive to ambient temperature due to the high boiling temperature of the heavy fuel components. Furthermore, the wide range of temperatures in the heavy fuel droplet allows for the prediction of the initial condition of pyrolysis and thermal cracking of heavier components.

Al-Qubeissi [61] investigated the heating and evaporation of fuel droplets for a range of automotive fuels including biodiesel, diesel, gasoline, and blended diesel-biodiesel fuels under real internal combustion engine conditions. The Discrete Component model (DCM) was used to predict the evolution of droplet radii and temperatures for various biodiesel fuels and their selective diesel fuel blends, which were composed of up to 116 components of 98 hydrocarbons and 4-18 methyl esters. The results showed that the droplet evaporation time and surface temperature predicted for 100% biodiesel were highly dependent on the composition of the biodiesel fuel and not always close to those predicted for pure diesel fuel. However, by replacing the full composition of biodiesel fuels with just 5, 4, or 3 components using the MDQDM, the errors in predicting droplet evaporation times were negligible (less than 1.83%) compared to the DCM predictions, and the computational time was reduced by up to 0.04.

Pinheiro et al. [62] investigated the impact of ambient temperature, pressure, and vapor concentration on the evaporation of a single ethanol droplet. They varied the temperature from 400 to 1000 K, pressure from 0.1 to 2.0 MPa, and vapor concentration from 0.0 to 0.75. The study found that increasing ambient pressure increased the ratio of initial heat-up time to the

entire evaporation lifetime, resulting in enhanced unsteady effects of the droplet evaporation. This ratio was found to be almost independent of gas temperature at low ambient pressure, but it increased significantly with gas temperature as the ambient pressure increased. Moreover, there is a threshold ambient temperature that determines whether the average area reduction rate will increase or decrease with an increase in ambient pressure. The study also observed condensation effects for non-zero ambient vapor concentration, and there is a threshold ambient temperature that determines whether the average area reduction rate will increase or decrease with an increase in ambient vapor concentration. Many studies focused on the ambient temperature and pressure effect on the droplet evaporation rate for hydrocarbon fuel such as **[20, 63-65]**.

Lupo et al. [66] developed a new method called Immersed Boundary Method (IBM) to simulate the evaporation of spherical droplets in gas flow. This method involves direct numerical simulation of momentum, energy, and species transport in the gas phase while exchanging these quantities with the liquid phase through global mass, energy, and momentum balances for each droplet. This method is applicable for small spherical droplets and accurately captures physical phenomena and their interactions for both laminar and turbulent gas flows, saving computational costs by not directly solving for the liquid phase fields. The team provided validation results for several test cases, including fixed rate and free evaporation of a static droplet, displacement of a droplet by Stefan flow, and evaporation of a hydrocarbon droplet in homogeneous isotropic turbulence. The method was validated against experimental data, demonstrating its potential for simulating real-life spray fuel applications.

Markadeh et al. [67] studied the evaporation of a multicomponent droplet in a hypothetical spherical bubble in a spray. They employed a fully

transient approach and investigated the variations in the extents of heat and mass influence during evaporation for three different fuels, heptane, hexadecane, and a blend of both. The study also considered the effects of neighboring droplets on temperature and species concentration in both liquid and gas phases and compared them to those of an isolated droplet. The results showed that the effects of neighboring droplets become significant for spacing parameters less than 55, corresponding to an equivalence ratio of around 10, and that this effect diminishes at higher ambient temperatures and lighter fuels. The study found that increasing the spacing between droplets results in a decrease in the droplet lifetime, and the effect of neighboring droplets becomes less significant at higher ambient temperatures. The effects of droplet spacing are more pronounced for less volatile fuels and smaller droplets. Furthermore, the impact of droplet spacing on the lifetime of the bi-component droplet is greater than that of the two single component droplets.

Veronika et al. [68] developed physical and mathematical models to study the combustion of multicomponent and multi-phase fuels in rocket engines. They considered the effect of poly-dispersed non-uniform mixtures, which consist of a hydrocarbon liquid and solid combustible material, on the conditions of ignition and modes of propagation of combustion. In this case, the combustion of different droplet fractions occurs in different modes: the volatile fraction evaporates and burns in the gas-phase mode, while the solid fuel fraction reacts with the oxidizer in the heterogeneous mode. The study also took into account the effect of the presence of a solid fraction in droplets reacting in a heterogeneous regime on the evaporation rate of the volatile fuel component, as well as the effect of tightness due to the presence of other drops on the evaporation rate of each drop. The results of computational modeling of flame propagation

during ignition of poly-dispersed mixture of liquid hydrocarbon fuel droplets with solid fine carbon particles were presented.

Gong et al. [69] investigated the mechanism and criteria for the change in dominant mixing mode during the evaporation of multi-component hydrocarbon mixtures under supercritical conditions. They utilized molecular dynamics to examine the behavior of three-component hydrocarbon fuel droplets (consisting of 5.3 wt% isooctane, 25.8 wt% n-dodecane, and 68.9 wt% n-hexadecane) and single-component n-hexadecane droplets in sub- and supercritical nitrogen environments. The initial diameters of the droplets were 25.5 nm (for the three-component droplets) and 26.5 nm (for the single-component droplets). Their findings revealed that the density difference between the vapor and liquid phases gradually decreased as the ambient pressure increased or the ambient temperature decreased, leading to a transition in the dominant mixing mode from evaporation to diffusion. However, increasing ambient pressure did not necessarily result in phase transition, while increasing ambient temperature accelerated it. Moreover, the presence of light fuel components raised the minimum pressure of the diffusive mixing zone.

Saufi et al. [70] studied a simulation of the combustion of a fuel droplet under normal gravity conditions. They utilized DropletSMOKE++, a solver that can model droplet vaporization and combustion in convective conditions. The analysis provides a detailed understanding of the physical properties of the problem and shows good agreement with experimental results in terms of diameter decay, radial temperature profiles, and sensitivity to oxygen concentration. The thermal conduction from the fiber, which occurs at high temperatures, impacts the vaporization rate. Additionally, the fiber influences the flame and causes it to quench at its surface. The researchers compared the combustion physics to that predicted

at zero gravity and found a lower standoff ratio, a higher flame temperature, and strong internal circulation. The distribution of species around the droplet revealed a local buildup of intermediate oxidation products at the fiber surface and water absorption in the liquid phase, which affected the vaporization rate.

Ruitian et al. [71] conducted a study on the behavior of n-heptane and multi-component diesel droplets under spray conditions. They used a multi-component diffusion sub-model along with real vapor-liquid thermodynamic equilibrium to analyze the phase change rate on the droplet surface. They also considered the finite thermal conduction model to calculate the temperature distribution within the droplets. The study highlights the impact of ambient composition on the evaporation and condensation characteristics of the droplets. They found that an increase in vapor concentration leads to a reduction in the droplet evaporation rate and an increase in the diffusional enthalpy flux. The study also defined two thresholds based on ambient composition that determine the condensation occurrence on the droplet surface and the droplet's approximately stable state. The authors observed that heavy-end fuel vapor had a greater effect on the droplet's lifetime compared to the light-end vapor. They also found that the influence of pressure on the droplet evaporation rate depends not only on the ambient temperature but also on the ambient composition. There are many studies that focus on the effect of vapor concentration on the droplet evaporation such as **[72, 73]**.

Gong et al. [74] investigated the evaporation of a six-component hydrocarbon fuel droplet containing toluene, n-decane, n-dodecane, n-tetradecane, n-hexadecane, and n-octadecane in different nitrogen environments using molecular dynamics simulations. The simulations were carried out at pressures ranging from 2 MPa to 16 MPa and temperatures

ranging from 750 K to 1350 K. The researchers found that the behavior of the mixed fuel was not a simple linear combination of the individual components' physical properties based on their mole fractions. They also observed that the average resultant force on an individual fuel atom increased with increasing pressure or decreasing temperature at the supercritical temperature, and diffusion dominated the mixing process of the fuel. Furthermore, the study discussed the clustering behavior of the fuel under supercritical conditions. The evaporation of droplets in supercritical circumstances has been reviewed from a variety of perspectives **[75-78]**.

Dodd et al. [79] studied the evaporation of n-heptane fuel droplets in forced homogeneous isotropic turbulence using Direct numerical simulations (DNS). They varied the ratio of initial droplet diameter to Kolmogorov length scale and the liquid volume fraction. The results showed that increasing the liquid volume fraction of droplets decreased the evaporation rate and caused the evaporation rate to deviate from the classical d^2-law. The study also tested evaporation models based on the Frössling correlation and found that the correlation was inaccurate when predicting the droplet Sherwood number in turbulent conditions. The study also discussed modeling aspects of the Spalding number in the context of multiple interacting droplets. The DNS results were validated against experimental data for an isolated droplet evaporating in HIT. The study provides insights into the complex interplay between droplet evaporation and turbulence in practical combustion systems.

2.4. Experimental and Theoretical Literature.

Wu et al. [80] studied the general evaporation model of a liquid fuel droplet, both theoretically and experimentally, under intermediate droplet Reynolds numbers and various ambient turbulence conditions. They

conducted extensive experiments on the evaporation of single fuel droplets, using hydrocarbon fuels such as pentane, hexane, heptane, octane, and decane, in quasi-laminar and turbulent environments with Reynolds numbers ranging from 72 to 333 at room temperature. The experiments were carried out using flow fields generated by a perforated plate or a circular disk in a vertical low-speed wind tunnel to provide the necessary ambient turbulent environments. The ambient turbulence intensities ranged from 1% to 60%, and the integral length scales ranged from 0.5 to 20 times the initial droplet diameter. The results indicated that the normalized evaporation rate (K/KL) decreased with an increase in the effective Damköhler number ($0.0001 < D_{av} < 0.1$) and was approximately equal to unity with a further increase in the Damköhler number ($0.1 < D_{av} < 1$).

Mouvanal et al. [81] studied experimentally and numerically the evaporation of a thin fuel film on a heated wall, using various single component hydrocarbons such as n-hexane, n-heptane, iso-octane, and n-decane, as well as a two-component and a three-component mixture representing gasoline. The thickness of the film was measured using a highly precise confocal device that can detect thickness down to 2-3 micrometers, enabling the measurement of film thickness in wet-components of gasoline injection systems. The researchers observed that the variation of film thickness with time was linear for single component fuel and exhibited fractional distillation for the multi-component fuel. A mathematical model was developed to estimate the temporal variation of film thickness and evaporation time for both single and multi-component fuels, which included a constant determined by the saturation temperature of the fuel and the wall temperature. The results showed that the model accurately predicted the time of evaporation of thin films, indicating its usefulness as a tool for designers of engines and fuel injection systems.

Poulton et al. [82] studied the heating and evaporation of suspended kerosene and kerosene surrogate droplets, using a Discrete Component Model (DCM). They considered the effects of natural convection using the Churchill approximation, and modeled the effects of heat addition from the supporting fiber by assuming that the heat is uniformly distributed within the droplet volume. The researchers found that the effect of the supporting fiber can be neglected, but natural convection cannot. The DCM predictions of droplet radii, taking into account natural convection and supporting fiber effects, were in good agreement with experimental measurements for gas temperatures between 500 °C and 700 °C. The study also compared the heating and evaporation of kerosene droplets with various kerosene surrogate fuels, including 11 surrogates proposed in the literature and two original compositions.

2.5. Concluding Remarks

It is noticed throughout the previously literature that the surrounding condition effected on droplet evaporation has been focused on different evaporation technique were used. In this work the effect of surrounding temperature and liquid type on evaporation characteristic specially, droplet lifetime will be using the free flying droplet technique.

CHAPTER THREE

EXPERIMENTAL WORK

Chapter Three: Experimental Work

In this chapter a detailed description of the experimental setup used in this work is given. The complete setup is fabricated in the post-gradual laboratory of department of mechanical engineering. Measuring apparatus used to measure properties (density, thermal conductivity and viscosity) are clarified in this chapter. The process of measuring the droplet evaporation and monitoring the evaporation process are explained. The rig is used to investigated the droplet evaporation for different hydrocarbon liquids fuel includes water, acetone, gasoline, kerosene, and ethanol.

3.1 Experimental Setup

In order to observe the evaporation process of a falling droplet, a rig was constructed that is fully depicted in the Figure (3-1) and illustrated in the schematic diagram shown in the Figure (3-2). This Rig is consisting of the following units:

1- Evaporation chamber.

2- Droplet injector.

3- Pressure gauge.

4- Temperature sensor.

5- Capture unit.

6- Control panel.

7- Air blower and heater.

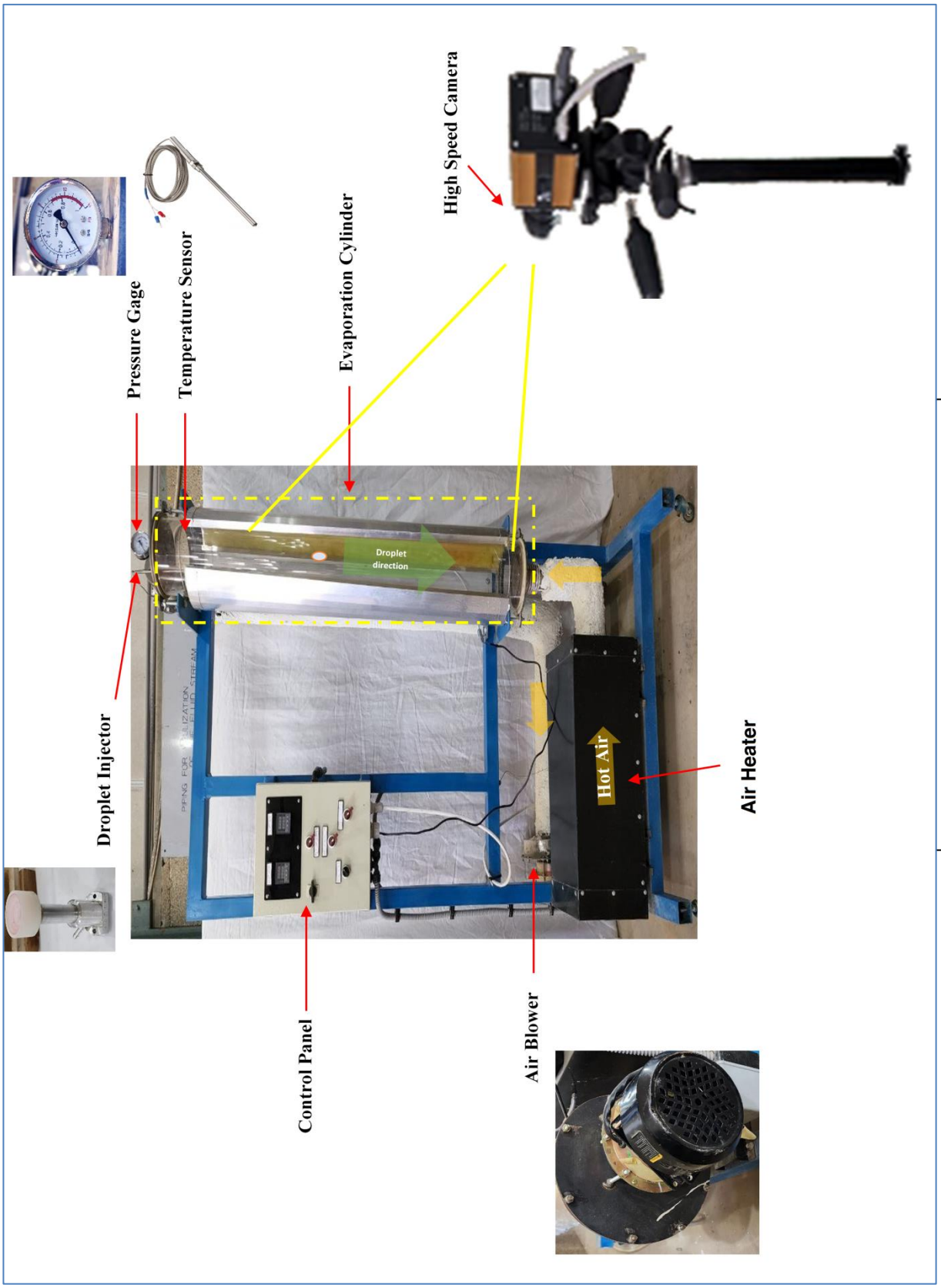

Figure (3- 1) Experimental Rig.

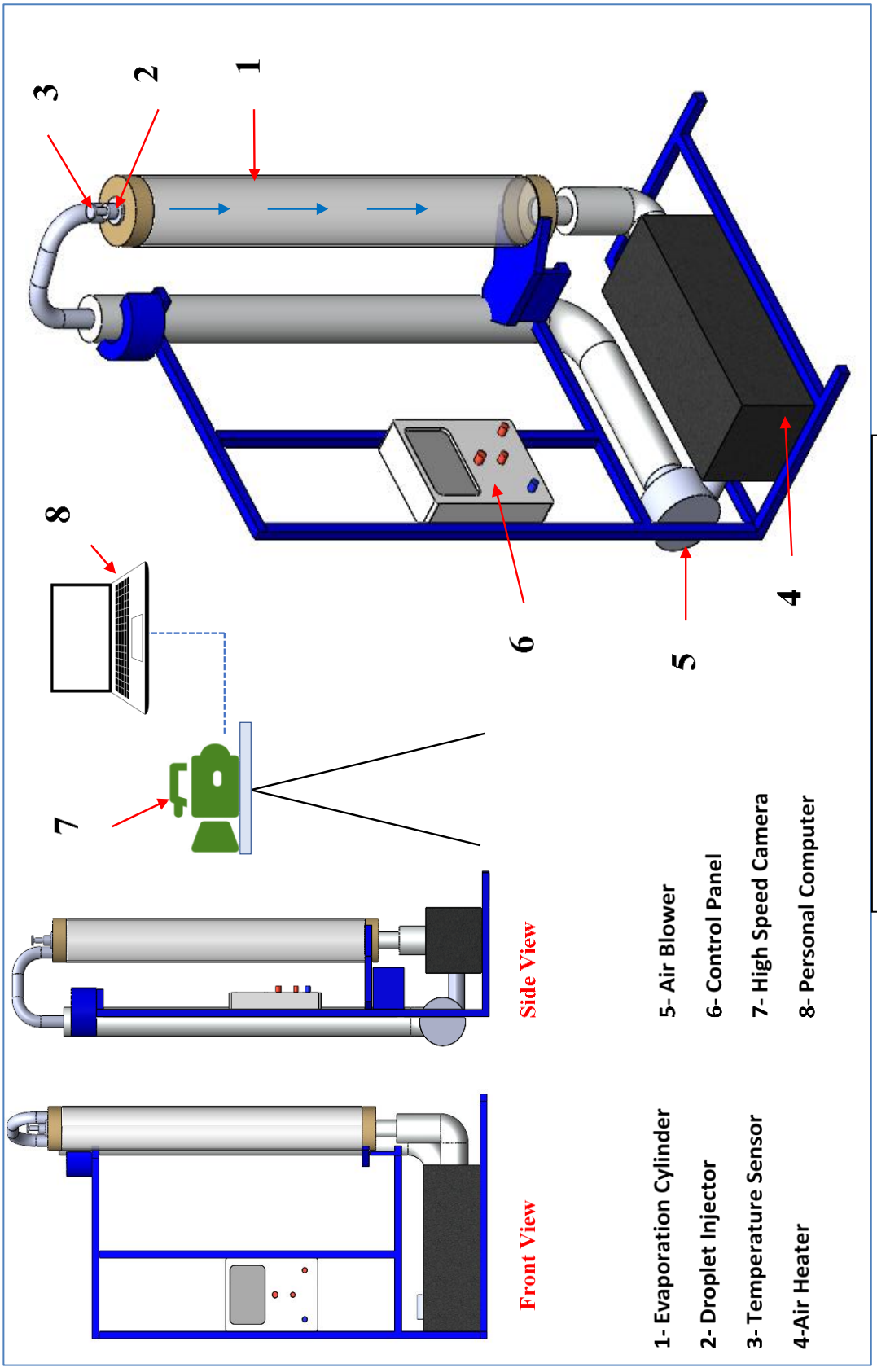

Figure (3- 2) Experimental Rig Layout.

3.1.1 Evaporation Chamber

For the purpose of following the liquid droplet and the change in its size due to evaporation the photography technique is used. Therefore, a glass chamber is needed to facilitate the photography process.

A clear glass tube with suitable length and size is needed. After looking in local market a glass tube with above mentioned specification is found. Therefore, the evaporation chamber is made of heat-resistant, transparent Pyrex glass. The cylinder has with 175mm inner diameter, 180 mm outer diameter and 1300 mm length. It is installed vertically. The cylinder is closed and supported by an iron flange from its lower end. The flange has an opening in its center to allow air hot circulation. The upper end of the cylinder is also closed by an iron flange with central opening to allow for air circulate also. On this flange the pressure gage, the thermocouple and droplet generator are mounted. Figure (3-3) show the Pyrex cylinder and its lower and upper flanges.

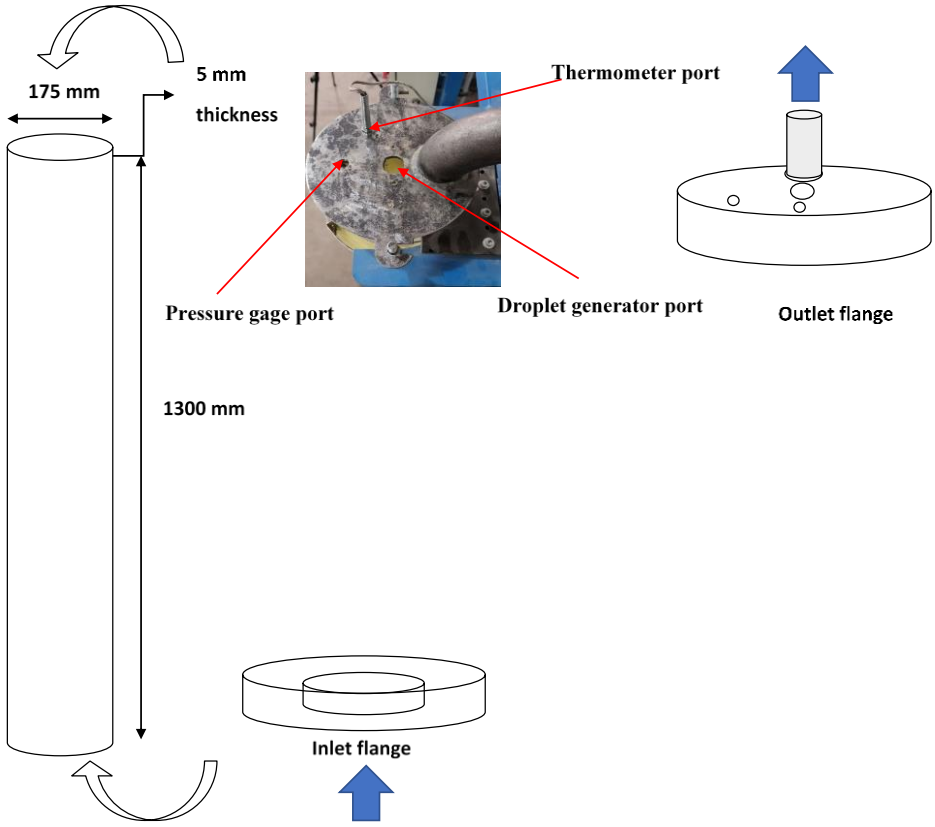

Figure (3- 3) Evaporation Chamber

3.1.2 The Droplet Generator

In order to generate a droplet that can be photographed clearly different techniques for were tried including:

1- The use of a special syringe for insulin treatment as shown in Figure (3- 4) for the purpose of generating the droplet. It is operated manually. However, this technique produces large droplet and it is difficult to control the plunger movement. Therefore, this technique was not used.

2- The burette device shown in Figure (3-5) was also tried to generate the droplet with the required size. However large size droplet was also generated, therefore this technique was also rejected.

3- The micropipette technique shown in Figure (3-6) was tried. This device is operated mechanically and used in many laboratories. However, it was found that this technique is not practical and also produces large size droplet.

4- Therefore, a special droplet generator is designed and fabricated for this purpose. The shape and dimension of this generator as show in Figure (3-7).

A pressure-driven droplet generator is a type of device that uses a compressed air to force a liquid through a small orifice or nozzle to create small droplets in a controlled and precise manner. The droplet size and shape are affected by various parameters such as the liquid properties, nozzle size, geometry, and the flow rate. The size of the droplets produced by a pressure-driven droplet generator can be varied from a few micrometers to several millimeters. As shown in Figure (3-7) the liquid is first drawn into a syringe or a reservoir and is then pushed through a narrow orifice or nozzle by compressed air. As the liquid leaves the nozzle it breaks up into droplets due to the shearing forces and surface tension of the liquid. The droplet generator was made of aluminum with a diameter of 7 cm from the bottom and perforated with two holes to be fixed with screws on the flange. The needle was made of stainless steel and the end of the needle had a diameter of 0.26 mm. The lever at the top of the injector was made of thermal Teflon with an outer diameter of 5 cm and is hollow for the purpose of pouring liquid into the cavity. Which has a diameter of 0.82 cm to flow around the surface of the needle after turning the lever manually and letting go. A hollow tube with a length of 4 cm and a diameter of 0.85 cm was attached for the purpose of compressing air from the compressor to the surfaces of the needle for the purpose of accelerating the flow of the liquid or breaking the adjacent layer that prevents the liquid from flowing. Figure (3-8) shows air compressor used with droplet generator.

Figure (3- 4) A special Syringe for Droplet Generation

Figure (3- 5) The Burette Device

Figure (3- 6) Micropipette

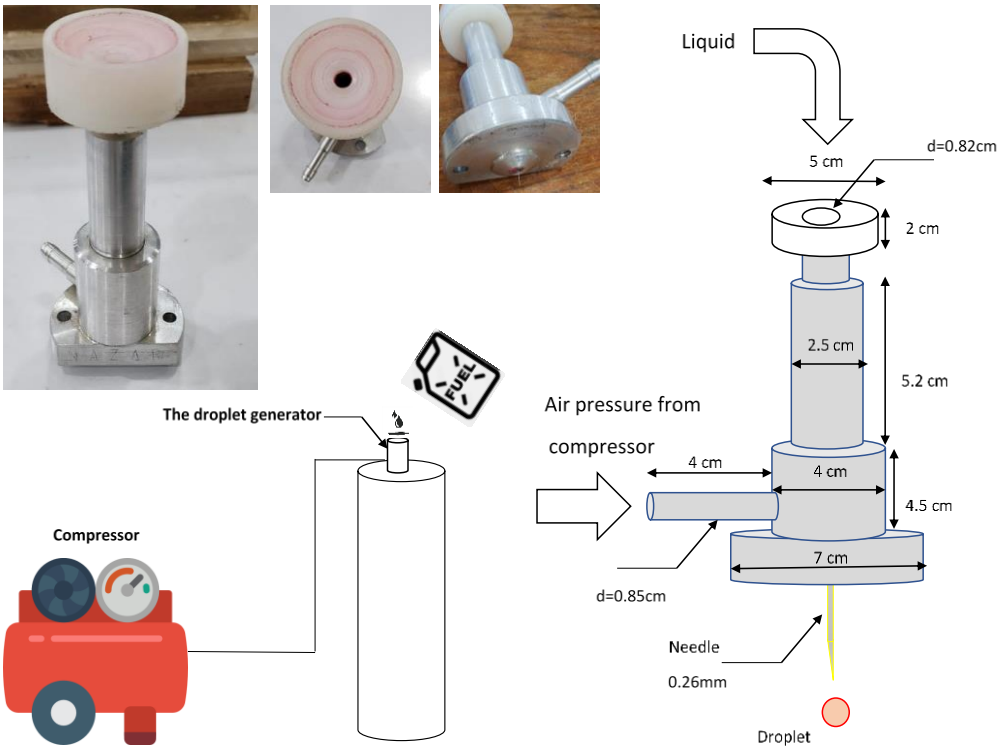

Figure (3- 7) Droplet Generation Process with Injector Dimensions

Figure (3- 8) The Compressor

3.1.3 Pressure gage

In the current study, the pressure in the evaporation chamber was not changed, but to ensure the stability of the pressure during the various experiments, a gauge pressure was placed to monitor the pressure variation as a result of heating the air inside the evaporation chamber. The gauge pressure mounted in upper end of the cylinder as depicated in Figure (3-9).

Figure (3- 9) The Gage Pressure

3.1.4 Temperature Sensor

Thermocouple type K is placed inside the evaporation chamber to monitor the temperature of the evaporation chamber. The thermocouple is connected to the control panel, which displays the digital reading of the temperature as shown in Figure (3-10).

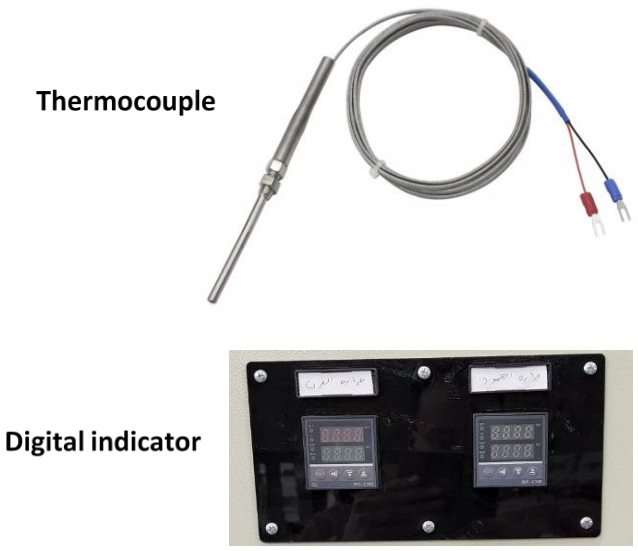

Figure (3- 10) Temperature Measurements

3.1.5 Photography Unit

An optical system is used to visualize the droplet evaporation process with a high – speed camera as shown in Figure (3-11, a,b). High speed camera type AOS-Q-PRI with image resolution of 3 Mega pixels is used in this study. The internal memory is 1.3 GB, and the frame rate is 16000 FPS. The setting used in the experiment is 500 FPS and the total time of recording is 2 sec. 10% of the time is set as pre-triggering to ensure that all evaporation process is recorded. The camera is connected to the computer, and through a camera software, the video time and frame rate is controlled, the video resolution is processed. Figure (3-11 c,d) explain the connections between the camera and PC.

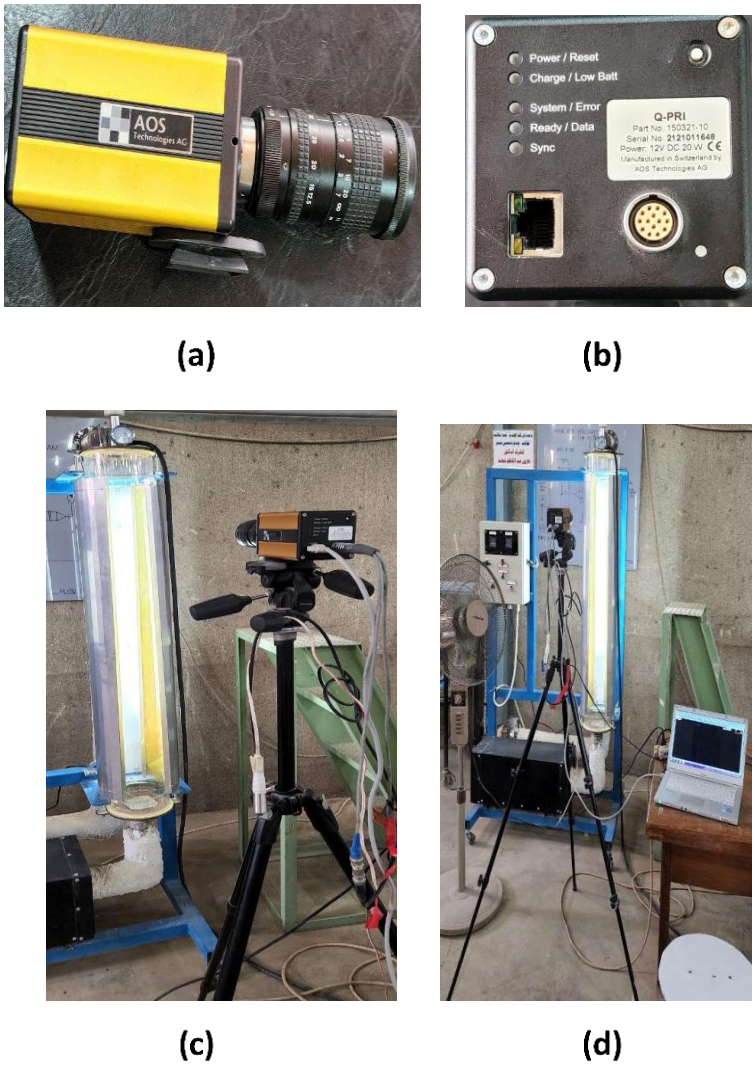

Figure (3- 11) Capture Unit, (a) AOS-Q-PRI High Speed Camera, (b)Camera Ports, (c) Install The Camera in The Appropriate Location in Front of The Evaporation Chamber, (d) Connect The Camera to The Computer.

3.1.6 Control Panel.

The control panel includes the operating switches of the controller as well as the temperature sensors of the evaporation chamber and the heater. Through the control panel, it is possible to operate the air heater and then operate the fan that blows air through the evaporation chamber. The control panel also contains digital screens to display the temperature inside the evaporation chamber. The temperature is fixed inside the evaporation chamber through the control panel, and when the chamber reaches the required temperature, the heater and the air blowing fan are stopped. The

lights can be controlled through the keys on the control panel. Figure (3-12) shows the control panel used in this study.

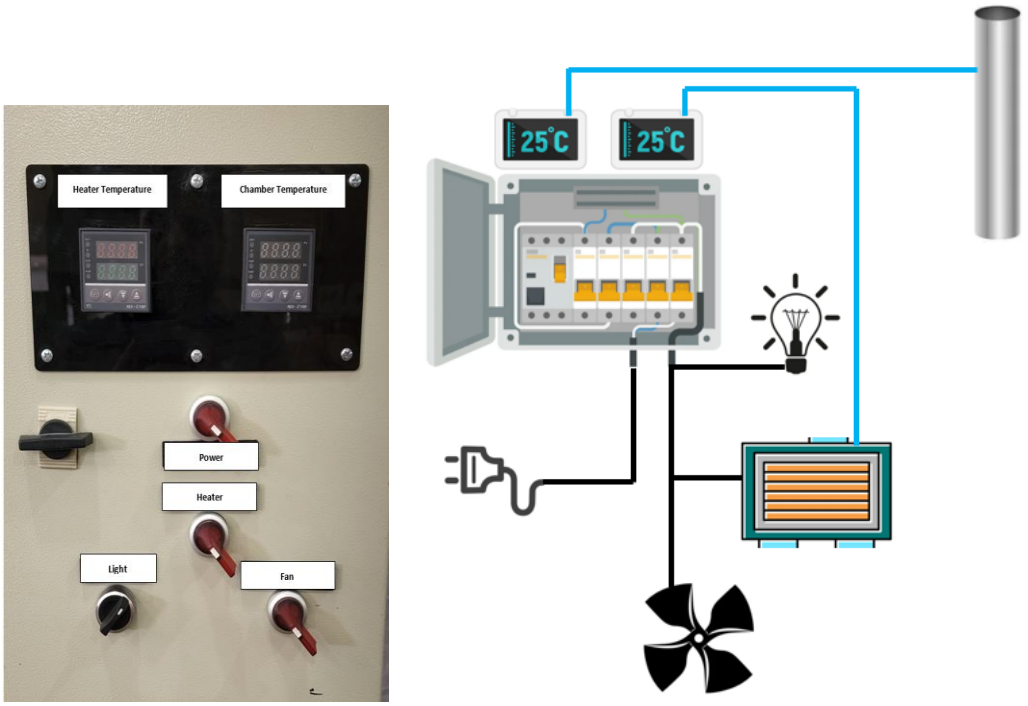

Figure (3- 12) Control Panel with Electrical Connections

3.1.7 Heating system

This system consist of three parts:

1. Air heating Chamber: Four electric heaters with 1000 W are installed inside the air chamber to heat the air which passed to the evaporation chamber as shown in Figure (3-13). The heating chamber is made form 410 stainless steel and thick layer of glass wool. The dimensions of heating chamber are 26×26×70 cm. To monitor the temperature of the air heating chamber, a thermostat is used inside the chamber and is connected to the control panel. The electric power of the heating chamber is supplied by connecting it with the control panel.
2. Air blower: Figure (3-14) shows the fan pushes the hot air from the heating chamber to the evaporation chamber through a tube and then withdraws it from the evaporation chamber and returns it to the heating

chamber until the temperature of the heating room reaches the required degree. It turns off automatically through a switch located in the control panel after setting it to the required temperature.

3. Air circulation tubes: Metal tubes with a diameter of 60 mm and a thickness of 2 mm are used to circulate air between the two chambers, as shown in the Figure (3-15). These tubes are insulated using rock wool to avoid heat losses and thus reach the required temperature as quick as possible.

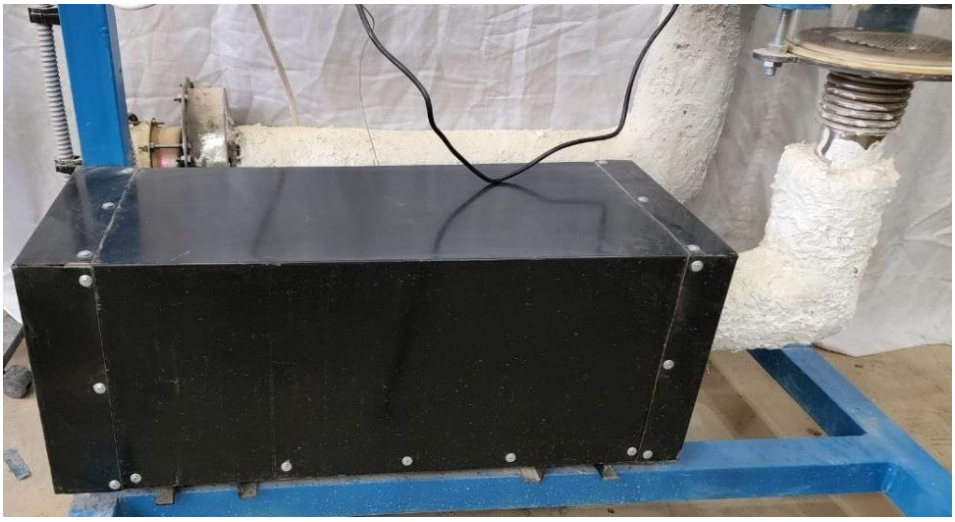

Figure (3- 13) Heating Chamber

Figure (3- 14) Air Blower

Figure (3- 15) ***Air Circulation Tubes***

3.2 Device calibration

The temperature sensor was calibrated by comparing the sensor readings with another more accurate temperature recorder. The temperature recorder thermocouple wire placed inside the evaporation chamber, then the temperature is gradually raised and recorded in both devices as in the Figure (3-16). Then draw a relationship between the readings between the two devices to extract the calibrator equation as in the Figure (3-17). The equation is a polynomial equation and the perfection of the following:

$$T_{cal} = 2.7019 + 0.8377\,T_{read} + 0.0029\,T_{read}^{2} - 2 * 10^{-5} * T_{read}^{3} \qquad (3.1)$$

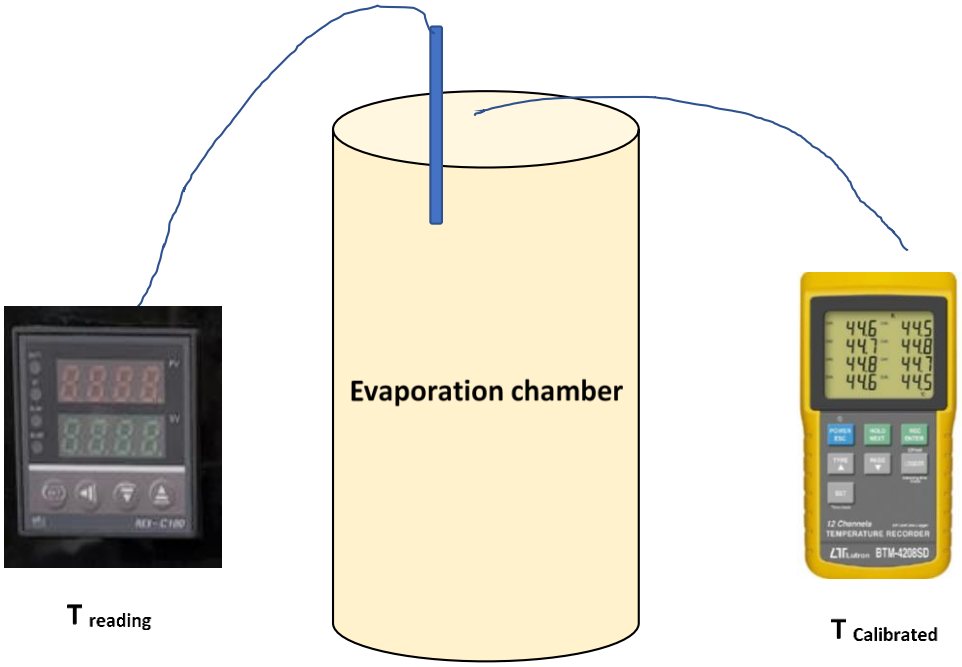

Figure (3- 16) Temperature Calibration Process

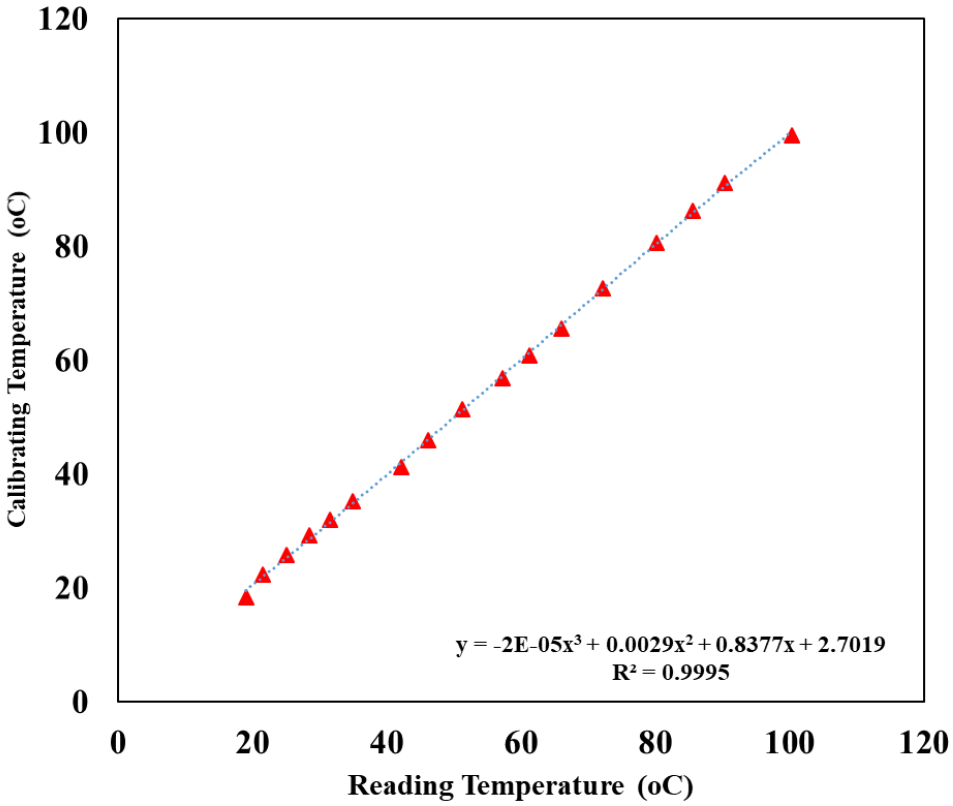

Figure (3- 17) Temperature Calibration Curve

3.3 Liquid physical properties

In this study five liquids are used (Water, Ethanol, Acetone, Kerosene, Gasoline). Which are four important fuels and water.The physical properties including thermal condictivity, density and viscosity are measured in the laboratories of the faculty of Materials Engineering at the unversity of Babylon.

3.3.1 Density measuring

Liquid density was measured using bulk density tester (GP-1205) as shown in Figure (3-18) . By adding suitable volume of a liquid to container and measuring the weight of this liquid the density can be obtined. The liquid is kept in a chamber insulated from surrounding air to prevent any evaporation process. Table (3-1) shows the results of the test to measure the density of the liquids used during the current study.

Figure (3- 18) Bulk Density Tester

Table (3- 1) Density Measurement Results

No.	Subject name	Measured density(g/cm^3)
1	Ethanol	0.7862
2	Acetone	0.7811
3	Gasoline	0.7392
4	Kerosene	0.7961
5	Water	0.9895

3.3.2 Dynamic viscosity measurement

Liquid dynamic viscosity is measured using Brook field viscometer DV3TLV with Rheocalc software as shown in Figure (3-19). The dynamic viscosity is measured by using viscometer type (Cone plate test DV-III ULTRA). It consists of a water jaket, cylindrical sample holder, small adaptor and spindle. The spindle of the viscometer drives was submerged in the sample holder that contains the test sample of the fluid by rotating of spindle the viscous drag of the fluid started by measuring against the spindle. The temperature sensor observed the temperature of the sample. The dynamic viscosity is measured at 30°C and the viscosity result as shown in Table (3-2).

Figure (3- 19) Dynamic Viscosity Measuring Device

Table (3- 2) Dynamic Viscosity Measurement Results.

No.	Subject name	Measured viscosity (mPa.s)
1	Acetone	0.421
2	Ethanol	0.316
3	Gasoline	0.494
4	Kerosene	0.523
5	Water	0.89

3.3.3 Thermal conductivity

The KD2 pro is a portable instrument that measures thermal conductivity as shown Figure (3-20). It includes aportable controller as well as sensors. That may be put into partically any material. Thermal conductivity and resistivity are measured by single needle sensors . The sensor connects to a cord that is immersed at any fluid for measuring data on the micro controller. The thermal conductivity result as shown in Table (3-3).

Figure (3- 20) Liquid Thermal Conductivity Measurements (KD2 pro).

Table (3- 3) Thermal Conductivity Measurement Results.

Fluid Type	thermal conductivity from device (W/m.K)	Average value (W/m.K)
Acetone	0.16 0.15 0.17	0.16
Ethanol	0.18 0.16 0.14	0.16
Gasoline	0.152 0.15 0.14	0.15
Kerosene	0.148 0.145 0.142	0.145
Water	0.607 0.609 0.611	0.609

3.4 Expermantal procedure

The experimental rig is installed in post-graduate laboratory of the Department of Mechanical Engineering. The experimental procedure is as follows:

1-The camera is installed at a distance of 103 cm from the evaporation chamber. The camera and the computer are connected to each other, and then they are connected to the electrical power

2- The camera is connected through the camera's software on the computer, and the camera settings are installed, which is a shooting rate of 500 FPS, as well as (1600*600). The length of the photographed section of the evaporation chamber is 240 mm. as shown in Figure (3-21)

3- Fix a measuring rule on the evaporating chamber for purpose of length calibration.

4- Set the evaporation chamber temperature.

5- Switch the air heater to heat the circulating air until the required set temperature in the chamber is reached, the heater, are switched off by the control unit.

6- A quantity of fuel is taken and withdrawn by means of a syringe, then it is injected into the droplet generator. The compressed air, connected to the droplet generator is turned on. When a droplet of liquid falls through the needle, the compressor is turned off.

7- The camera is switch on to record the free flying droplet as it falls in the chamber.

8- At the end of the experiment the chamber is flushed by fresh air to scavenge any remaining liquid.

9- Repeat the previous steps but at other chamber temperature for the same liquid.

10- Repeat the same procedure for other liquids.

11- The captured video is transferred to the MATLAB program in AVI format, by designing image processing code. The evaporation rate and droplet diameter are calculated as explained in next section.

3.5 Data Analysis

3.5.1 Image processing

A code script is developed in MATLAB to analyze video data of a droplet and plots various graphs related to the droplet's size and evaporation rate over time. The analyzes product as follows:

1-The video file that was recorded in the experiment is exported to the code because it does not read the video in "raw3" format of the camera, but

rather reads a video file named "VI. avi" using the video Reader function video and image processing Toolbox of MATLAB.

2- The code defines a vector called *stopFramesVector* which represents the frames at which the user is prompted to select the droplet in the video using the input function. These frames represent 0.1, 0.5, and 0.75 of the total number of frames in the video which only the droplet was seen.

3-The code then loops through all of the frames in the video and displays each frame using imshow. If the current frame is one of the frames specified in *stopFramesVector*, the user is prompted to select the droplet using the ginput function as shown in Figure (3-22). The selected area is zoomed in and displayed again for further user input. The area and size of the droplet are calculated and stored in the arrays Areas and Sizes.

4- After the loop, the code plots the size of the droplet over time, the amount of evaporation over time, and the evaporation rate over time. The last two charts are neglected because they were calculated from the difference between the two diameters, as the calculation of the amount and rate of evaporation is calculated from the mass difference over a period of time.

5- Finally, the code defines a function called *fit The Curve* which takes a vector of sizes as input and sorts them in descending order.

The purpose of using ruler in this work is to calibrate the system, to relate the pixels and distance travelled because it has a significant effect on the final calculated size of droplet (The Camera does not read dimensions, but reads pixels) . The following steps describes the procedure to find this relationship:

1- Get the pixel vector projected from the ruler line.
2- Get the pixel number at (0 mm) of ruler which is (200).

3- Get the pixel number at (240mm) of ruler which is (1508).

4- Use the linear relationship to find the relation between pixel and millimeter in equation:

At 0 mm number pixel =200

At 240 mm number pixel =1508

$$(240 - 0)mm = (1508 - 200)pixels \quad (3.2)$$

240 mm=1308 pixels

1 pixel $= \frac{240}{1308}\ mm = const$

Figure (3-23) shows an illustration of the dimension seen in the video. According to the previous setting of the camera, the percentage of clear vision is $\frac{240}{1300}$ % of the total length of the cylinder.

AB= 120 mm the length of the line from the tip of injector to the beginning of the ruler, which is not visible with the camera.

BC= 240 mm the length of the line viewed by the Camera, according to the settings.

CD=940 mm the remaining length of the cylinder, which is not visible with the camera, from point C to point D.

The time recorded in the video for the arrival of the point B to point C is 450 ms

t_{BC}=450 ms for BC

since that BC = 240 mm

Now we find the time taken from the point A to point B.

AB= $\frac{1}{2}$ BC $\longrightarrow$ $t_{AB}= \frac{1}{2}(450)= 225ms$

To find the time taken for the arrival of the droplet at each point depending on the drop- up points, which are selected 0.1f, 0.5f and 0.75f within the code for the purpose of calculating the size.

The video of the droplet from B to C will be divided into frames over the 450 ms time period.

At point s= 0.1f $t_1=0.1*450+225$

$t_{1=}270$ ms=0.27 sec

At point m=0.5f $t_2=0.5*450+225$

$t_2=450$ ms= 0.45 sec

At point n=0.75 $t_3=0.75*450+225$

$t_3=$ 562.5 ms= 0.5625 sec

The size of droplet at any moment can be calculated as the follows steps:

1- Surround the droplet manually using left click of the mouse.
2- Calculate the enclosed area based on trapezoidal numerical method. (in pixels)
3- The code converses the area from pixels to millimeters square.
4- Approximate the shape to a circle and calculate the radius using the following equation

$$r = \sqrt{\frac{A}{\pi}} \quad \text{(mm)} \qquad (3.3)$$

$$D = 2r$$

5- Approximate the shape of droplet to a sphere and calculate the size based on equation:

$$v = \frac{4}{3}\pi r^3 \quad (3.4)$$

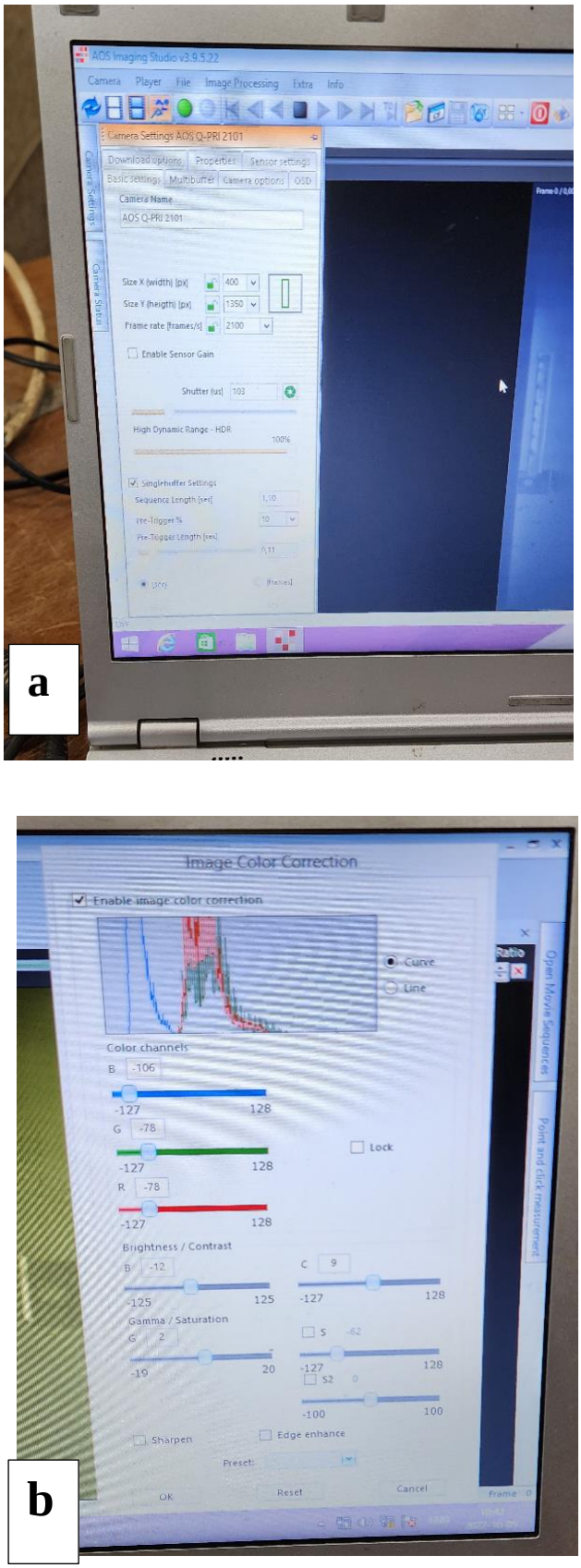

Figure (3- 21) (a) Adjust The Imaging Size Through The Software, (b) Adjust The Color of The Image Through The Software.

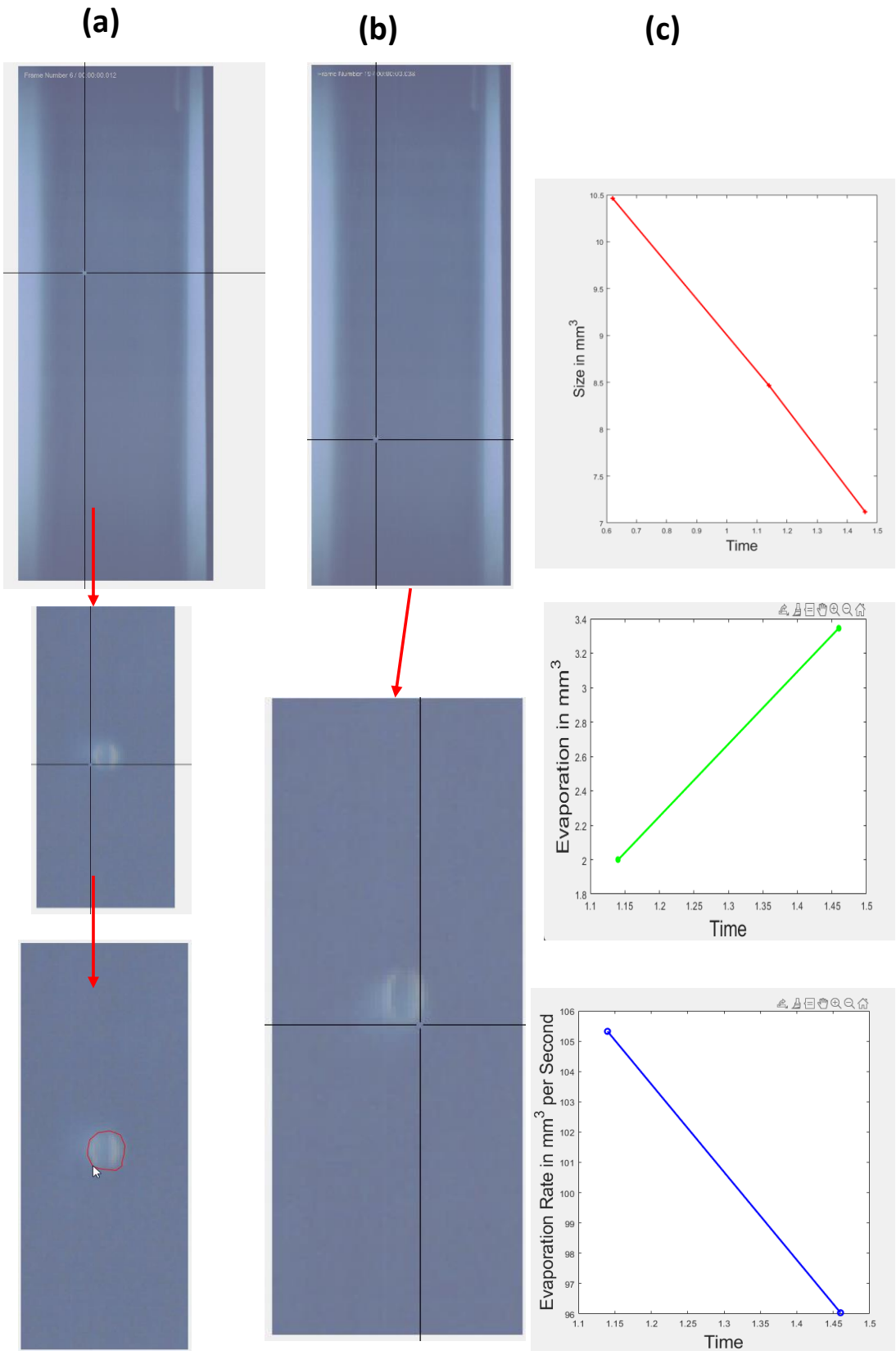

Figure (3- 22) Image Process by Using MATLAB (a) Droplet at Location. 1, (b) Droplet at Lactation 2, (c) Program Results.

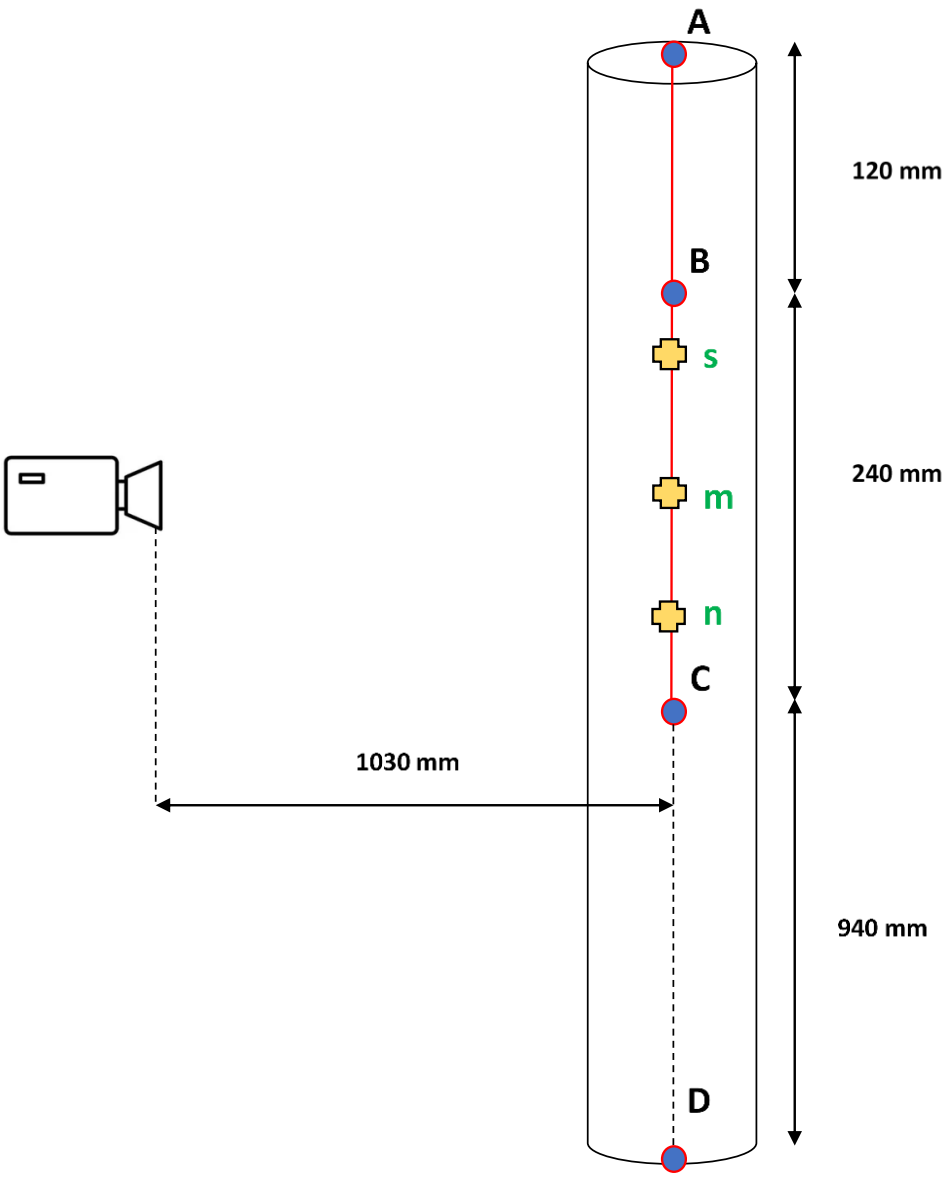

Figure (3-23) Location of Droplet in Evaporation Chamber.

3.5.2 Evaporation characteristics

1- Evaporation Rate

Through the MATLAB program, the volume and diameter of the droplet were calculated at different times. So the droplet evaporation rate can be calculated through the following relationship:

$$\dot{m} = \frac{\rho_l \Delta v}{\Delta t} \quad \text{where} \qquad (3.5)$$

$$\Delta v = v_1 - v_2 \,, \quad \Delta t = t_2 - t_1 \quad , \rho_l = liquid\ density$$

2- Evaporation Constant

The evaporation constant is a parameter that describes the rate of evaporation of a liquid into the surrounding environment. It is often represented by the symbol K and has units of (mm^2/s). The evaporation constant depends on various factors such as the properties of the liquid, the temperature and humidity of the surrounding environment, and the flow conditions around the droplet. Here are the general steps for the experimental determination of the evaporation constant:

1- calculate the initial droplet diameter D_0

2- measured the change in diameter over the time by using MATLAB image process.

3- Fitting the data: Plot $\frac{D^2}{D_\circ{}^2}$ versus $\frac{t}{D_\circ{}^2}$ and fit a curve with liner equation. The slope of the curve will be the negative and equals of the evaporation constant (K). Ochowiak et al. [83] found the evaporation rate constant by using D^2-Law as following:

$$\frac{D^2}{D_0^2} = -K\left(\frac{t}{D_0^2}\right) + 1 \tag{3.6}$$

$$\frac{p_{sat}}{p_{(=1atm)}} = exp[-\frac{h_{fg}}{(R_\circ/MW_L)}\left(\frac{1}{T} - \frac{1}{T_{boil}}\right)] \tag{3.7}$$

$$X_L = P_{sat}$$

$$y_{l,i} = X_L \frac{MW_L}{MW_{mix}} \tag{3.8}$$

$$MW_{mix} = X_L.MW_L + (1 - X_L)MW_{air} \tag{3.9}$$

$$B_{y_{L,i}} = \frac{Y_{A,i} - Y_{A,\infty}}{1 - Y_{A,i}} \tag{3.10}$$

Turns [84] explained the evaporation constant as following:

$$K = \frac{8\rho_{air} D_{AB}}{\rho_L} \ln(1 + B_{y_{L,i}}) \quad (3.11)$$

$$\rho_{air} = \frac{p}{RT} \quad (3.12)$$

D_{AB}: diffusion coefficient(m^2/s).

h_{fg}: heat of vaporization(J/kg)

$R_\circ$: universal gas constant (J/kmol. K)

X: Mole fraction.

MW: Molecular weight(kg/kmol).

B_Y: Dimensionless transfer number or Splading number.

R: specific gas constant (J/kmol.K).

T: Temperature (K)

$Y_{A,\infty}$: mass fraction of A in the free stream flow.

$Y_{A,i}$: interface mass fraction.

Example to calculate value of K

T= 273+25= 298 K

$T_{boil} = 273 + 56.08 = 329.08\ K$

$$\frac{p_{sat}}{p(=1atm)} = exp\left[-\frac{534000}{8314/58}\left(\frac{1}{298} - \frac{1}{329.08}\right)\right]$$

$p_{sat} = \exp[-1.18] = 0.307$

$X_L = 0.307$

$MW_{mix} = 0.307 * 58 + (1 - 0.307) * 28.82$

$= 37.77826$

$$y_{L,i} = 0.307 * \frac{58}{37.77826} = 0.4713$$

$$B_{y_{L,i}} = \frac{0.4713}{1 - 0.4713} = 0.891$$

$\rho_{air} = \frac{101325}{288*273} = 1.18$ kg/m^3

$K = \frac{8*1.18*1.32*10\text{^}-5}{782} \ln(1 + 0.891)$=0.101mm^2/s

3- Droplet Lifetime

Droplet lifetime refers to the duration of time during which a liquid droplet remains suspended in the air until it is completely evaporated. This depends on various factors such as the size of the droplet, the ambient temperature and humidity, and the velocity of the surrounding air. The lifetime of the droplet is calculated using the following equation:

$$t_d = \frac{D_\circ^{\,2}}{K} \quad (3.13)$$

Where $D_\circ$ =is the initial diameter of droplet.

$K = evaporation\ constant$

3.6 Uncertanty analysis

Uncertainty analysis is a process that involves quantifying and analyzing the uncertainties associated with the results of scientific measurements. In any scientific experiment, there are always inherent uncertainties due to various sources of error, such as measurement errors, model assumptions, or data variability. The standard uncertainty (Su) can be calculated by equation detailed by Bell [85] as:

$$Su = \frac{S.D}{\sqrt{N}} \quad (3.14)$$

$$S.D = \sqrt{\frac{\sum_{i=1}^{N}(X_i - X_{average})^2}{(N-1)}} \quad (3.15)$$

$$X_{average} = \frac{1}{N}\sum_{i=1}^{N} X_i \ \ldots\ldots \quad (3.16)$$

$$X_{average} = \frac{2.816 + 2.863 + 2.863 + 2.823 + 2.829 + 2.840 + 2.826 + 2.836 + 2.818 + 2.817}{10}$$

$X_{average} = 2.8331$

$\sum_{i=1}^{N}(X_i - X_{average})^2 = (2.816 - 2.8331)^2 + (2.863 - 2.8331)^2 + (2.863 - 2.8331)^2 + (2.823 - 2.8331)^2 + (2.829 - 2.8331)^2 + (2.840 - 2.8331)^2 + (2.826 - 2.8331)^2 + (2.836 - 2.8331)^2 + (2.818 - 2.8331)^2 + (2.817 - 2.8331)^2 = 0.00279$

$$S.D = \sqrt{\frac{0.00279}{(9)}} = 0.01762$$

$$Su = \frac{0.01762}{\sqrt{10}} = 0.00557$$

Where N is the total number of measurements, Where X_i is represented the values for measurements data.

The main reasons of causing error encountered in the data analysis process are the uncertainty of droplet diameter. The Dia et al. [36] explained the error analysis way was used in this study.

If a physical backward value R is expressed as:

$$R = R(X1, X2, \ldots, Xn) \quad (3.17)$$

The relative uncertainty of R is

$$\frac{\Delta R}{R} = \left[\left(\frac{\partial R}{\partial X_1}\frac{\Delta X_1}{X_1}\right)^2 + \left(\frac{\partial R}{\partial X_2}\frac{\Delta X_2}{X_2}\right)^2 + \ldots + \left(\frac{\partial R}{\partial Xn}\frac{\Delta X_n}{Xn}\right)^2\right]^{0.5} \quad (3.18)$$

In this experiment, the droplet volume is measured by using image process in MATLAB after assuming that the droplets are spherical. The droplet diameter found by using equation (3.4). The standard uncertainty of the droplet diameter measurement found by repeated the experiment 10 times with same conditions and then found (Su) for diameter as explained in Table (3-4). The uncertainty propagation for evaporation rate and droplet lifetime found by using equation (3.12) calculated by using EES software as explained in Figure (3-24).

Table (3- 4) Stander Uncertainty for Diameter Measurement.

Fuel type	Uncertainty of diameter measurements (mm)
Water	0.00501
Kerosene	0.00557
Gasoline	0.00542
Ethanol	0.00582
Acetone	0.00623

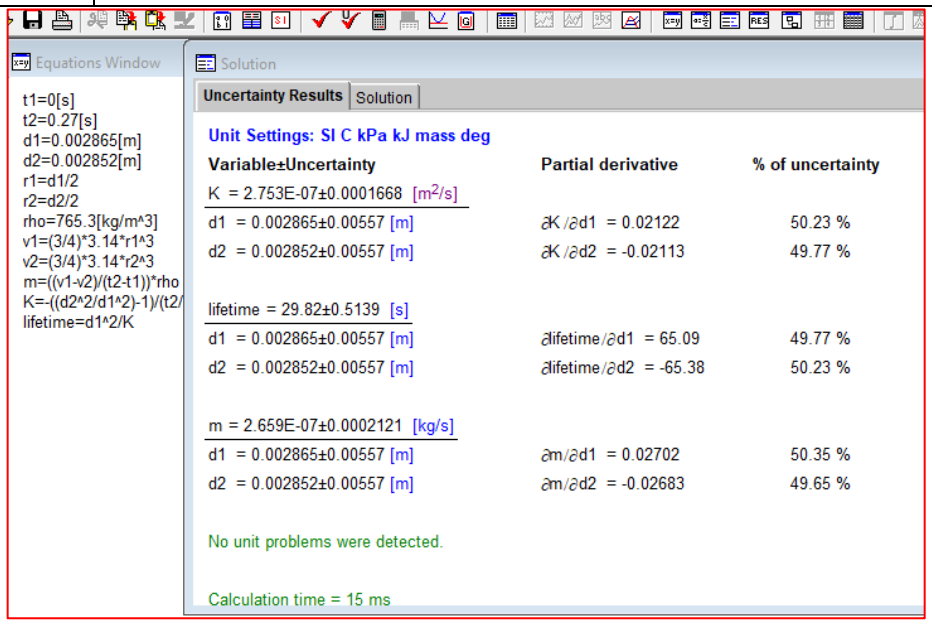

Figure (3-24) Uncertainty Analysis by Using EES Software.

CHAPTER FOUR

RESULTS AND DISCUSSIONS

Chapter Four: Results and Discussion

4.1. Introduction

In this chapter, the experimental results of different types of liquid will be presented and discussed. The effect of temperature and fuel type on evaporation rate and evaporation constant as well as lifetime will be discussed.

4.2. Repeatability test

In order to confirm the practical results, the experiment was repeated for three times at different dates for the evaporation of liquid water droplet.

After analyzing these experiment results and calculating the rate of evaporation of this droplet. The results showed that there was an error in the rate of evaporation of the droplet ranging from (1%- 4%) at 25 ^{o}C and (8%-12%) at 95 ^{o}C as shown in Figure (4-1), which are acceptable.

$$\text{Error percentage} = \frac{\max value - \min value}{\max value} \quad (4.1)$$

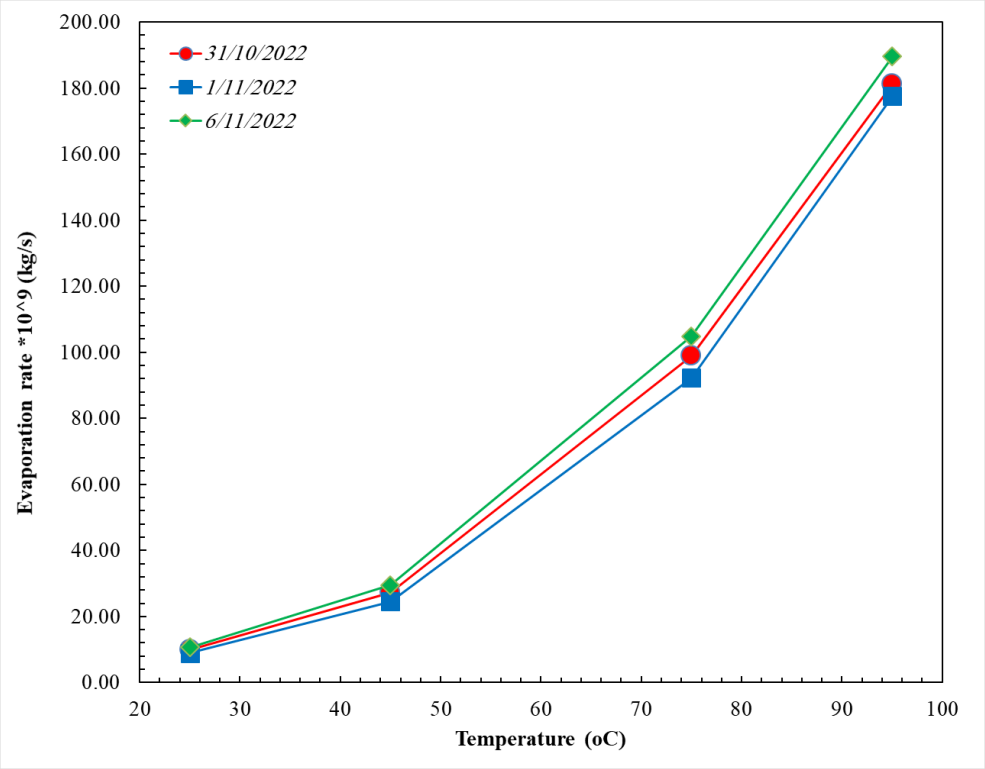

Figure (4- 1) Variation of The Evaporation Rate with Temperature (Repeatability Test)

4.3. Droplet evaporation test results

The data obtained from the present set of experiments provides suitable condition to explore droplet evaporation when raising the temperature for different types of liquid .The most important variables that occurred from droplet evaporation were calculated, which are the variation in droplet diameter, the evaporate rate, evaporation constant and droplet lifetimes.

4.3.1. Droplet diameter results

4.3.1.1 Effect of temperature on droplet diameter.

The variation of droplet diameter with time is due to the evaporation process as the droplet falls in the chamber. When a liquid droplet is released into the air, it immediately begins to evaporates, as the liquid vaporizes and diffuses into the surrounding air.

Figure (4-2) shows the decrease in the droplet diameter of the liquids with time after injection in to the evaporation chamber. The initial droplet diameter for the different liquids, acetone, ethanol, gasoline, kerosene and water are 2.82,2.807,2.58,2.44 and 2.12 mm respectively.

The difference in initial diameter is due to the difference in liquid densities and viscosities. The liquid collects at the end of the injector needle, and when its mass reaches a force higher than the adhesion force of this liquid to metal, the droplet falls free fall due to gravity. The large liquid density leads to a low mass droplet, while a high liquid viscosity leads to a large droplet mass. These liquids that were used in the experiment decreased in droplet diameter after being injected with 0.27 sec in to the evaporation chamber at a temperature 25°C, as shown in Table (4-1) below.

Table (4-1) Shows The Decrease in Diameter After 0.27 sec at 25°C of Droplet Liquids Injection.

Liquid substance	Initial diameter in (mm)	Diameter after injection by 0.27 sec in (mm)
Acetone	**2.82**	**2.815**
Ethanol	**2.807**	**2.8059**
Gasoline	**2.58**	**2.5789**
Kerosene	**2.44**	**2.4397**
Water	**2.12**	**2.1196**

This difference in the decreasing diameter of each liquids droplet is due to the difference in the initial diameter and the evaporation rate of each liquid under the same condition.

The decrease in droplet diameter continues as time progresses, so at 0.5625 sec the diameter becomes as shown in the Table(4-2).

Table(4-2) Shows The Decrease in Diameter After 0.5625 sec at 25°C of Droplet Liquids Injection.

Liquid substance	Initial diameter in (mm)	Diameter after injection by 0.5625
Acetone	2.82	2.809
Ethanol	2.807	2.8048
Gasoline	2.58	2.5778
Kerosene	2.44	2.4395
Water	2.12	2.1193

This decrease in droplet diameter increases with increasing temperatures. When the temperature of the evaporation chamber is raised to 45°C , the diameter becomes as shown in Table (4-3).

Table (4-3) Shows The Decrease in Diameter After 0.27 sec and 0.5625 sec at 45°C of Droplet Liquids Injection.

Liquid substance	Initial diameter in (mm)	Diameter after injection by 0.27	Diameter after injection by 0.5625
Acetone	2.82	2.806	2.792
Ethanol	2.807	2.8038	2.8004
Gasoline	2.58	2.5774	2.5746
Kerosene	2.44	2.4393	2.4385
Water	2.12	2.1189	2.1174

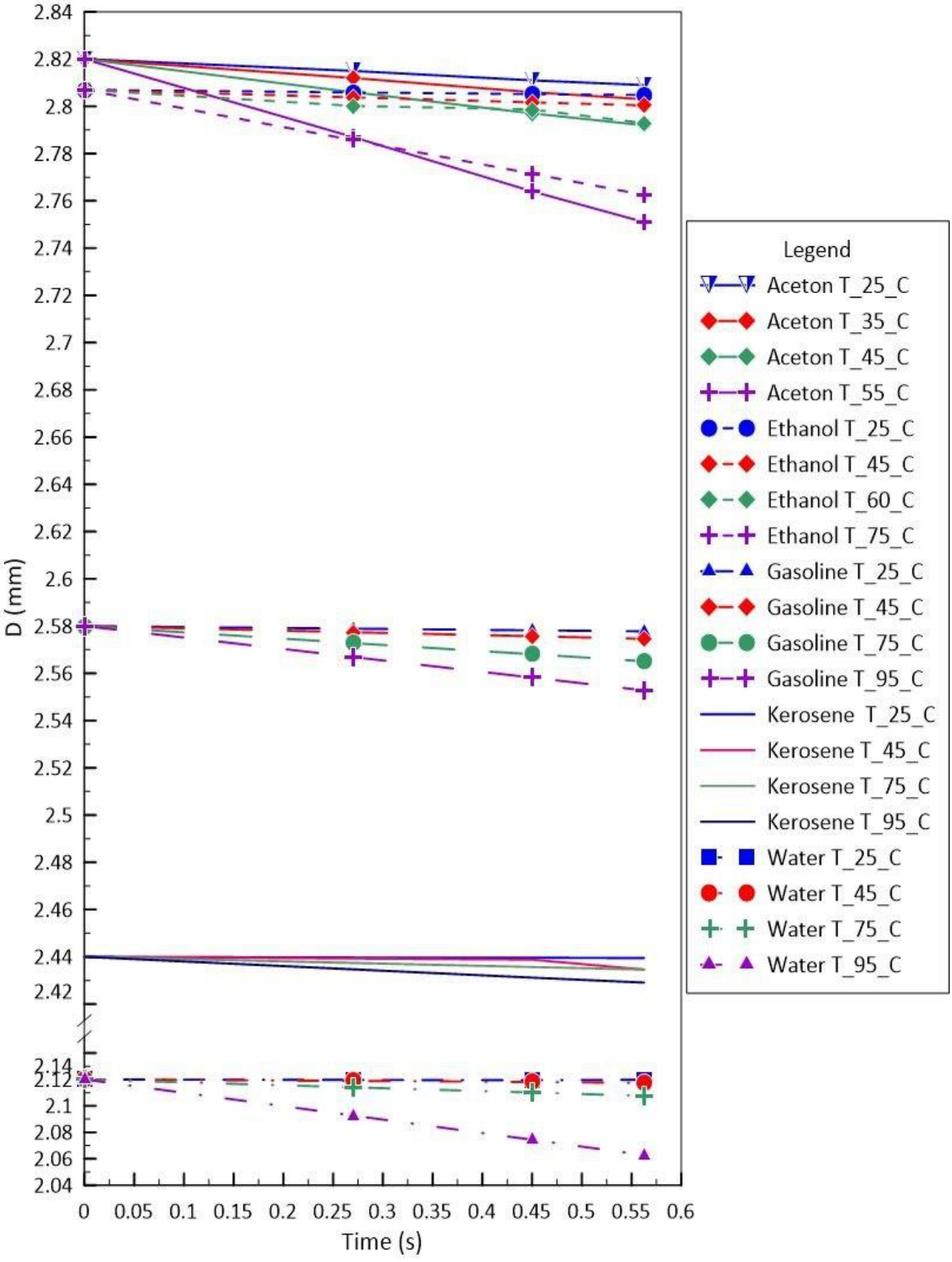

Figure (4- 2)Variation of Droplet Diameter of Liquids with Time

Figures (4-3),(4-4),(4-5) ,(4-6) and (4-7) show the variation of droplet diameter due to evaporation with chamber temperature for acetone, ethanol, gasoline, water, and kerosene respectively with time of the injection. All Figures show the same trend where the droplet diameter decreases with increasing the chamber temperature. As the temperature increases and approaching the boiling temperature of the specific liquid the rate of diameter decreases rises due to high rate of evaporation as will be seen later.

The initial droplet diameter of acetone is 2.82 mm and decreases by 0.39% at temperature 25°C during 0.5625 sec. While, when the temperature of the evaporation chamber is raised to 55°C and during the same period of time, which is close to its boiling point, the percentage of decrease increases to 2.446%.

The gasoline droplet decreases by 0.084% from the initial diameter, which is 2.58 mm, when the temperature of the evaporation chamber is 25°C, and within 0.5625 sec, while raising the chamber temperature to 95°C, the percentage of decrease increase to 1.053%.

Likewise, a droplet of ethanol with an initial diameter of 2.807 mm decreases by 0.077% when the evaporation chamber temperature is 25°C after 0.5625 sec the droplet into the chamber, which raising the evaporation chamber to 75°C the percentage of decrease increases to 1.583%.

During the same period of time used (0.5625 sec), the water droplet was tested at 25°C and decreased by 0.031%. In the case of raising the temperature of evaporation chamber to 95°C , the percentage increased to 2.695%.

Kerosene decreases its droplet under the same experimental condition (25°C, 0.5625 sec) by 0.018% and when changing the temperature only to 95°C, the percentage of decrease increases slightly and becomes 0.446%.

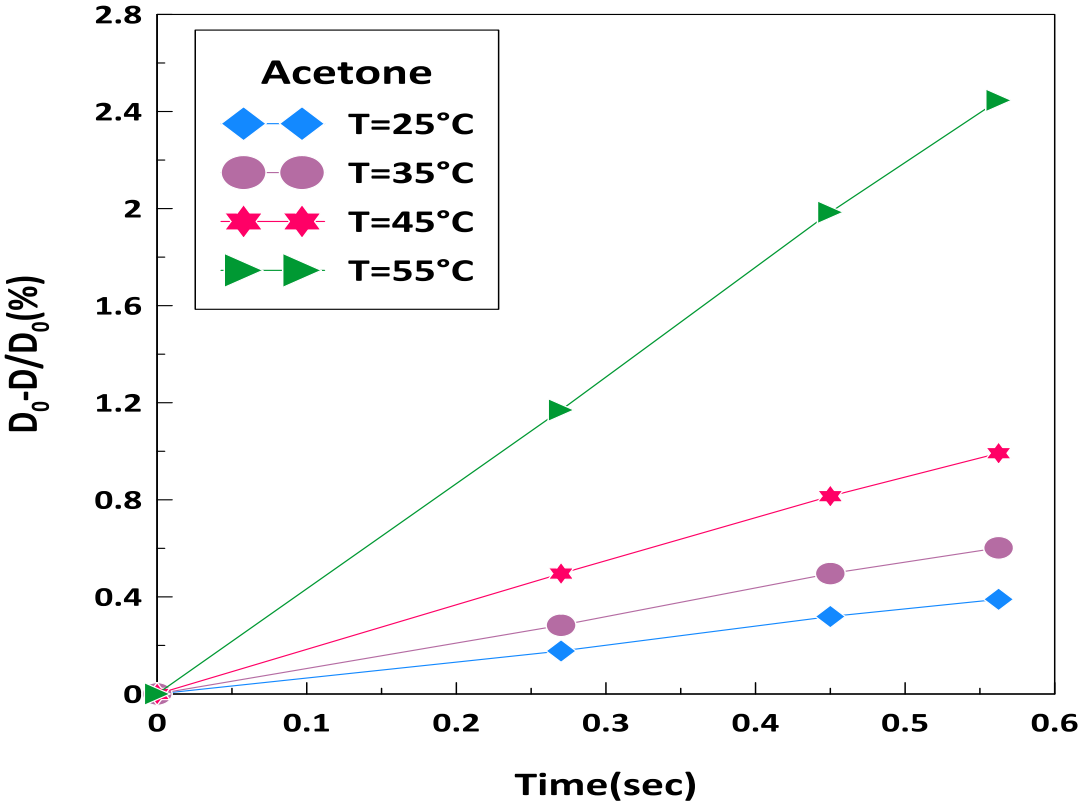

Figure (4- 3)The Percentage Decrease in Diameter in A Droplet of Acetone with Time

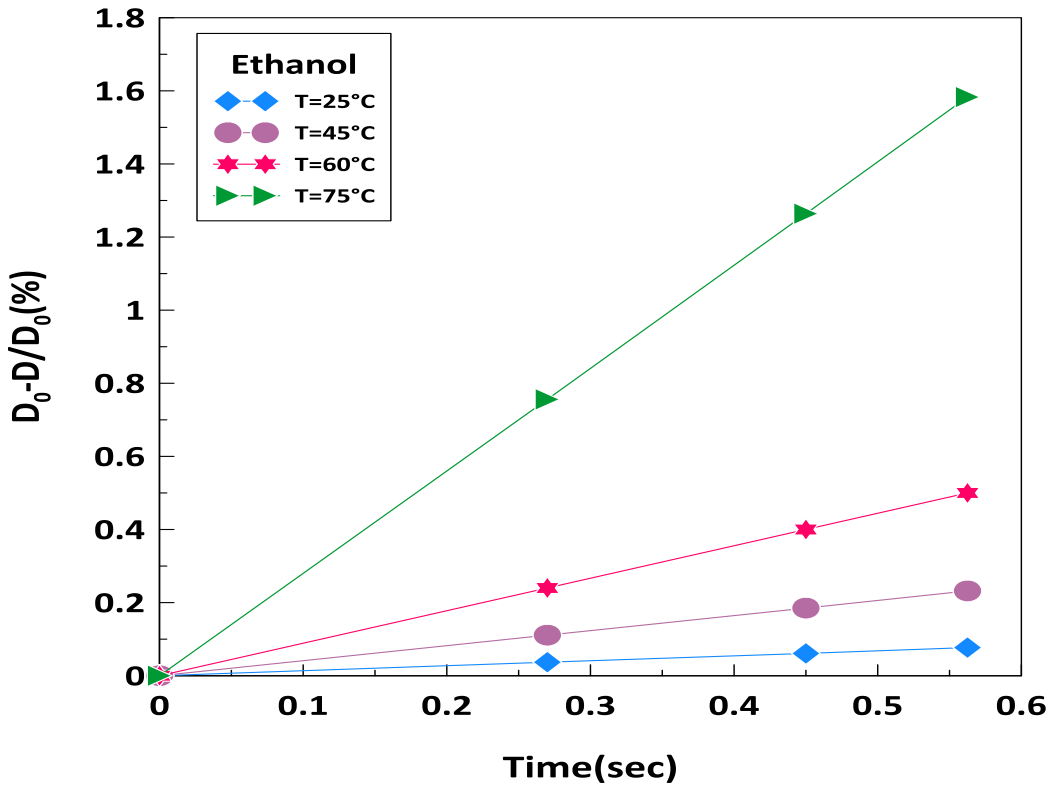

Figure (4- 4) The Percentage Decrease in Diameter in A Droplet of Ethanol with Time

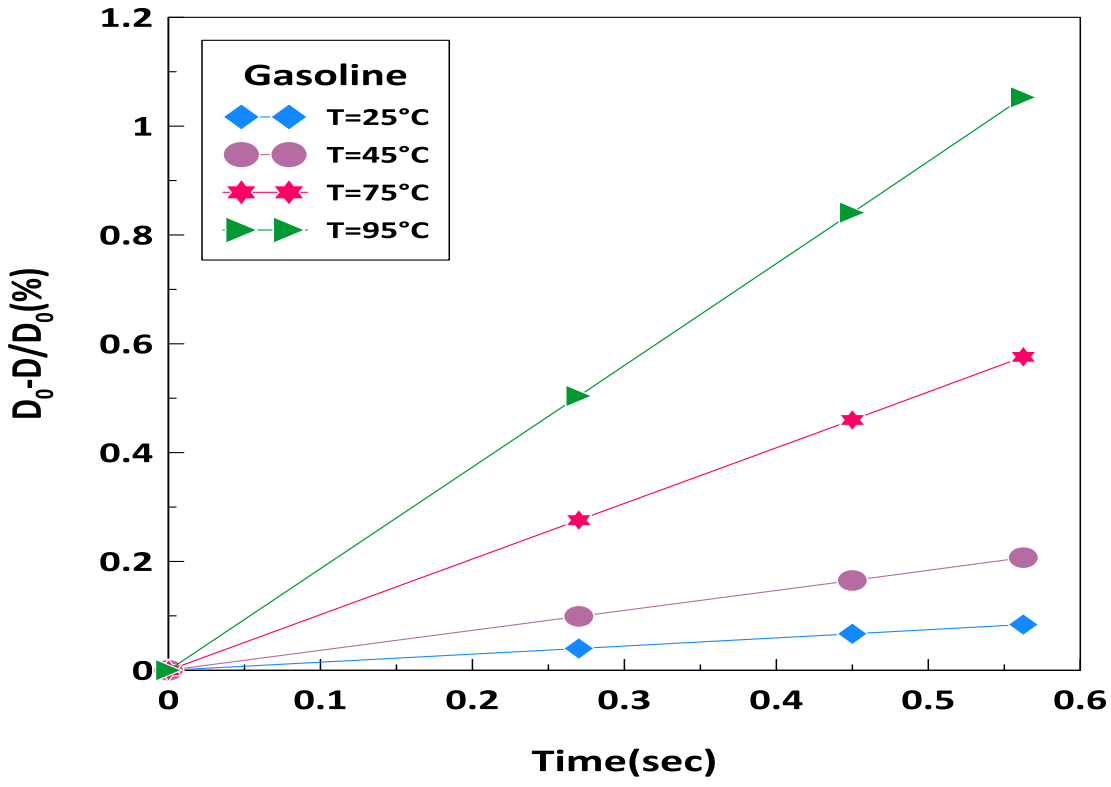

Figure (4- 5) The Percentage Decrease in Diameter in A Droplet of Gasoline with Time

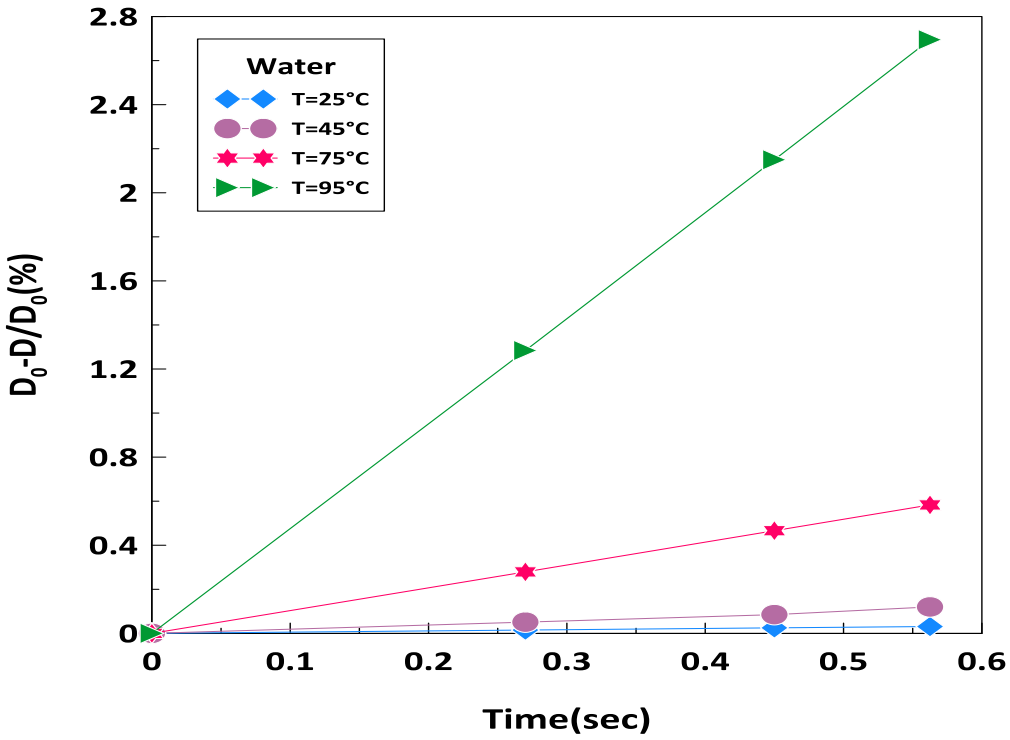

Figure (4- 6) The Percentage Decrease in Aiameter in Adroplet of Water with Time

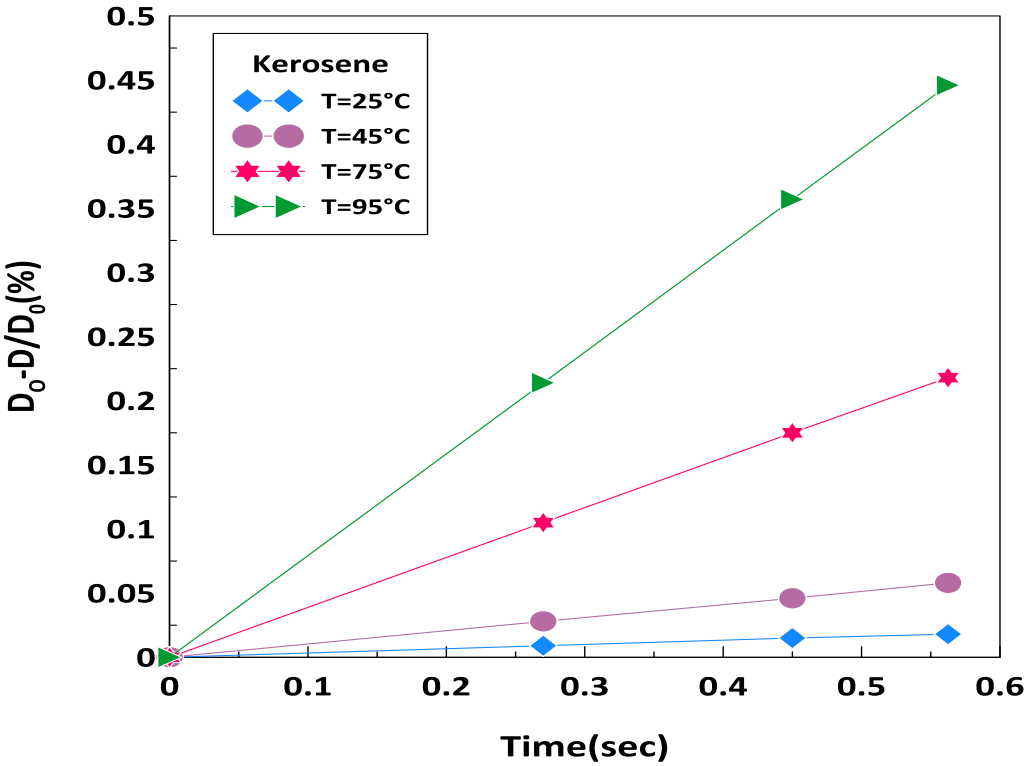

Figure (4- 7) The Percentage Decrease in Diameter in A droplet of Kerosene with Time

4.3.1.2 Effect of liquid type on droplet diameter.

In the Figures (4-8), (4-9), (4-10),(4-11),(4-12),(4-13), (4-14), (4-15), (4-16), (4-17),(4-18), and (4-19) show the percentage decrease of droplet diameter for the different liquids at different chamber temperatures and different times after injection. The percentage decrease of diameter is expressed as $(\frac{D_\circ - D}{D_\circ} * 100\%)$.

At a temperature of 25°C, the highest percentage of decrease in droplet diameter is acetone, gasoline, ethanol, water, and Kerosene, respectively, the percentage of decreasing droplet diameter of these liquid after 0.27 sec of injection 0.177% , 0.04% , 0.037%, 0.015% and 0.009% respectivly.

The percentage of droplet diameter decrease after 0.45sec injections inside the evaporation chamber also increases and takes the same behavior is show as at 0.27 sec, where the decrease percentage is 0.319% , 0.067%, 0.061% , 0.025% and 0.015%, respectively .

Likewise, at a time of 0.5625 sec, the percentage becomes 0.39%, 0.084%, 0.077% , 0.031%, and 0.018%, respectively

This difference in percentage of decreasing diameter between droplet liquids is due to the difference in the initial droplet diameter, as well as the difference in the evaporation rate of the liquid under these conditions. As for at a temperature of 45°C, the percentage of decreasing in acetone remains the highest of all time, while for ethanol, the percentage of decrease is higher than that of gasoline , unlike what was at 25°C, when gasoline was higher because the evaporation rate of gasoline was faster than of ethanol at 25°C. With regard to water and kerosene, the percentage of decrease in the diameter of the droplet increased, but the percentage of decrease of water is higher than of kerosene , although the diameter of the water droplet is smaller than the diameter of kerosene droplet, and this is

due to the fact that the evaporation of water is faster than that of kerosene and as shown in Table (4-4) below.

Table (4-4) Show The Percentage Decrease in Diameter After 0.27 sec,0.45 sec, and 0.5625 sec at 45°C of Droplet Liquids Injection.

Liquid substance	Decrease percentage in 0.27 sec	Decrease percentage in 0.45 sec	Decrease percentage in 0.5625 sec
Acetone	0.283%	0.496%	0.602%
Ethanol	0.111%	0.185%	0.232%
Gasoline	0.099%	0.165%	0.207%
Water	0.051%	0.085%	0.12%
Kerosene	0.028%	0.046%	0.058%

When the temperature of the evaporation chamber is raised to 75°C, the acetone disappears due to the rapid evaporation of its droplet while it is suspended in the needle. At this temperature, the decrease in droplet diameter of water is higher than the decrease in droplet diameter of gasoline, different from the previous temperatures, and as shown in Table (4-5) below.

This is due to the fact that the process of water evaporation is faster than the evaporation of gasoline at this temperature.

Table (4-5) Show The Percentage Decrease in Diameter After 0.27 sec,0.45 sec, and 0.5625 sec at 75°C of Droplet Liquids Injection.

Liquid substance	Decrease percentage in 0.27 sec	Decrease percentage in 0.45 sec	Decrease percentage in 0.5625 sec
Ethanol	0.756%	1.264%	1.583%
Gasoline	0.279%	0.466%	0.583%
Water	0.276%	0.46%	0.576%
Kerosene	0.105%	0.175%	0.218%

Also, when the temperature of the evaporation chamber is raised to 95°C, the percentage of diameter decrease, and ethanol disappears, in order to exceed its boiling point, which is 78.2°C, as shown in Table (4-6) below.

Table (4-6) Show The Percentage Decrease in Diameter After 0.27 sec,0.45 sec, and 0.5625 sec at 95°C of Droplet Liquids Injection.

Liquid substance	Decrease percentage in 0.27 sec	Decrease percentage in 0.45 sec	Decrease percentage in 0.5625 sec
Water	1.284%	2.15%	2.695%
Gasoline	0.504%	0.841%	1.053%
Kerosene	0.214%	0.357%	0.446%

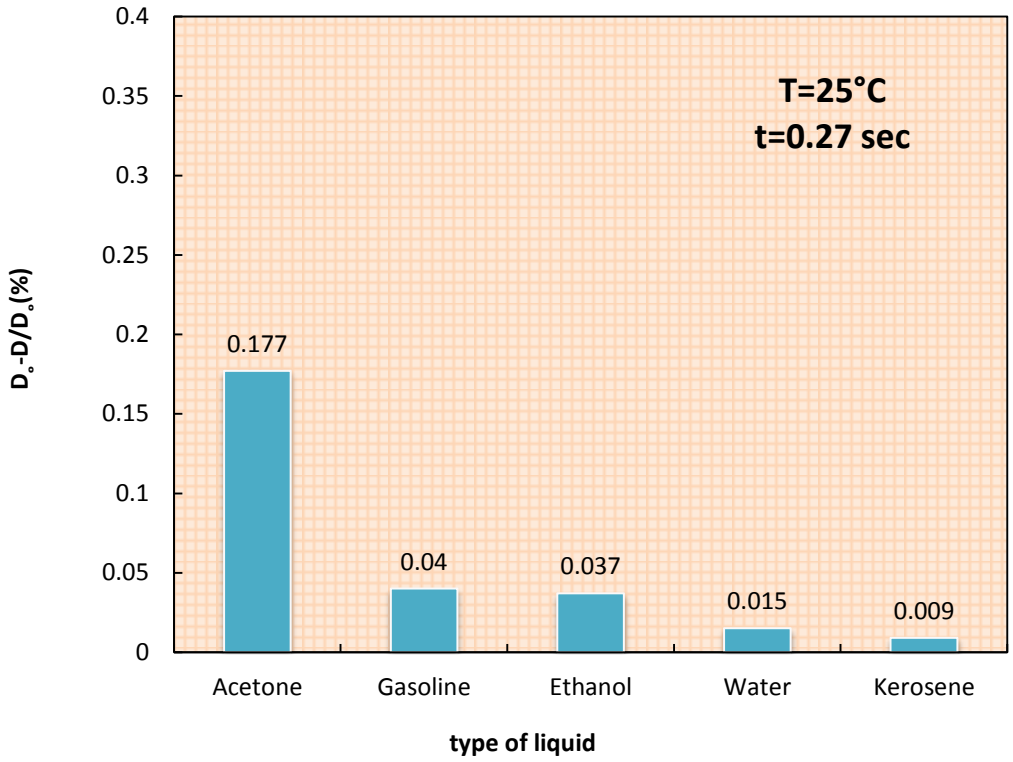

Figure (4- 8) Percentage Variation in Droplet Diameter for Different Liquids at T=25°C, t=0.27sec

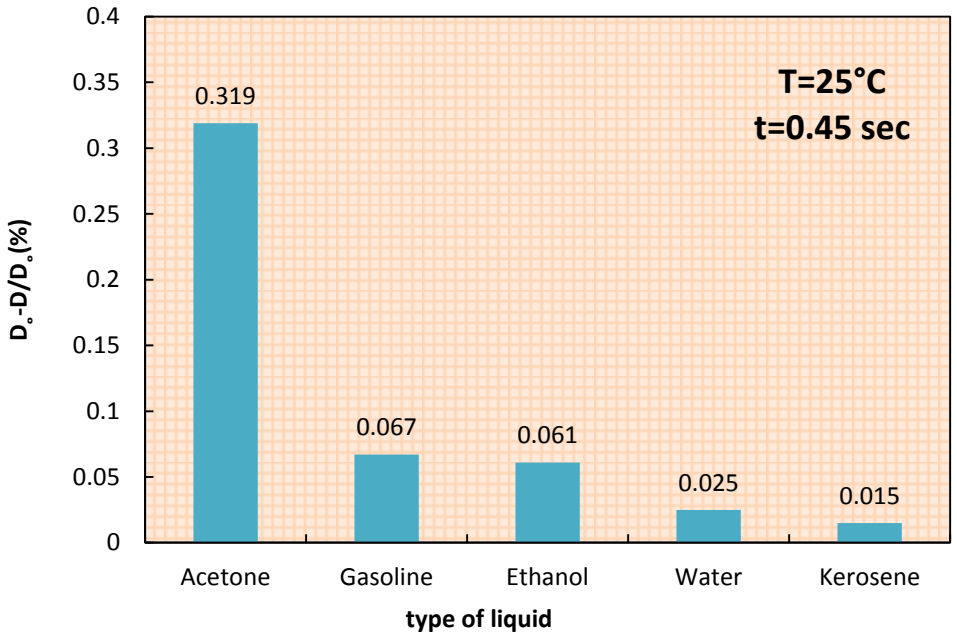

Figure (4- 9) Percentage Variation in Droplet Diameter for Different Liquids at T= 25°C, t= 0.45 sec

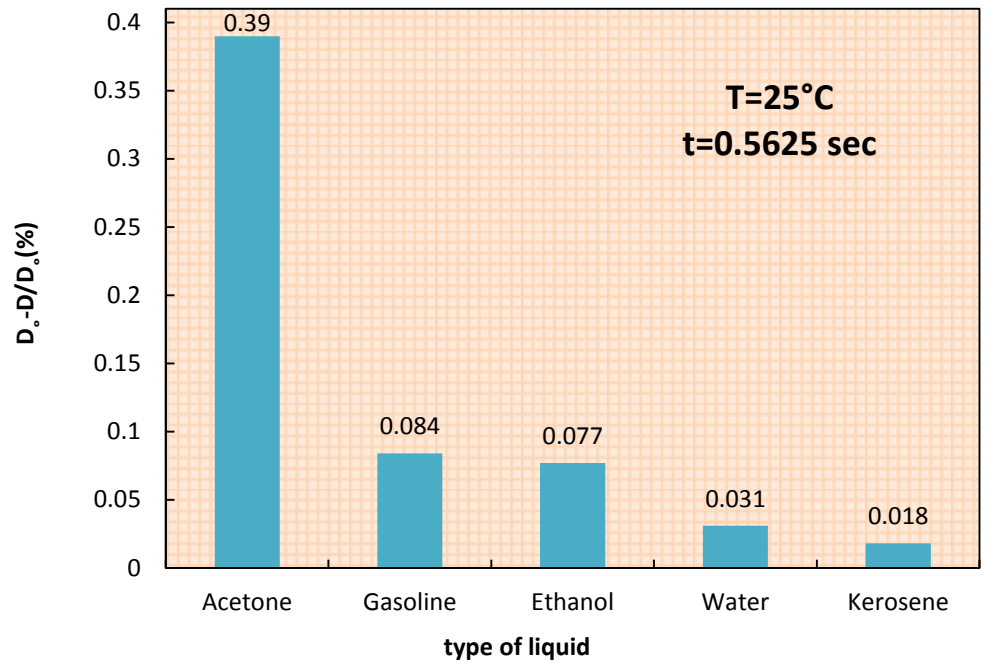

Figure (4- 10) Percentage Variation in Droplet Diameter for Different Liquids at T= 25°C, t= 0.5625 sec

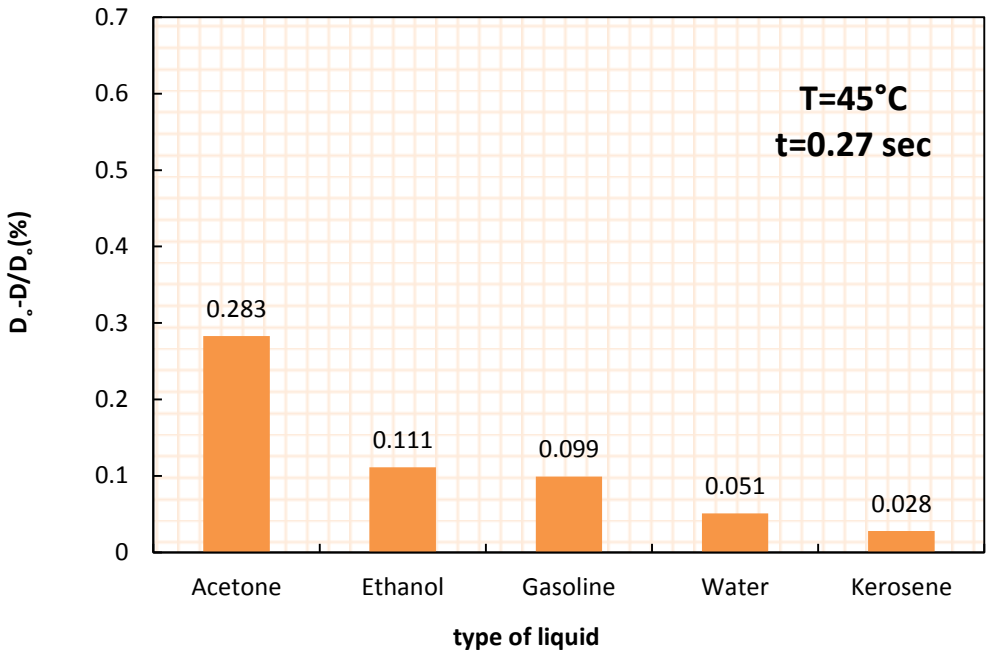

Figure (4- 11) Percentage Variation in Droplet Diameter for Different Liquids at T= 45°C , t= 0.27 sec

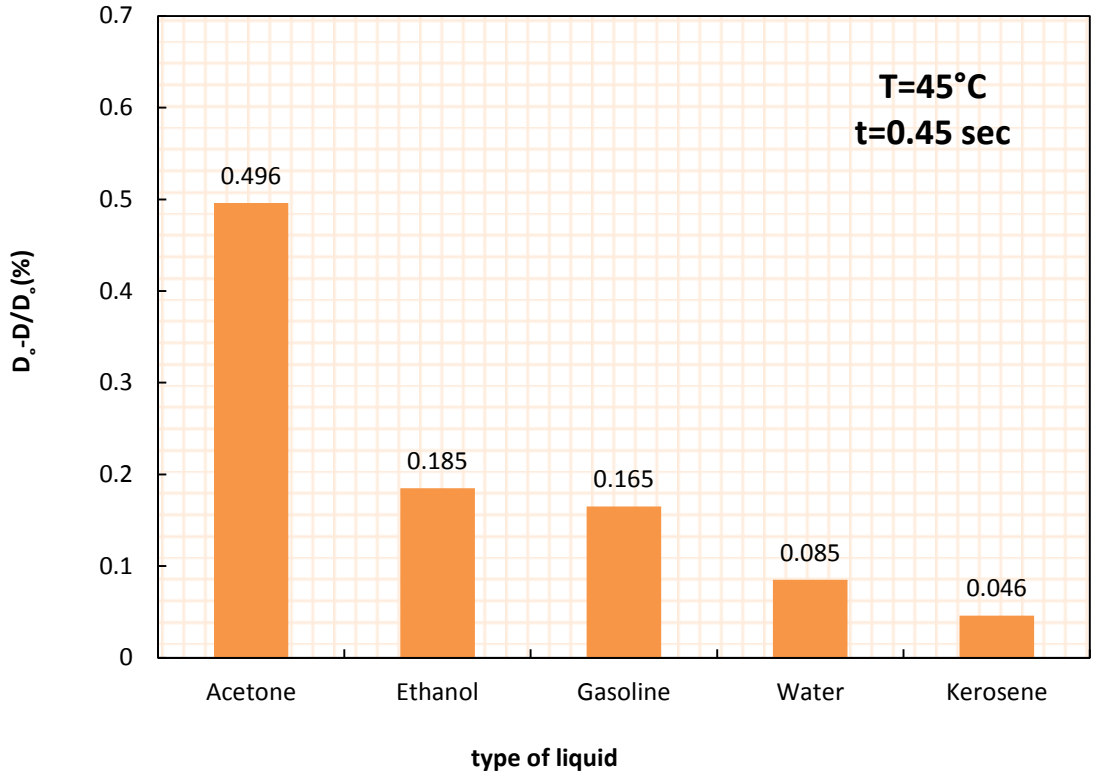

Figure (4- 12) Percentage Variation in Droplet Diameter for Different Liquids at T= 45°C, t= 0.45 sec

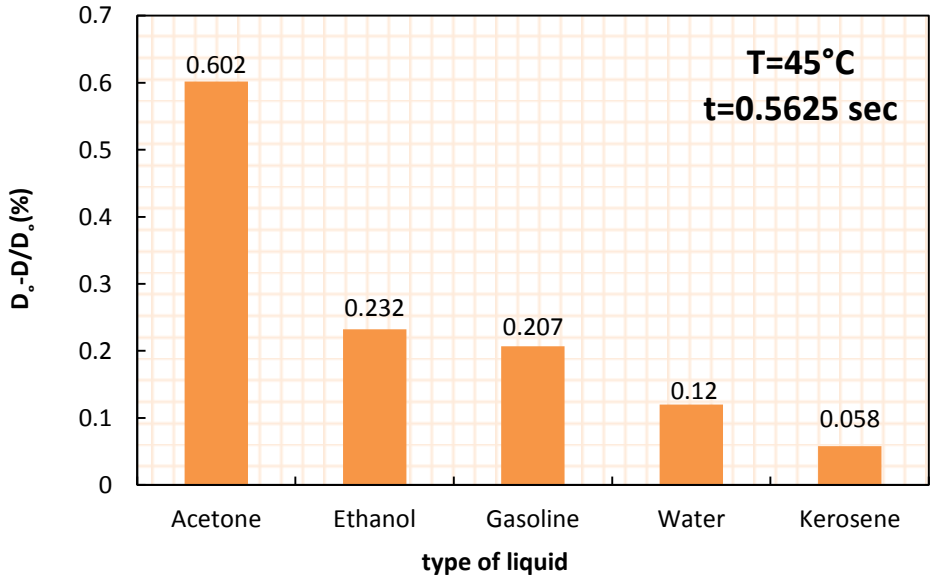

Figure (4- 13) Percentage Variation in Droplet Diameter for Different Liquids at T= 45°C , t= 0.5625 sec

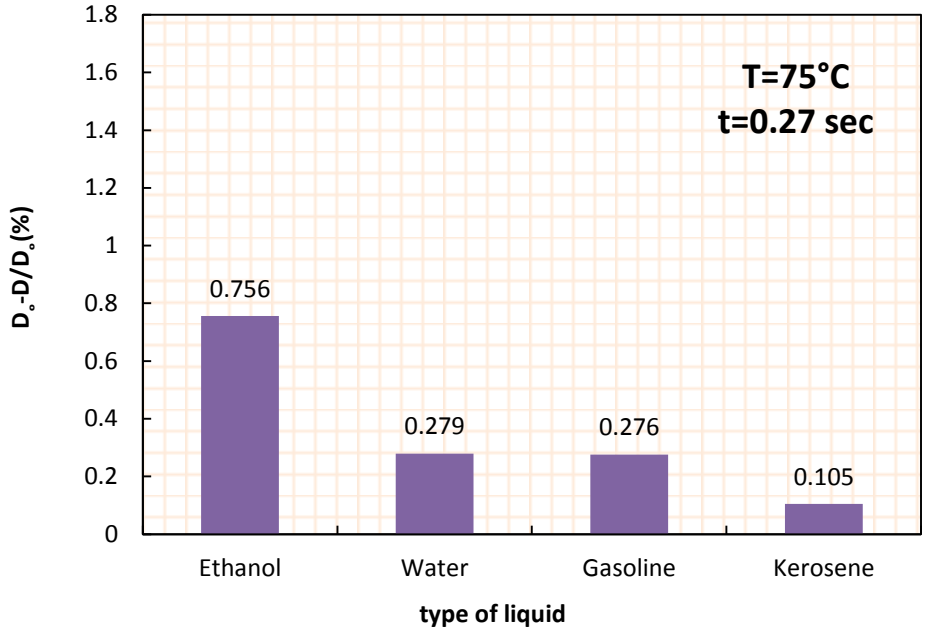

Figure (4- 14) Percentage Variation in Droplet Diameter for Different Liquids at T= 75°C , t= 0.27 sec

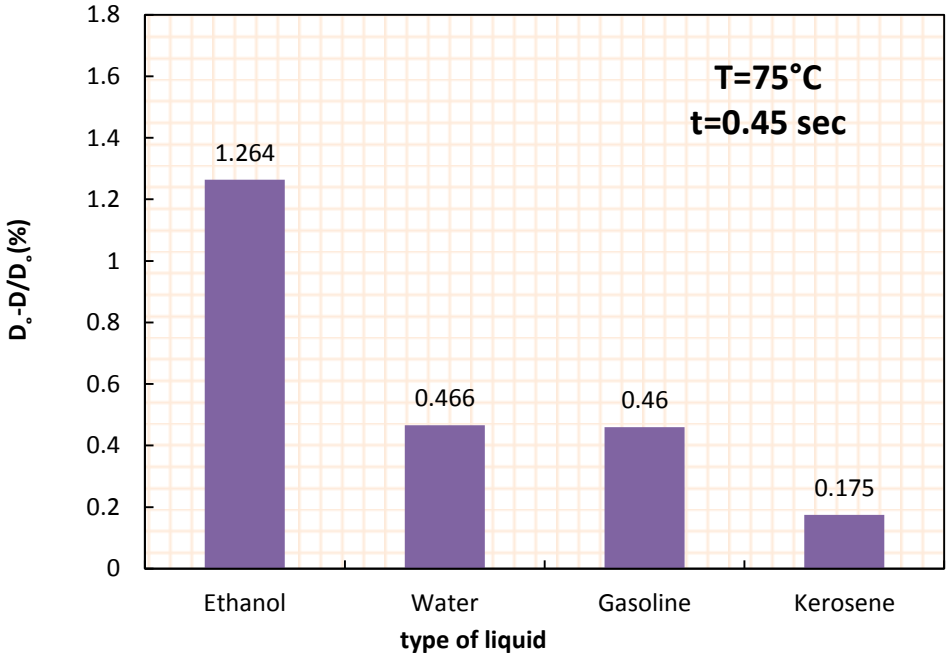

Figure (4- 15) Percentage Variation in Droplet Diameter for Different Liquids at T= 75°C , t= 0.45sec

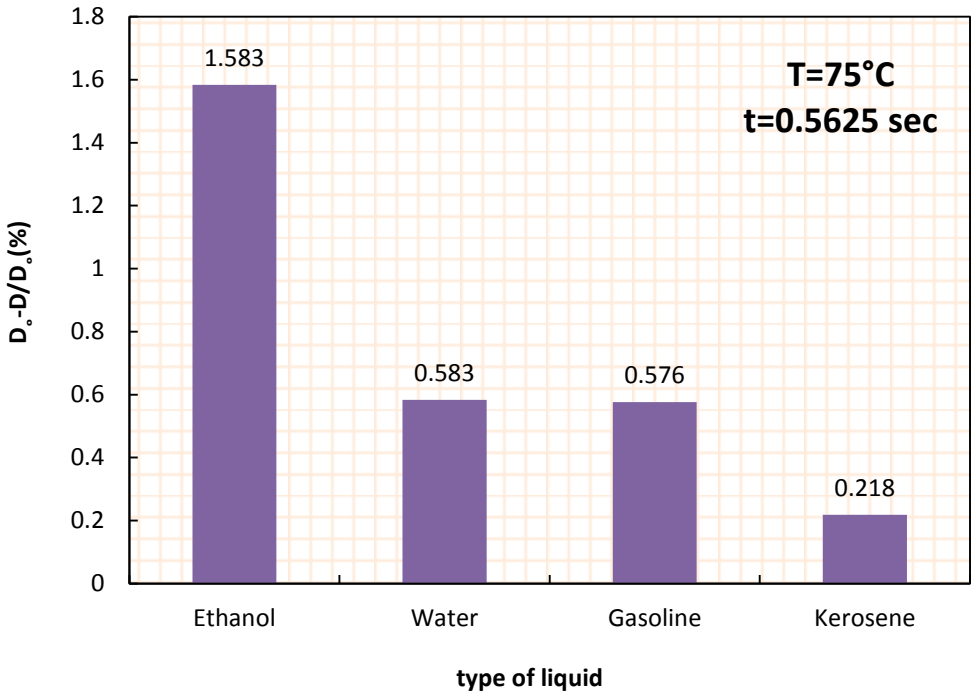

Figure (4- 16) Percentage Variation in Droplet Diameter for Different Liquids at T= 75°C , t= 0.5625 sec

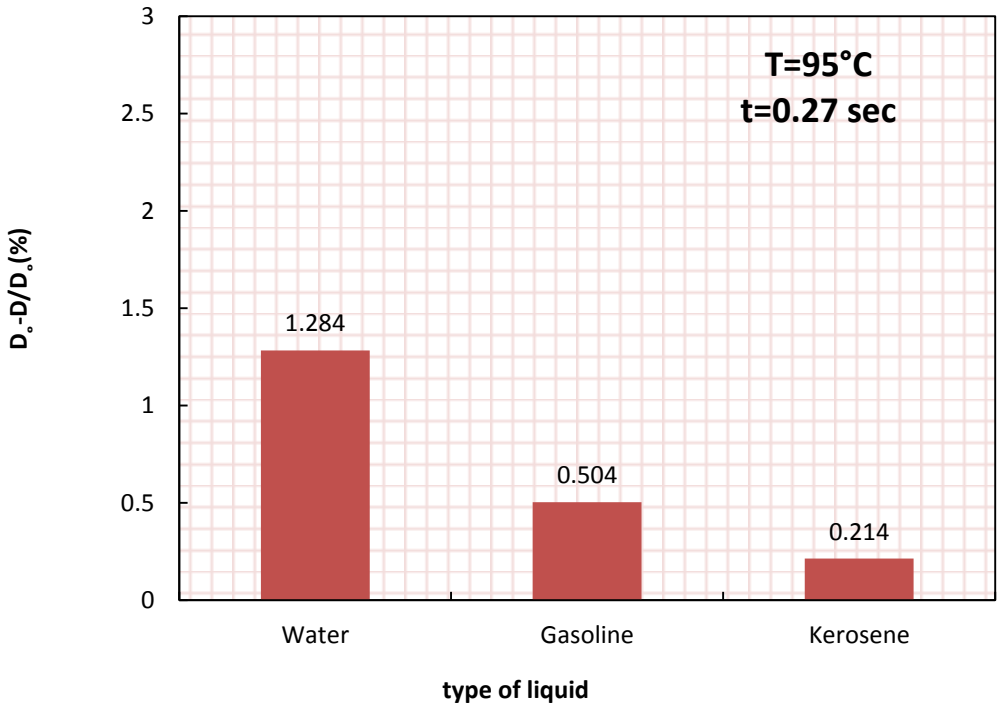

Figure (4- 17) Percentage Variation in Droplet Diameter for Different Liquids at T= 95°C , t= 0.27sec

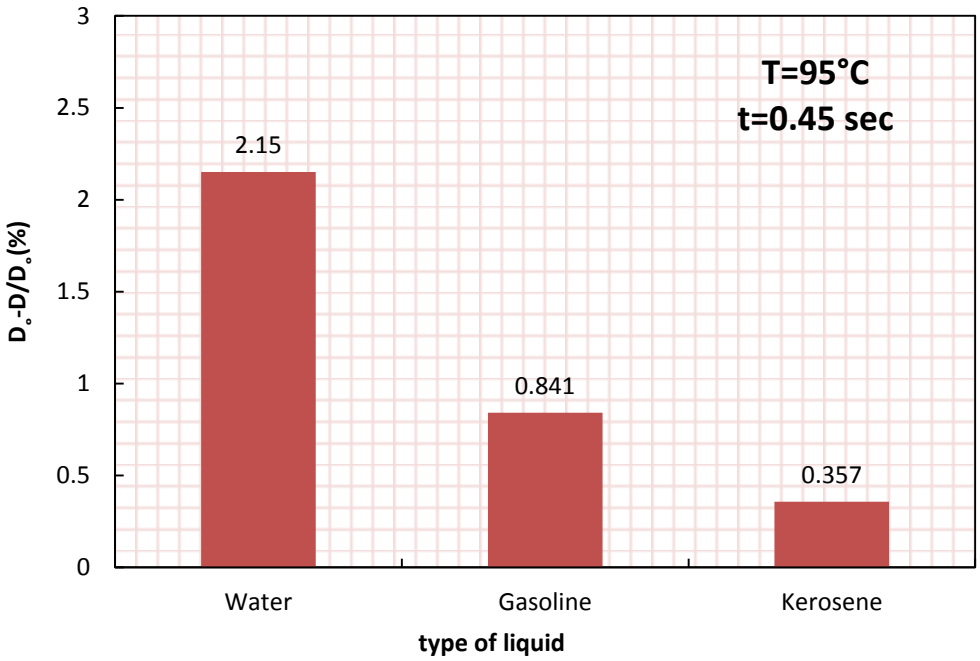

Figure (4- 18) Percentage Variation in Droplet Diameter for Different Liquids at T= 95°C , t= 0.45 sec

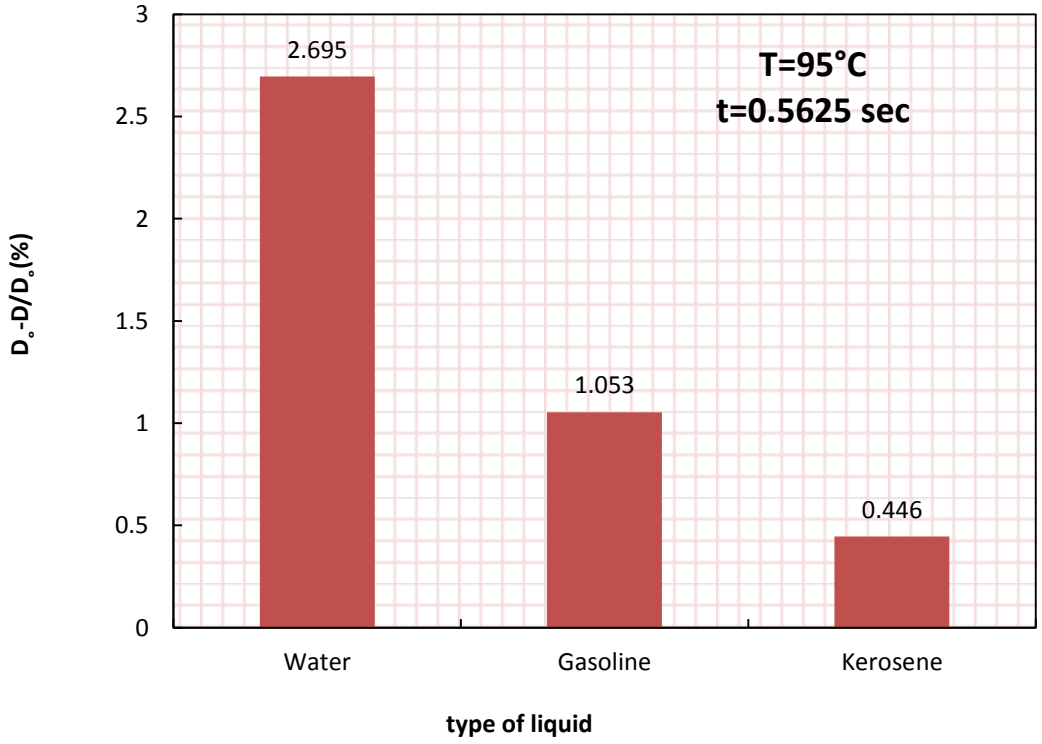

Figure (4- 19) Percentage Variation in Droplet Diameter for Different Liquids at T= 95°C , t= 0.5625 sec

4.3.2. Droplet evaporation rate results

4.3.2.1 Effect of temperature on evaporation rate

The ambient temperature can have a significant effect on the evaporation rate of a liquid. Generally, as the temperature increases, the evaporation rate of a liquid also increases. This is because at higher temperatures, the molecules of the liquid have more kinetic energy, which causes them to move faster and escape from the surface of the liquid more easily. As a result, the rate of evaporation increases. However, other factors such as humidity, air flow, and the properties of the liquid can also affect the evaporation rate. For example, at high humidity levels, the air is already saturated with water vapor, which reduces the driving force for evaporation and slows down the evaporation rate. Similarly, air flow can increase the rate of evaporation by carrying away the water vapor from the surface of the liquid, but it can also decrease the evaporation rate by reducing the amount of water vapor that accumulates above the surface of the liquid.

Figures (4-20), (4-21), (4-22), (4-23), and (4-24) show the effect of the evaporation chamber temperature on the evaporation rate of the tested liquid droplet. Acetone diagram shows that with an increase in the temperature of the evaporation chamber, the rate of evaporation increases. During the experiments, the evaporation temperature was changed to four different degrees for acetone liquid, which are 25, 35, 45, and 55^{o}C, where it can be observed that the evaporation rate rises from 190.282 $\times 10^{-9}$ kg/s to 1169.18 $\times 10^{-9}$ kg/s when the temperature increases from 25^{o}C to 55^{o}C. This is due to the fact that an increase in temperature means an increase in the kinetic energy of the molecules, and thus means that the molecules move and escape from the surface of the droplet, and thus the evaporation rate increases.

The rate of evaporation of ethanol droplet increasing with increasing in temperature of the evaporation chamber. The evaporation rate increased from 37.604×10^{-9} kg/s to 760.293×10^{-9} kg/s after increasing the temperature from 25°C to 75°C. This increase in the evaporation rate is due to the increase in the kinetic energy of the liquid molecules when the temperature is raised to a degree close to the evaporation temperature of the liquid.

Increasing the temperature of the evaporation chamber increases the rate of evaporation of the gasoline droplet, as shown in Figure. It can be seen that the rate of evaporation increased from 30.301×10^{-9} kg/s to 373.915×10^{-9}kg/s when the temperature increased from 25°C to 95°C. The evaporation rate of a gasoline fuel droplet can vary depending on several factors such as temperature, and air flow. Generally, as the temperature increases, the evaporation rate of gasoline increases as well, the evaporation rate of gasoline droplets can also be affected by the composition of gasoline itself. Gasoline is a complex mixture of hydrocarbons, and different hydrocarbons have different boiling points and rate of evaporation.

The rate of evaporation of a water droplet increases with increasing in temperature of the evaporation chamber. The temperature of the evaporation chamber ranged from 25°C to 95°C. It can be seen that the rate of evaporation increases when the ambient temperature of the water drop increases. The evaporation rate increased gradually from 8.323×10^{-9} kg/s to 32.154×10^{-9} kg/s when the temperature increased from 25°C to 45°C, then the evaporation rate increased linearly from 32.154×10^{-9} kg/s to 698.148×10^{-9} kg/s when the temperature increased from 45°C to 95°C. The rate of evaporation depends mainly on the evaporation pressure of the

liquid, because an increase in temperature means an increase in the evaporation pressure, and then the evaporation rate rises.

A droplet of kerosene liquid increases its evaporation rate also with increasing temperature. At room temperature (round 25^{o}C) and normal atmospheric pressure, the evaporation rate of kerosene can be relatively slow 6.185 $\times 10^{-9}$ kg/s. However, at higher temperature such as boiling point of kerosene which is a round 215^{o}C, the evaporation rate can be much faster. It's also worth noting that the vapor pressure of kerosene increases with temperature, meaning that at higher temperature, kerosene will evaporate more readily and produce more vapor.

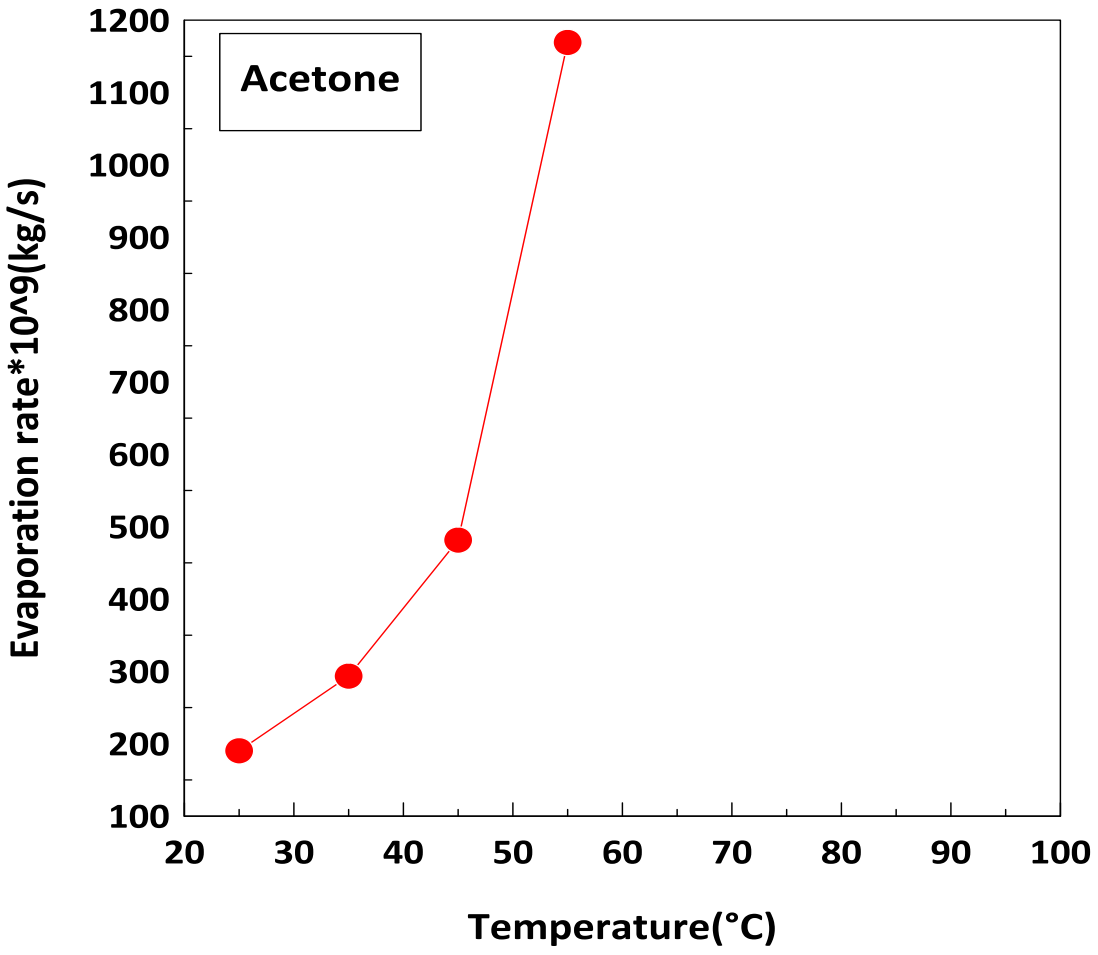

Figure (4- 20) Temperature Effect on Evaporation Rate for Acetone Liquid Droplet

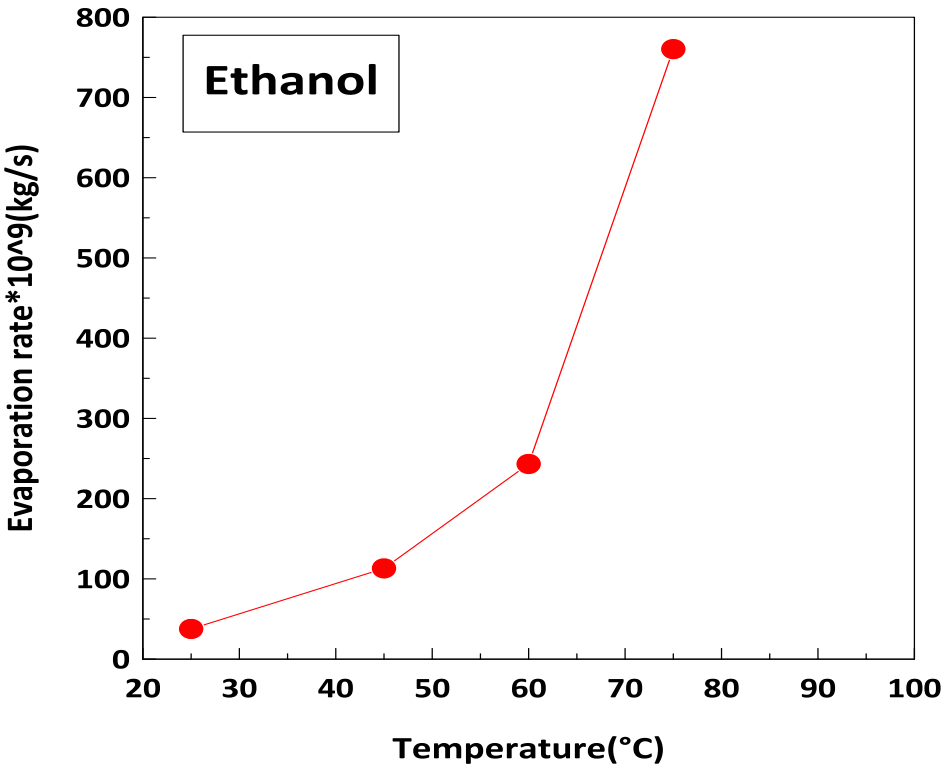

Figure (4- 21) Temperature Effect on Evaporation Rate for Ethanol Liquid Droplet

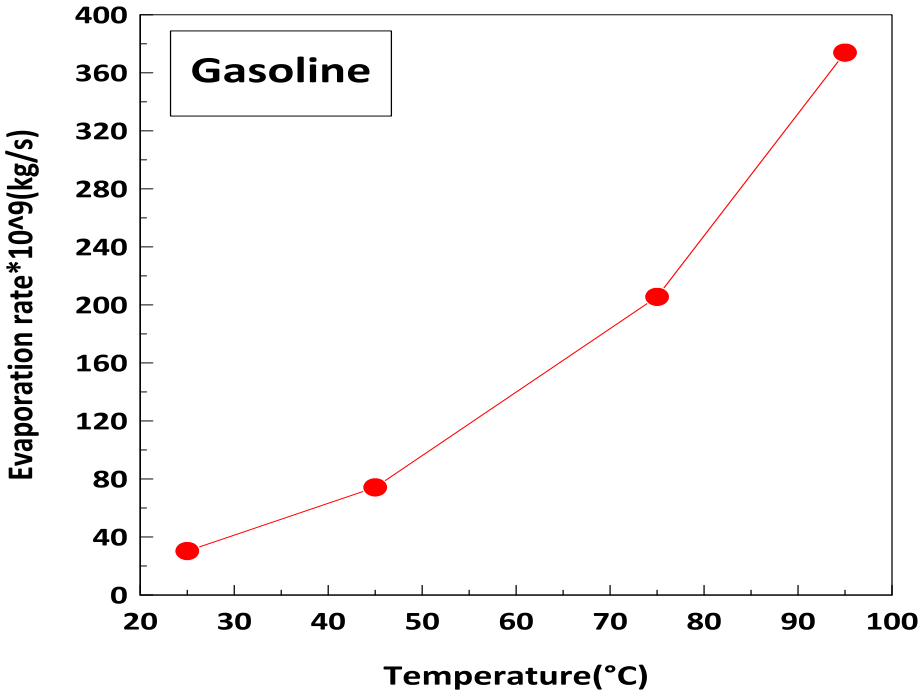

Figure (4-22) Temperature Effect on Evaporation Rate for Gasoline Liquid Droplet

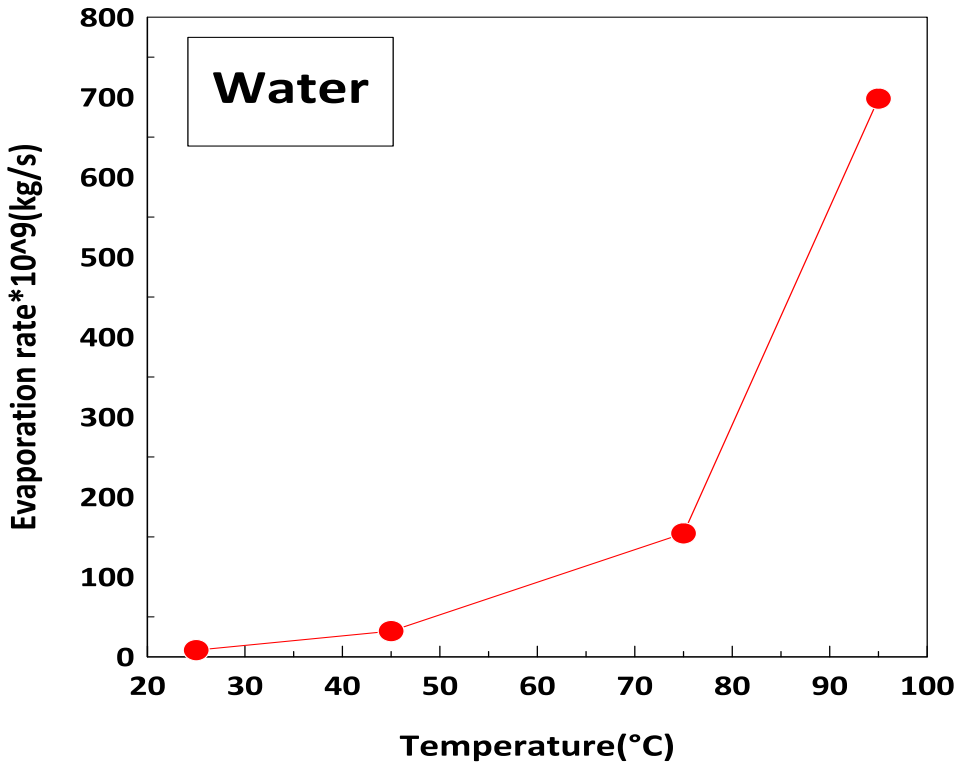

Figure (4- 23) Temperature Effect on Evaporation Rate for Water Liquid Droplet

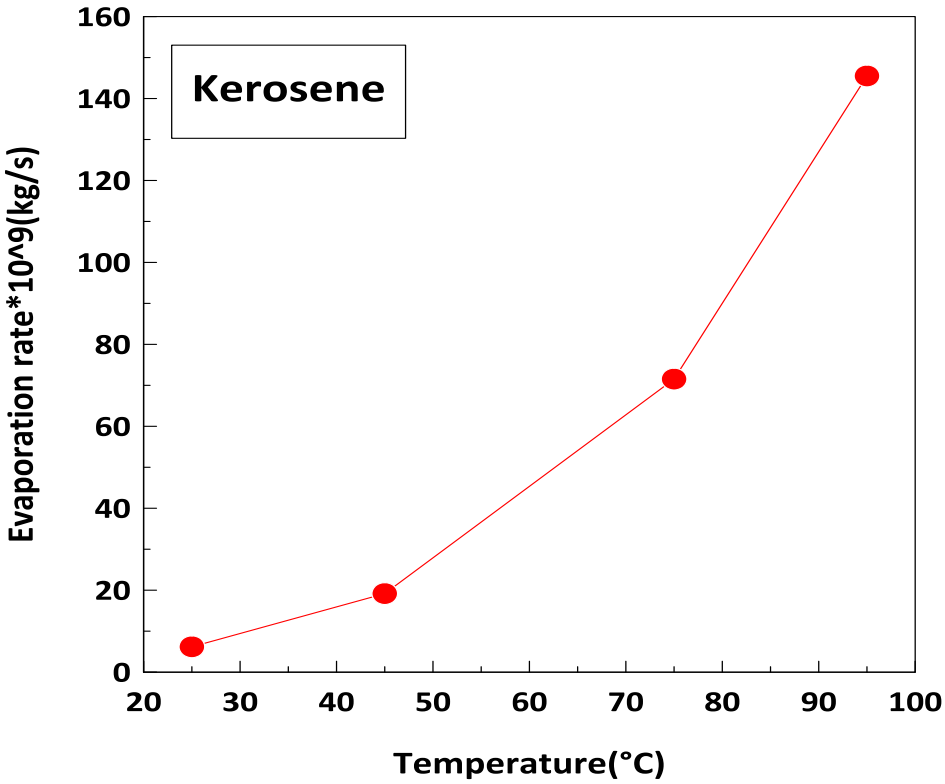

Figure (4- 24) Temperature Effect on Evaporation Rate for Kerosene Liquid droplet

4.3.2.2 Effect of liquid type on evaporation rate

Figures (4-25), (4-26), (4-27), and (4-28) explain the type of liquid of the evaporation rate at different temperatures. When the temperature of the evaporation chamber is equal to 25°C, it can be seen the evaporation rate at liquids acetone, ethanol, gasoline, water, and kerosene are 190.282 × 10^{-9},37.604×10^{-9}, 30.301×10^{-9}, 8.323×10^{-9}, 6.182×10^{-9} kg/s, respectively. A droplet of acetone has the highest evaporation rate than the rest of the liquids used in the experiment. We note that the difference between the evaporation rate of droplet of acetone and the rest of the droplet of other liquids, ethanol, gasoline, water, and kerosene are 1.526×10^{-7} ,1.599×10^{-7}, 1.819×10^{-7},1.840×10^{-7} kg/s respectively. This difference in evaporation rate is due to the difference in the initial diameter droplet as well as the difference in thermal conductivity between the liquids. When the temperature of the evaporation chamber is raised to 45°C, the evaporation rate of the aforementioned liquids increases. The same behavior of the previous at temperature 25°C, it can be noted that acetone liquid droplet is higher of evaporation rate and lower of evaporation rate is kerosene liquid droplet. Ethanol and gasoline are close in their droplet evaporation rate. A droplet of water has a higher rate of evaporation than kerosene. The difference between of a droplet of acetone and other droplets of liquids ethanol, gasoline, water, and kerosene are 3.683×10^{-7} ,4.072 ×10^{-7} , 4.492×10^{-7}, 4.622×10^{-7} kg/s.

Note when the temperature of the evaporation chamber is 75°C, there is no acetone liquid, and this is due to the fact that this temperature is higher than its boiling point of 56.08°C. Ethanol, which is close to its boiling point of 78.2°C, has a higher evaporation rate than other liquids.

The difference between the evaporation rate of ethanol and other liquids gasoline, water and kerosene are 5.547×10^{-7}, 6.058×10^{-7}, 6.887×10^{-7}

kg/s respectively. This variation in the evaporation rate is due to the difference in the initial droplet diameter and the area exposed to evaporation, as the larger the area, the higher the evaporation rate.

Figure showing the rate of evaporation between liquids at 95°C , we notice disappearance of ethanol because this temperature is higher than its boiling point. Water has the highest of evaporation rate as it approaches its boiling point of 100°C.

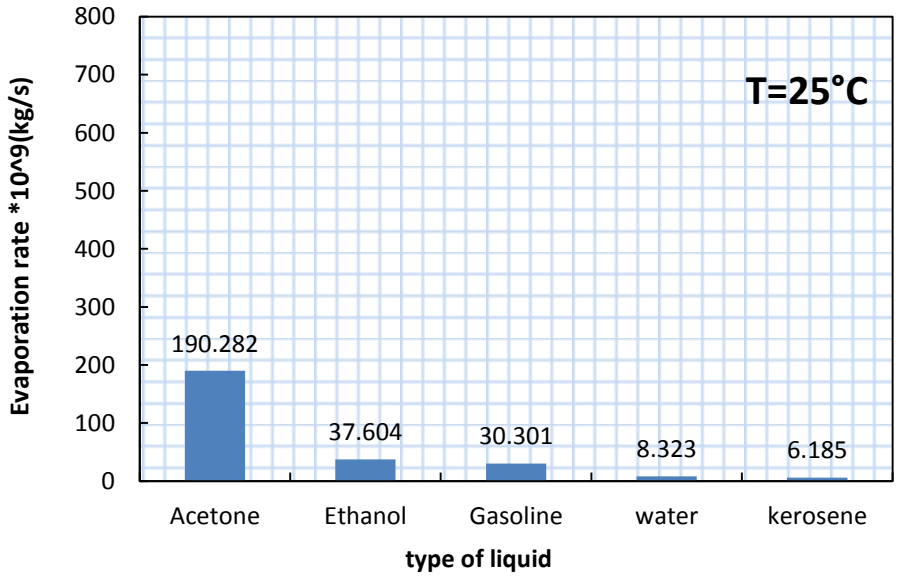

Figure (4- 25) Evaporation Rate for Different Liquid Droplet at T=25°C

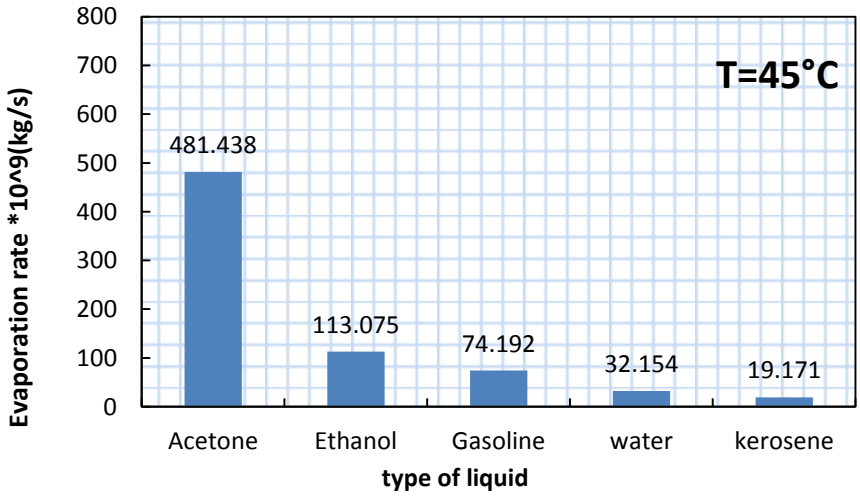

Figure (4- 26) Evaporation Rate for Different Liquid Droplet at T= 45°C

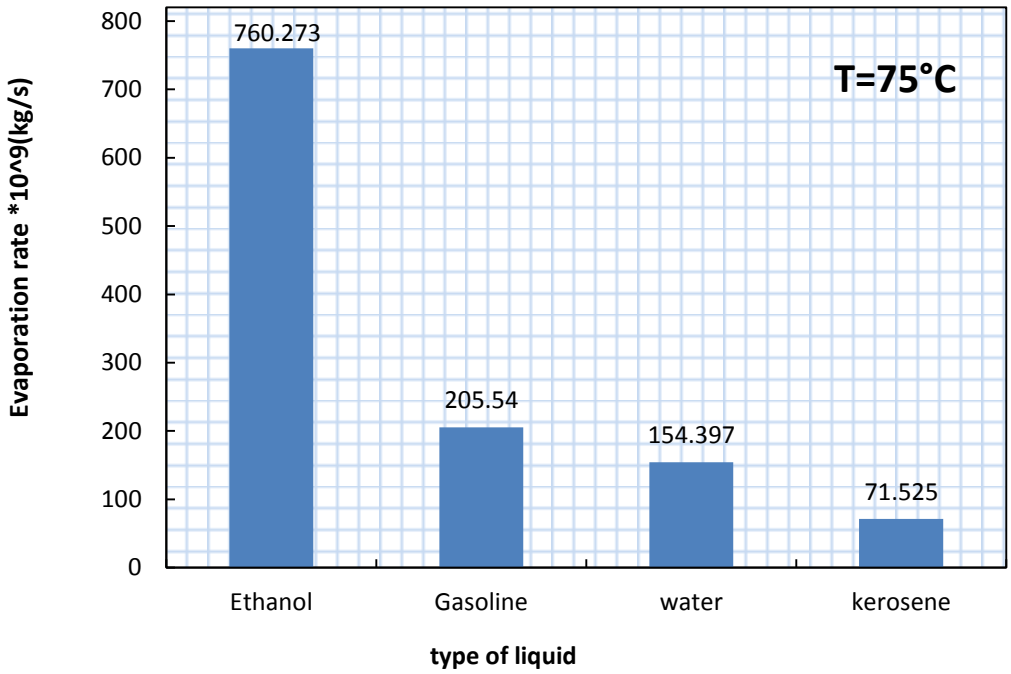

Figure (4- 27) Evaporation Rate for Different Liquid Droplet at T= 75°C

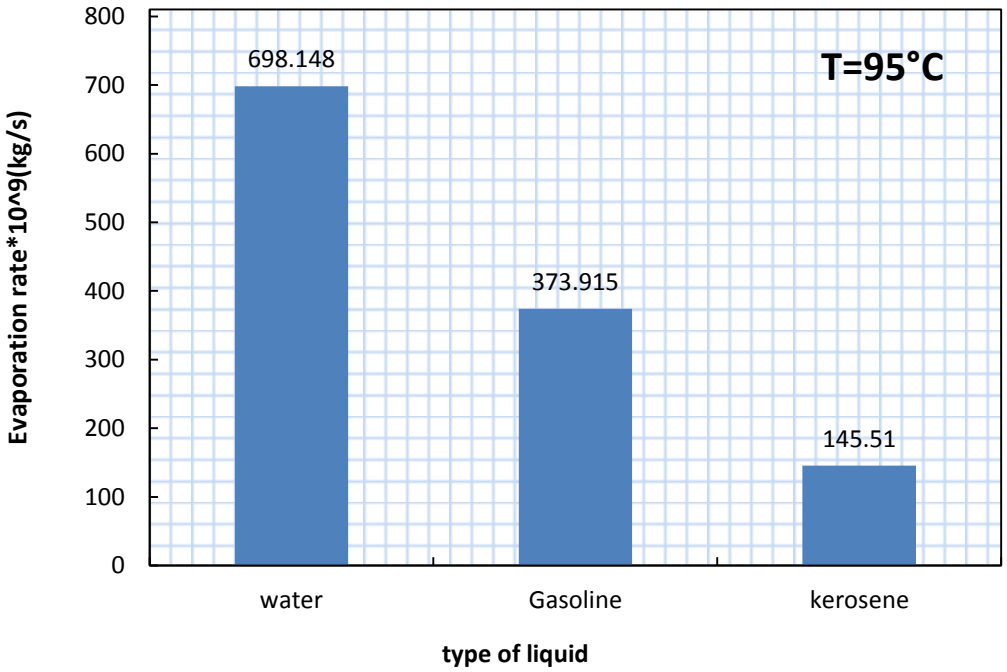

Figure (4- 28) Evaporation Rate for Different Liquid Droplet at T= 95°C

4.3.3. Droplet evaporation constant results

The equation (3.6) shows that the evaporation constant varies linearly with D^2.

$$\frac{D^2}{D_\circ^2} = -K\left(\frac{t}{D_\circ^2}\right) + 1$$

After setting

$$1 - \frac{D^2}{D_\circ^2} = K\left(\frac{t}{D_\circ^2}\right) \quad (4.2)$$

Since the magnitude $(1 - \frac{D^2}{D_\circ^2})$increases with a decrease in D^2 and equation (4.2)is linear, the increase in the magnitude $(1 - \frac{D^2}{D_\circ^2})$ is the increase in the value of K.

4.3.3.1 Effect of temperature on evaporation constant

Figures (4-29), (4-30),(4-31) , (4-32), and (4-33) shows the effect of temperature on evaporation constant for droplet liquids used in experiment. The value of the evaporation constant increases with increasing temperature. The relationship of increasing the value of the evaporation constant with the increase in temperature is a logarithmic relationship, as shown in the Figures, as the curves at low temperature have a slope angle curve is heading to 0°, while when the temperature is raised to temperature close to the boiling point of these liquids, the slope angle of these curves tends to 90°.

The evaporation constant of acetone droplet increases with increasing temperature , where at 25°C its value is 0.101 mm^2/s and when the temperature of the evaporation chamber is increased to 55°C , the evaporation constant becomes $0.683mm^2/s$. The slope angle of the curve between temperatures (25°C-35°C) is 20.68°, while between (25°C-45°C) and (25°C-55°C) are 29.05°, 63.678°, respectively .

This increase in the value of the evaporation constant is due to the increase in the mole fraction, which is directly proportional to the value of the evaporation constant. The value of evaporation constant for droplet

ethanol at temperature 25, 45, 60, and 75°C are 0.0216, 0.065, 0.14, 0.44, mm^2/s, respectively.

It can be seen that it increases with increasing temperature.

The slope angle increases from 7.123° at between temperature (25°C-45°C) to 27.46° when raised temperature (25°C-75°C). Evaporation constant for droplet gasoline at 25°C is $0.02mm^2/s$ and it increases with increasing temperature, when at 45°C is 0.049 mm^2/s , at 75°C is 0.136 mm^2/s and at 95°C is 0.248 mm^2/s . The slope angle of curve the evaporation constant between (25°C-45°C) is 4.76°, between(25°C-75°C) is 7.616° and between (25°C-95°C)is 10.69°.

As the temperature increases, the value of the mole fraction increases, and thus value of the evaporation constant increases. If we notice the Figure of the water droplet, we see that the evaporation constant also increases with increase in temperature of evaporation chamber. The evaporation constant of droplet water at 25, 45, 75, and 95°C are 0.005, 0.017, 0.093 ,0.425 mm^2/s, respectively. The slope angle between (25°C-45°C), (25°C-75°C), and (25°C-95°C) are 1.96°,5.77°, 19.69°.

The constant evaporation of droplet kerosene at environment temperature is low , and when the temperature of evaporation chamber is increased , it gradually increases , as it is at 25°C is $0.004mm^2/s$, at 45°C is $0.0124mm^2/s$, at 75°C is $0.0463mm^2/s$ and at 95°C is $0.0943mm^2/s$. The slope angle of curves between (25°C-45°C) is 1.37°, between (25°C-75°C) is 2.77° and between (25°C-95°C) is 4.23°.

This gradual increase in the value of the evaporation constant is due to the fact that the rate of evaporation of the droplet is gradually increasing.

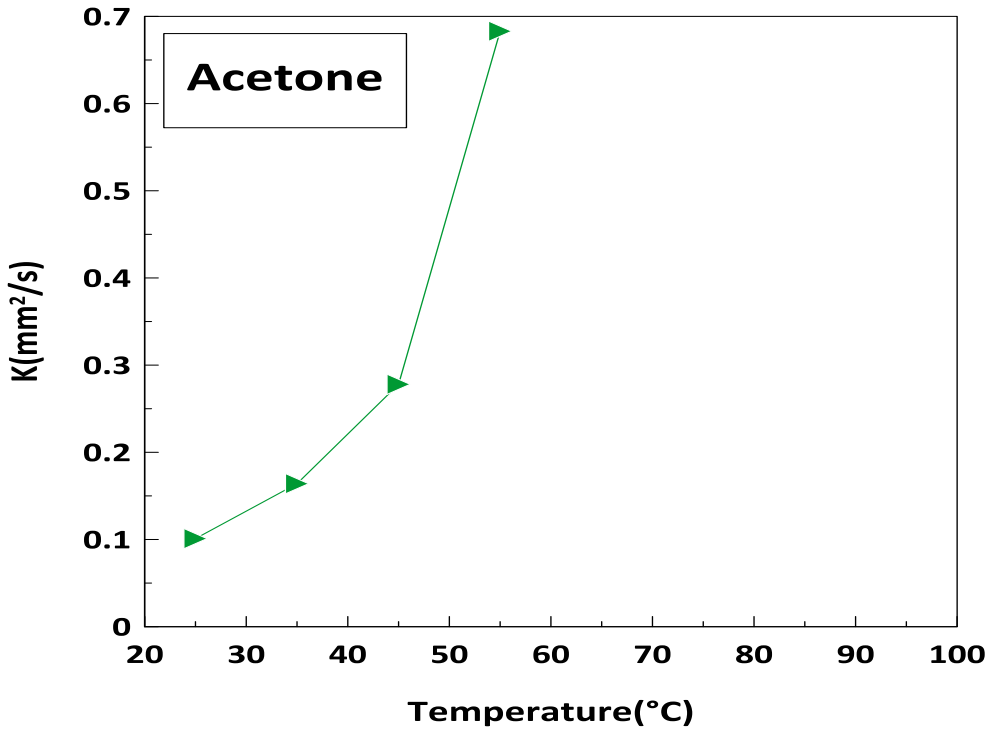

Figure (4- 29) Acetone Evaporation Constant Versus Ambient Temperature

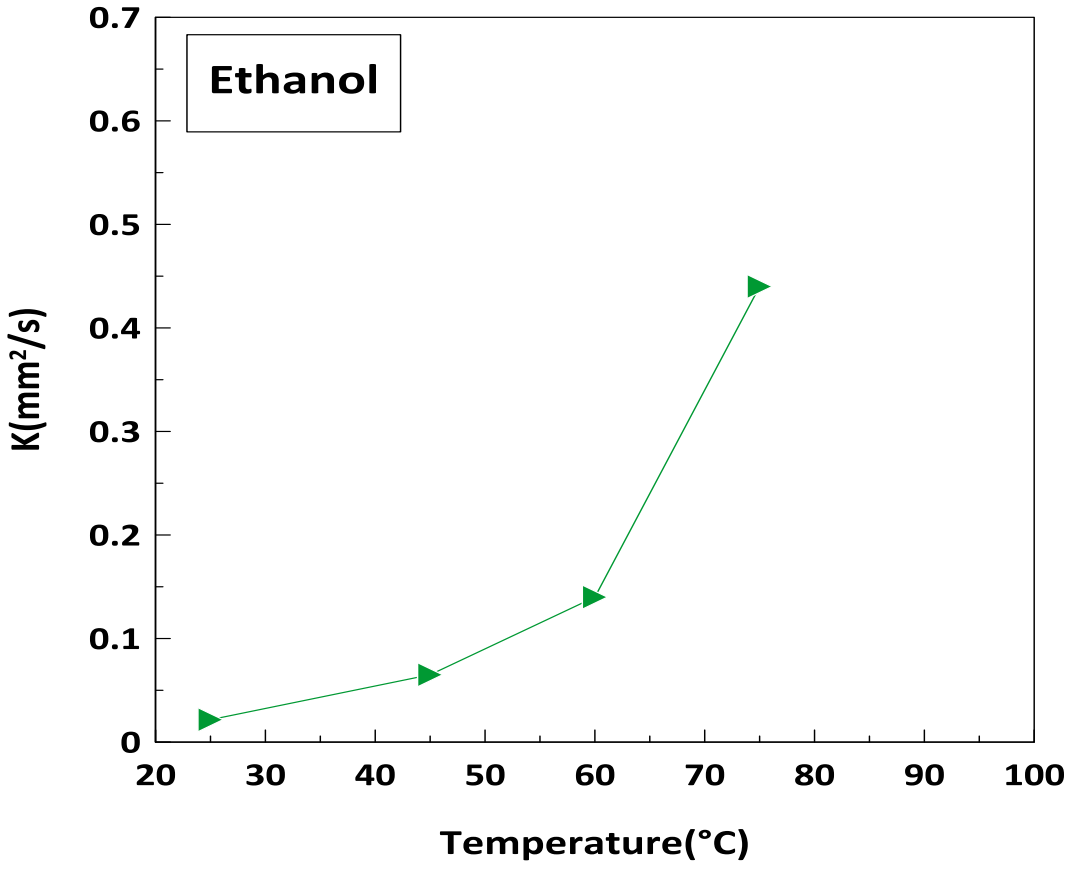

Figure (4- 30) Ethanol Evaporation Constant Versus Ambient Temperature

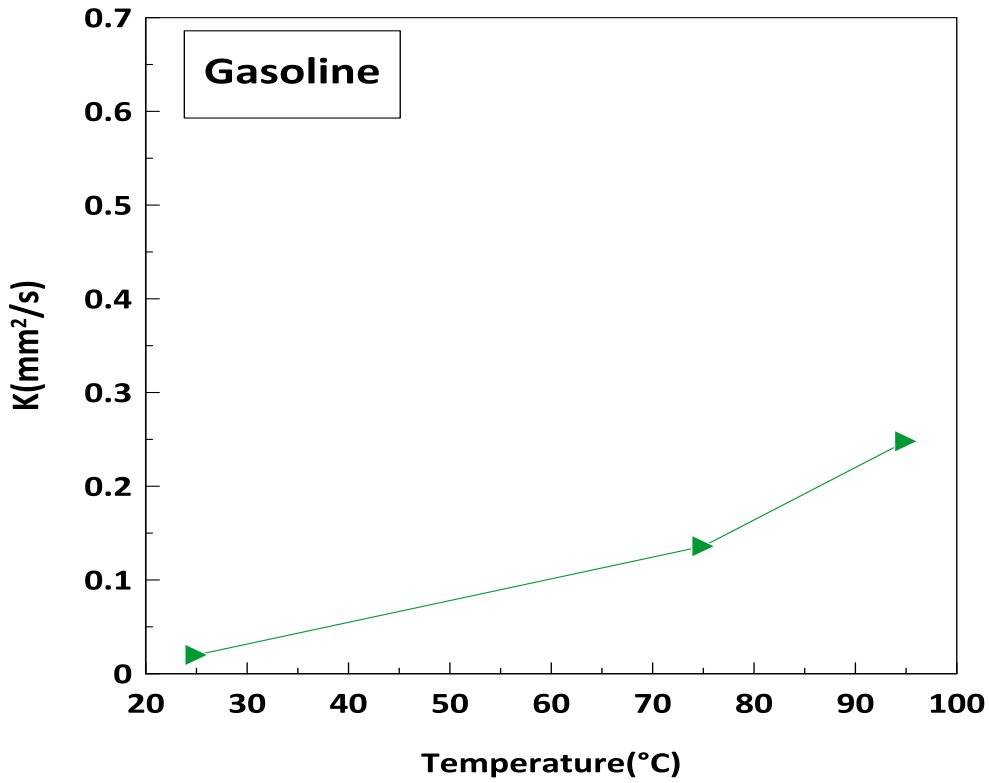

Figure (4- 31) Gasoline Evaporation Constant Versus Ambient Temperature

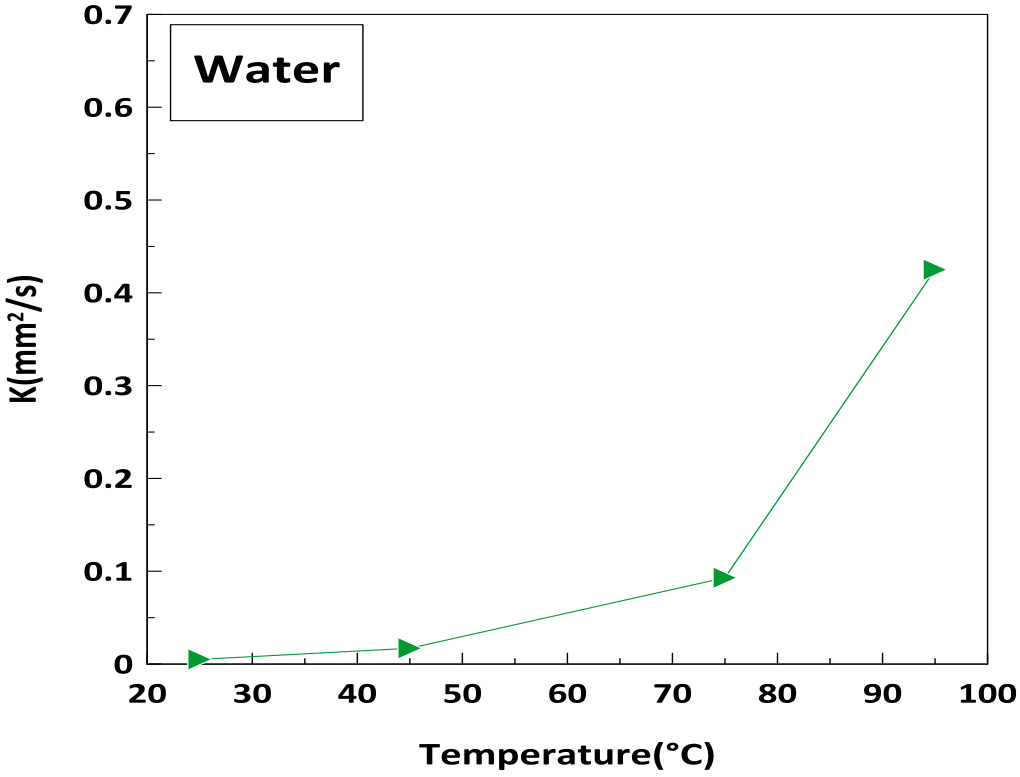

Figure (4- 32) Water Evaporation Constant Versus Ambient Temperature

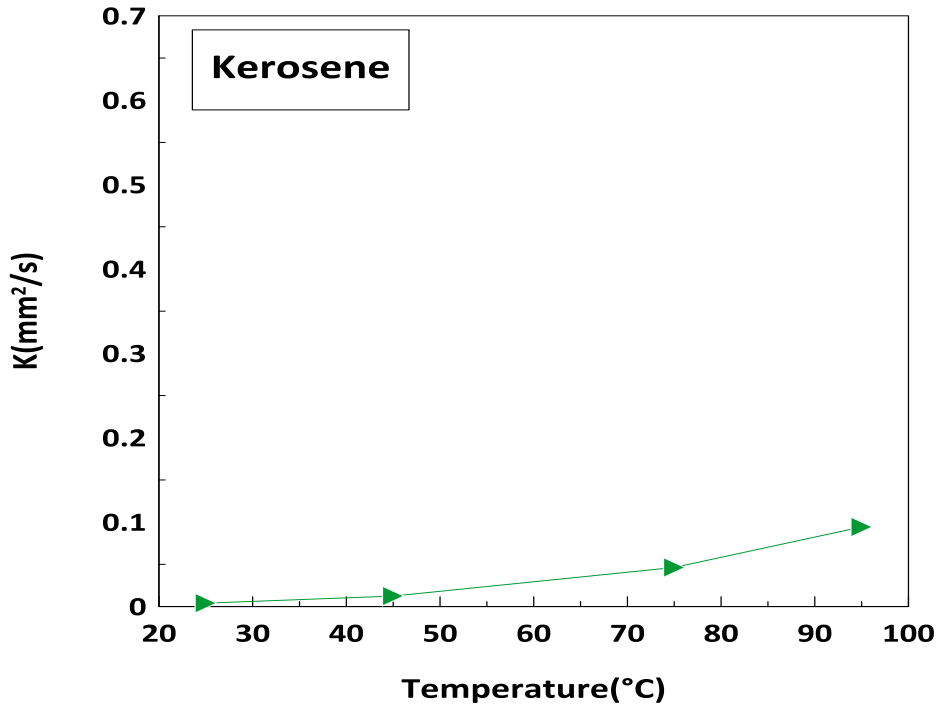

Figure (4- 33) Kerosene Evaporation Constant Versus Ambient Temperature

4.3.3.2 Effect of liquid type on evaporation constant

Figures (4-34), (4-35), (4-36), and (4-37) explain the effect type of liquid on evaporation constant at different temperature of evaporation chamber. The evaporation constant of a droplets varies from one liquid to another depending on its rate of evaporation and the value of the mole fraction at the specified temperature.

The Figure at the value of the evaporation constant at a temperature of 25°C shows us that the highest value is for a droplet of acetone, about 0.101 mm^2/s . Other liquids ethanol, gasoline , water and kerosene the value of its evaporation constant are 0.0216, 0.02, 0.005, 0.004mm^2/s , respectively. The difference between the value of evaporation constant for a droplet acetone and a droplet of liquids at this temperature is as shown in Table (4-7).

Table (4-7) Shows The Difference in Value Evaporation Constant Between Acetone and The Rest of The Liquids Used .

Acetone- another liquid	Difference value at T=25°C (mm^2/s)	Difference rate at T= 45°C (mm^2/s)
Acetone - Ethanol	**0.0794**	**0.213**
Acetone-Gasoline	**0.081**	**0.229**
Acetone – Water	**0.096**	**0.261**
Acetone – Kerosene	**0.097**	**0.2656**

When the temperature of the evaporation chamber is raised to 45°C , the evaporation constant also varies between liquids used. As the difference between acetone and other liquids at temperatures 25°C, 45°C is different as shown in Table (4-7).The difference is due to the rate of evaporation of the liquid droplet, as well as the mole fraction.

When the temperature of the evaporation chamber is 75°C, there is no acetone. Ethanol has highest value of the evaporation constant because it is close to the boiling point and about $0.44mm^2/s$.

Gasoline, water and kerosene are constant evaporation 0.136, 0.093, 0.0463 mm^2/s, respectively. This explains that the difference is due to the difference in the rate of evaporation at this temperature, as well as the difference in mole fraction between liquids, which increases or decreases the evaporation constant.

The absence of ethanol when the temperature is raised to 95°C because it is higher than its boiling point (78.2°C) and evaporates before reaching this temperature. At this temperature, we notice that the water droplet has a higher evaporation constant than gasoline, and this is due to its approaching its boiling point of 100°C, which led to an increase in its evaporation rate as a result of the energy gained by the liquid molecules.

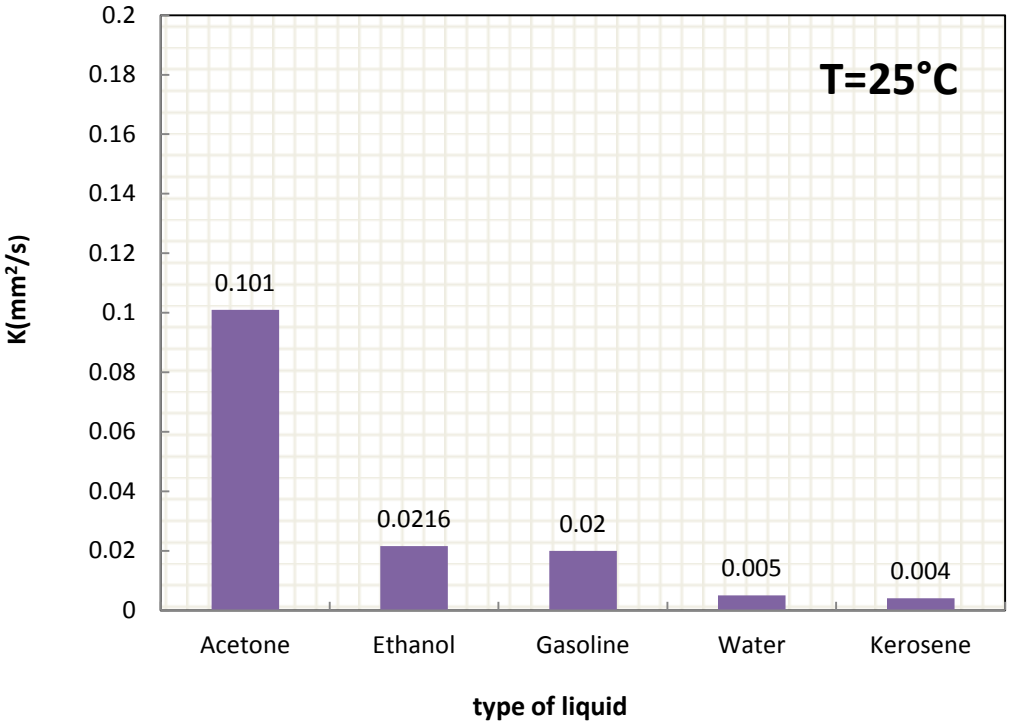

Figure (4- 34) Comparison Between Evaporation Constant for Different Liquids.at Temperature= 25°C

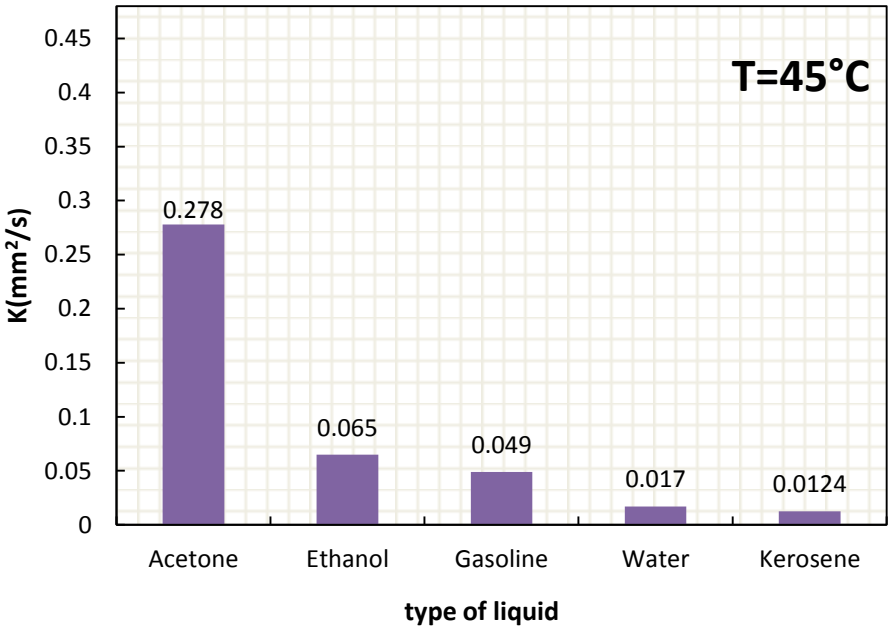

Figure (4- 35) Comparison Between Evaporation Constant for Different Liquids.at Temperature= 45°C

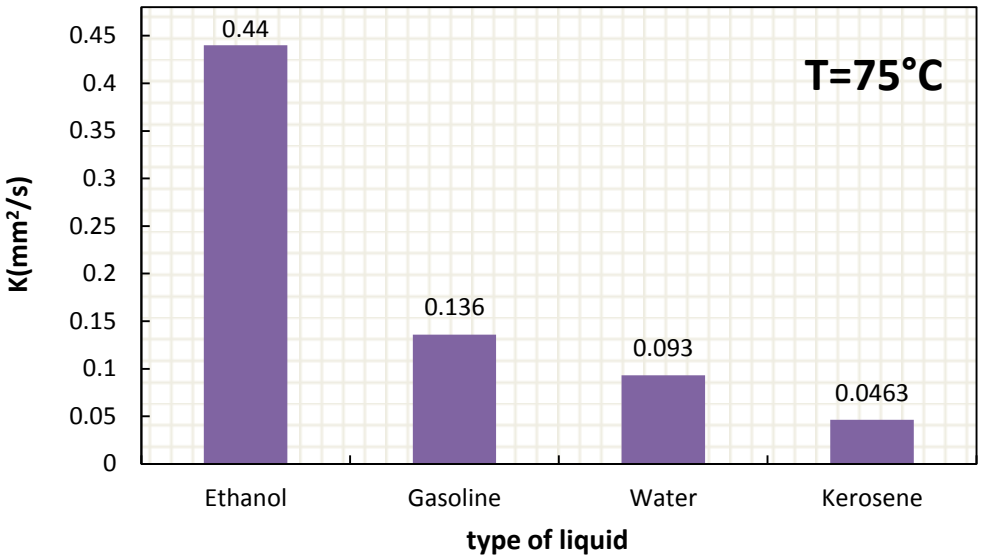

Figure (4- 36) Comparison Between Evaporation Constant for Different Liquids.at Temperature= 75^{o}C

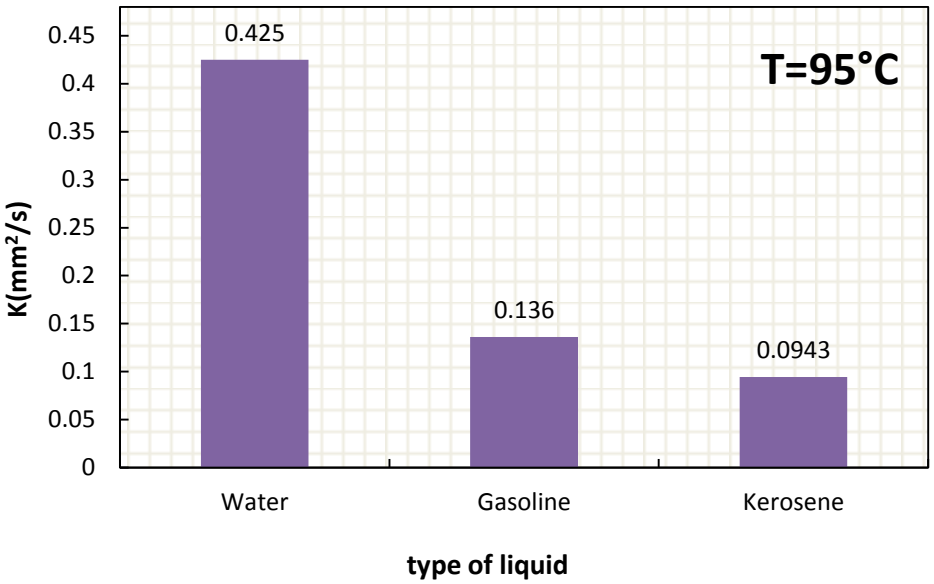

Figure (4- 37) Comparison Between Evaporation Constant for Different Liquids.at Temperature= 95^{o}C

4.3.4. Droplet lifetime results

Droplet lifetime typically refers to the length of time that a liquid droplet exists before it evaporates completely. The droplet lifetime can vary widely depending on several factors such as the size of the droplet, the

ambient temperature and the properties of the liquid. Smaller droplet tends to have shorter lifetime as they have a large surface area to volume ration and thus evaporate more quickly. Similarly, higher temperatures tend to accelerate droplet evaporation and reduce the droplet lifetime.

4.3.4.1 Effect of temperature on droplet lifetime results

Figures (4-38), (4-39), (4-40), (4-41), and (4-42) explains the effect of temperature on the droplet lifetime of the used liquids. The droplet lifetime decreases with increasing temperature. The evaporation of liquid particles from the surface of the droplet as a result of the high temperature and their escape to environment leads to a decrease in its diameter , and as a result this diameter decreases until it vanishes.

The droplet lifetime is depending on the temperature and its initial diameter. The droplet lifetime of acetone at 25, 35, 45, and 55°C are 78.736, 48.49, 28.605, 11.643 sec, respectively.

We note that the temperature is inversely proportional to the droplet lifetime. High temperature increases the rate of evaporation and leads to a gradual decrease in diameter and after a period of time it fades. The droplet lifetime of ethanol at 25°C is 364.78 sec, and when the temperature of the evaporation chamber is raised to 75°C , the droplet lifetime decreases to 17.907 sec.

As the droplet lifetime decreases when the temperature is raised to 45°C by 66.7% , at 60°C by 84.57%, and at 75°C by 95%.

As for gasoline, the droplet lifetime is at 25°C, 45°C, 75°C and 95°C are 332.82, 135.844, 48.944, 26.84, respectively.

That is decreases by 59.18% when the temperature is raised from 25°C to 45°C and when it is raised to 75°C by 85% and when raising it to

95°C by 91.93%. A droplet lifetime of liquid water reaches to 898.88 sec at a temperature 25°C and decreases to 264.376 sec at 45°C and reaches 48.326 sec at 75°C to become at 95°C is 10.575 sec. That is , it decreases by 70.58%, 94.62% and 98.8%, respectively with the above mentioned temperatures.

Kerosene is the droplet lifetime at 25°C is 1488.4 sec, at 45°C is 480.125 sec, at 75°C is 128.587 sec and at 95 °C is 63.134 sec. Its droplet lifetime decreases by 67.7%, 91.36%, 95% respectively with the above mentioned temperatures.

We notice in all Figure , as the temperature increases, the droplet lifetime decreases due to the increase in the rate of evaporation at high temperatures.

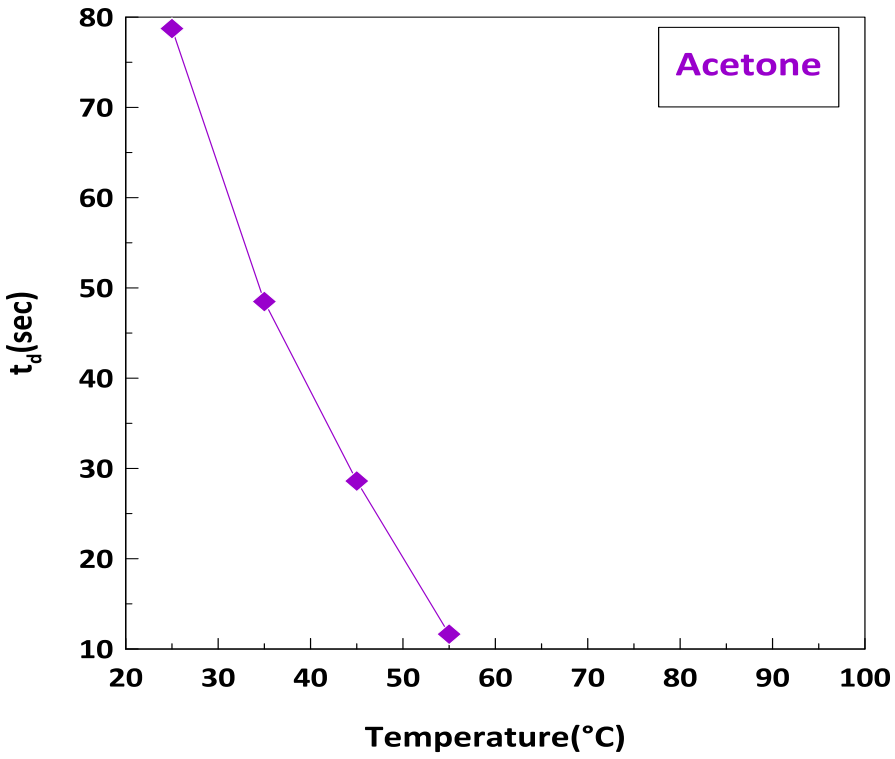

Figure (4- 38) Effect of Temperature on Droplet Lifetime of Acetone

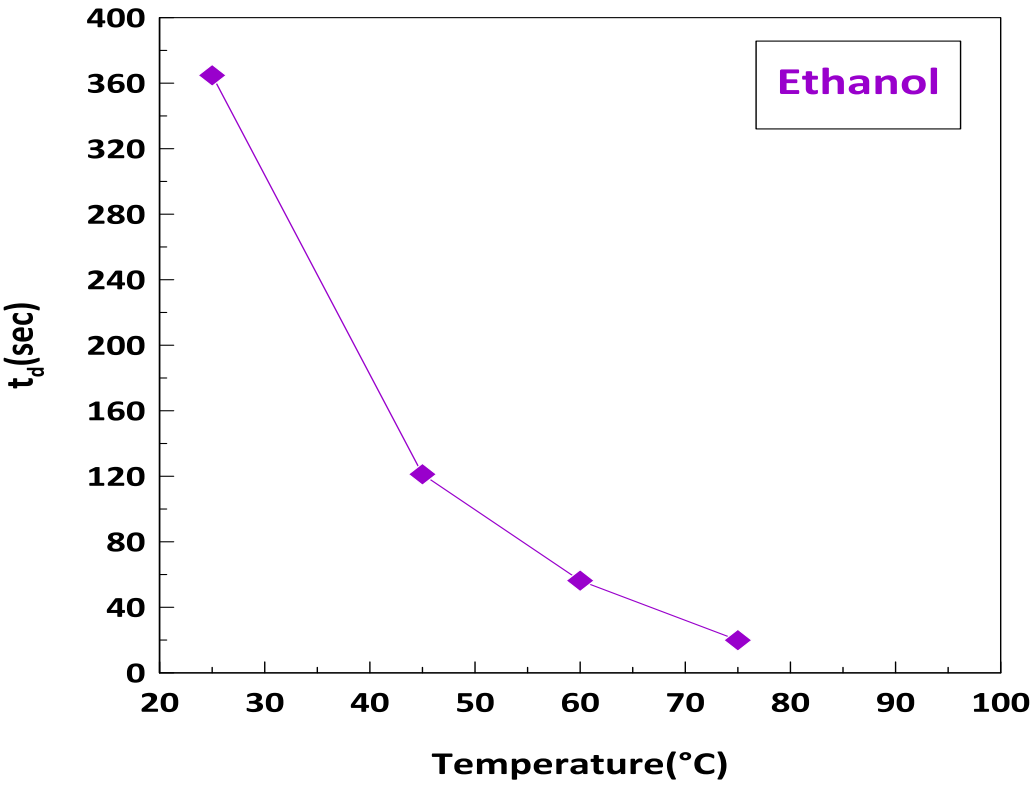

Figure (4- 39) Effect of Temperature on Droplet Lifetime of Ethanol

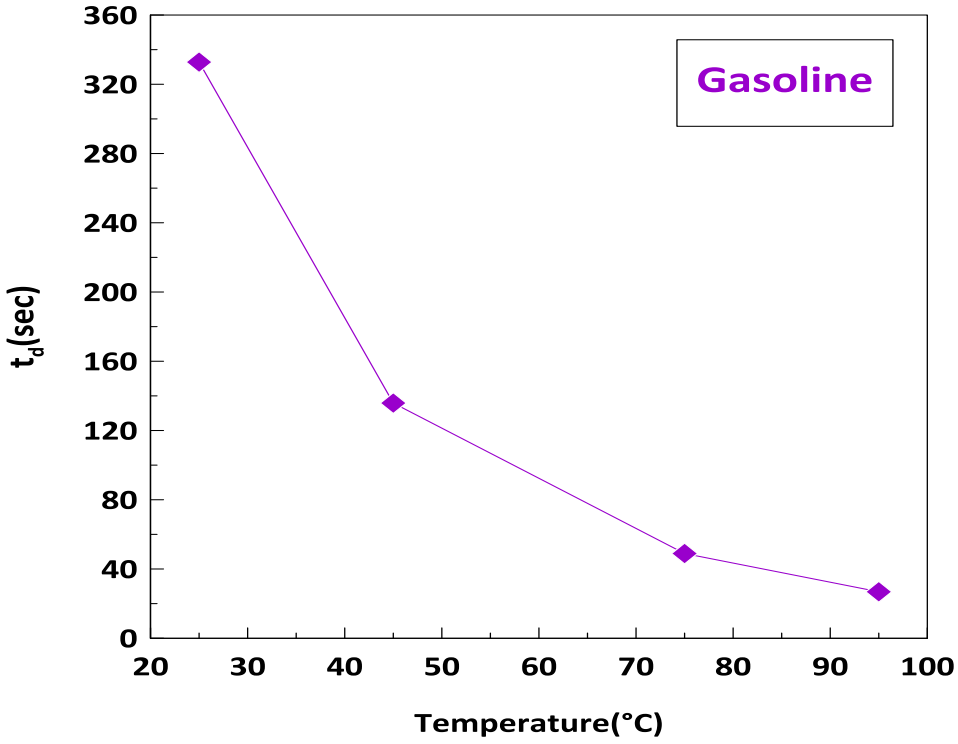

Figure (4- 40) Effect of Temperature on Droplet Lifetime of Gasoline

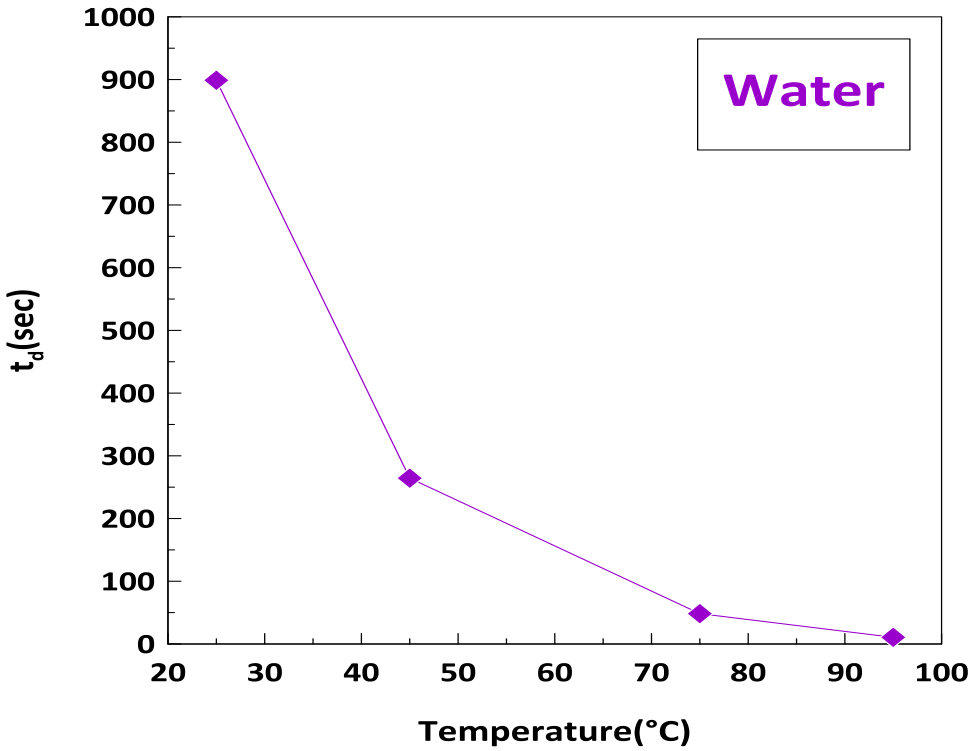

Figure (4- 41) Effect of Temperature on Droplet Lifetime of Water

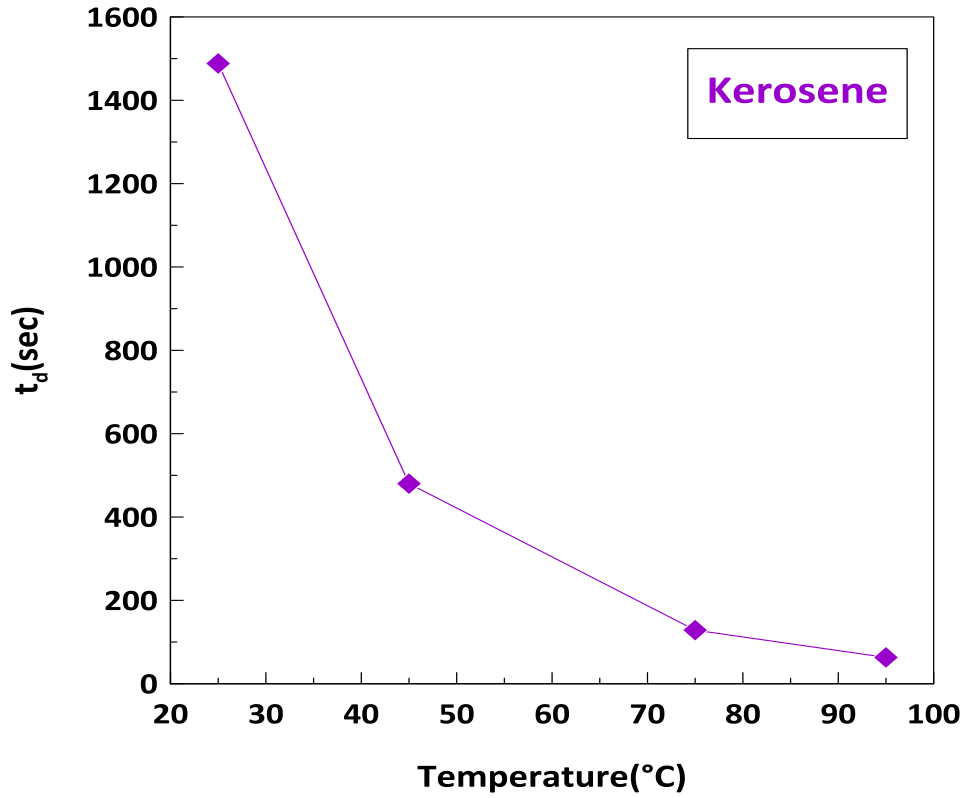

Figure (4- 42) Effect of Temperature on Droplet Lifetime of Kerosene

4.3.4.2 Effect of liquid type on droplet lifetime results

Figures (4-43), (4-44), (4-45) and (4-46) shows the effect of liquid type on droplet lifetime at different temperature in evaporation chamber.

The lifetime of droplet varies between the liquids, as the droplet of liquid that has a high evaporation rate has a shorter lifetime. Likewise, the larger droplet diameter, the longer lifetime of droplet.

At a temperature of 25°C, the minimum droplet lifetime is acetone about 78.736 sec. As for other liquids are gasoline, ethanol, water and kerosene, the droplet lifetime are 332.82, 364.78, 898.88, 1488.4 sec, respectively . This is due to the fact that the rate of evaporation of acetone is higher than the rest of the liquids used, as the evaporation process reduces the size of the droplet until it fades and disappears. Also, at a temperature of 45°C, a droplet lifetime of acetone has the least lifetime and it is about 25.605 sec, but a droplet of ethanol has a shorter lifetime than a droplet of gasoline, regardless of its lifetime at 25°C, as a droplet lifetime of ethanol and gasoline at this temperature are 121.219, 135.844 sec, respectively .

A droplet of water , despite its small size, has a longer lifetime than acetone, ethanol and gasoline, which is about 264.376 sec, because its evaporation rate is low. Because kerosene has the lowest evaporation rate , its droplet lifetime is the longest. When the temperature of the evaporation chamber is raised to 75°C, the acetone disappears, and the ethanol is the least, about 17.907 sec, due to its fast of evaporation. The droplet of water is less lifetime than the droplet of gasoline due to its fast of evaporation, unlike what was in temperatures 25°C and 45°C. The droplet of kerosene is the longest lifetime, about 128.587 sec , because it is slow evaporation.

At the temperature of 95°C , the ethanol disappears, and the droplet of water is the least lifetime of gasoline and kerosene , as the lifetime of a droplet of water 10.575 sec, gasoline 26.84 sec, and kerosene is 63.134 sec. This due to the water droplet approaching the boiling point , and the evaporation rate is fast.

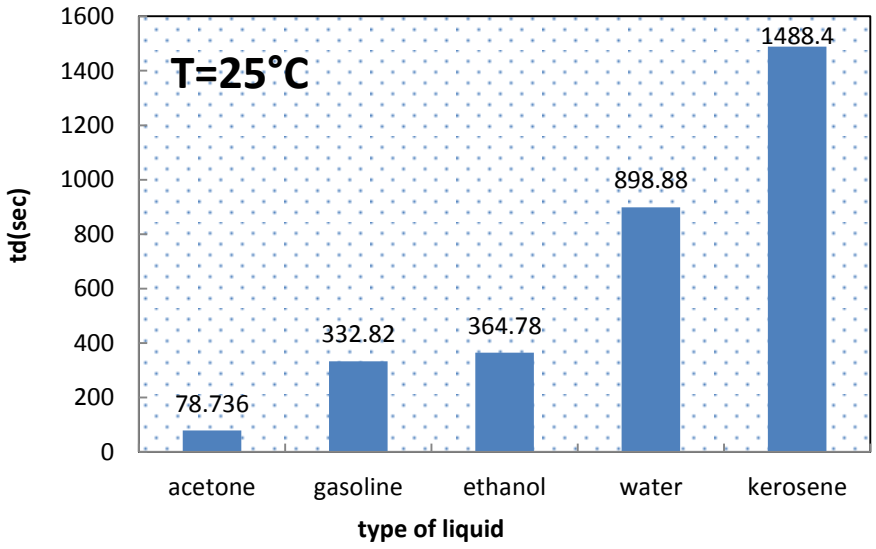

Figure (4- 43) Lifetime for Different Liquid Droplet at T= 25°C

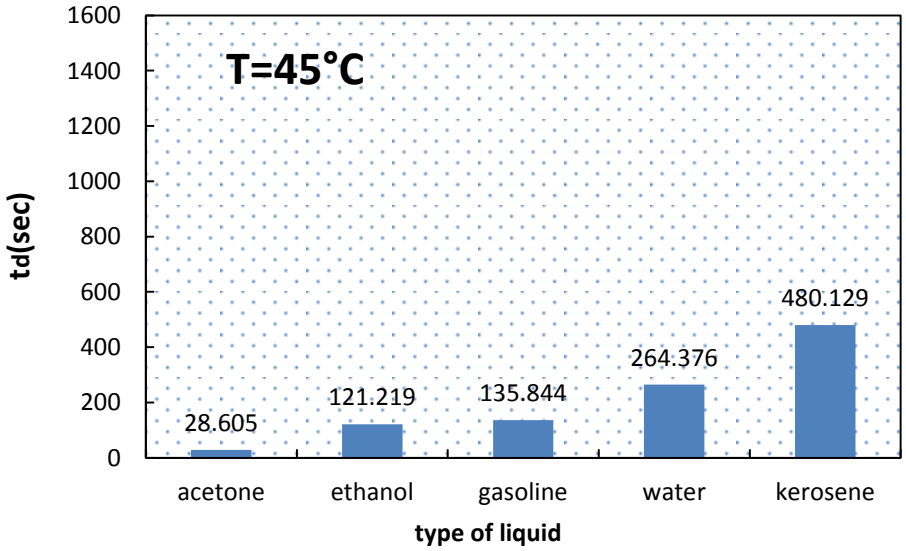

Figure (4- 44) Lifetime for Different Liquid Droplet at T= 45°C

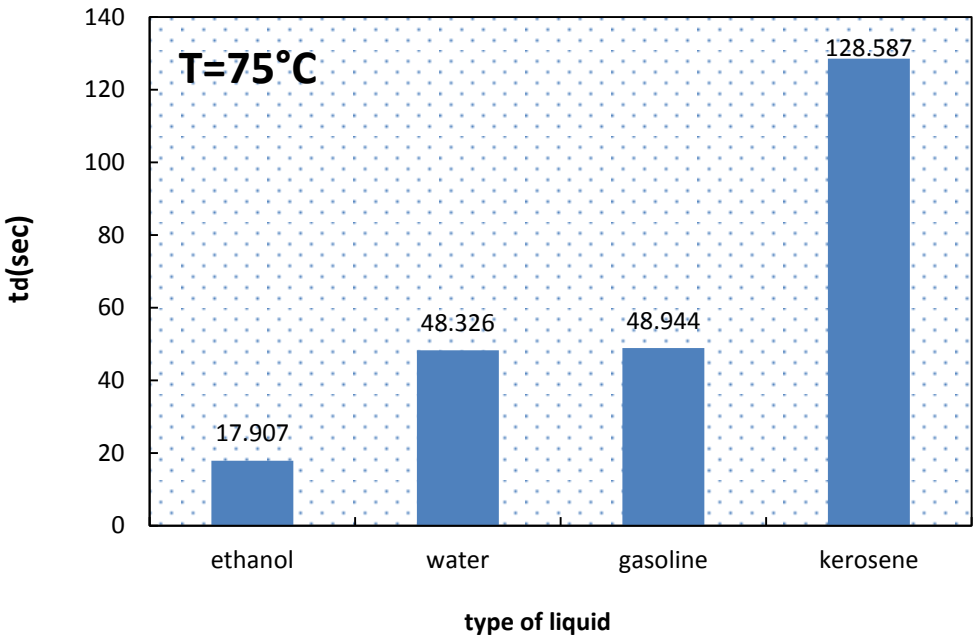

Figure (4- 45) Lifetime for Different Liquid Droplet at T= 75°C

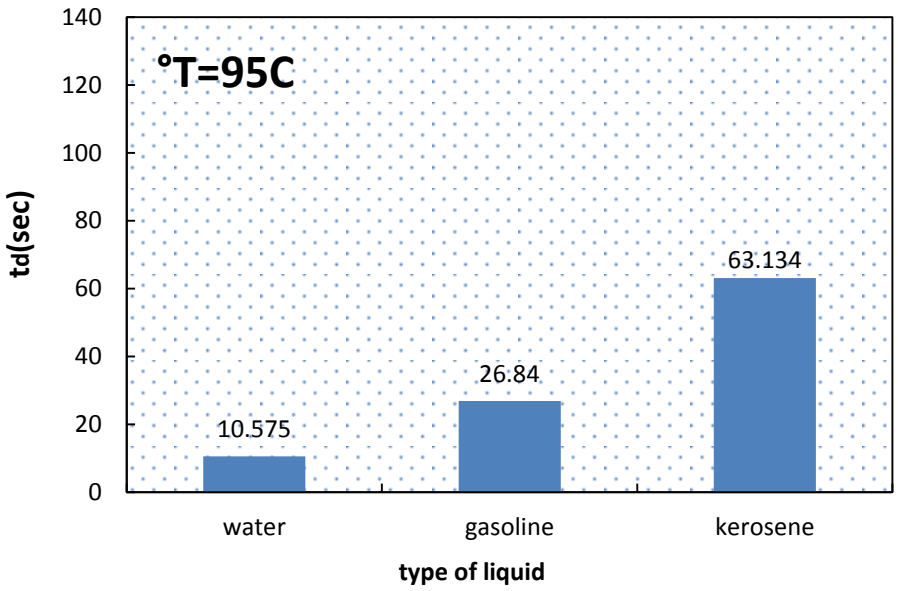

Figure (4- 46) Lifetime for Different Liquid Droplet at T= 95°C

Figure (4.47) shows the evaporation rate of acetone and ethanol droplets with different diameters during fixed time periods. At the initial droplet diameter of acetone, which is 2.82 mm , and within a period of time 0.27 sec, the evaporation rate is 504×10^{-9} kg/s, so that the diameter becomes 2.806 mm ,and this diameter decreases to 2.797 mm during a period of 0.18 sec, at an evaporation rate of 482.034×10^{-9}kg/s, and at an evaporation rate of 426.336×10^{-9}kg/s during a period of 0.1125sec, it becomes diameter 2.792 mm. This difference in the evaporation rate is due to the difference in the droplet diameter over the time periods, meaning that the smaller the diameter, the lower the evaporation rate.

A droplet of ethanol decreases from 2.807 mm to 2.803 mm in 0.27 sec, with an evaporation rate of 113.143×10^{-9} kg/s , and within 0.18 sec the evaporation rate is 113.038×10^{-9} kg/s, and the diameter becomes 2.801 mm. Also, during a period of 0.1125 sec, the diameter becomes 2.8 mm , with an evaporation rate of 112.97×10^{-9} kg/s. This explains that acetone evaporates at a faster rate than ethanol, because the boiling point of acetone is lower than that of ethanol.

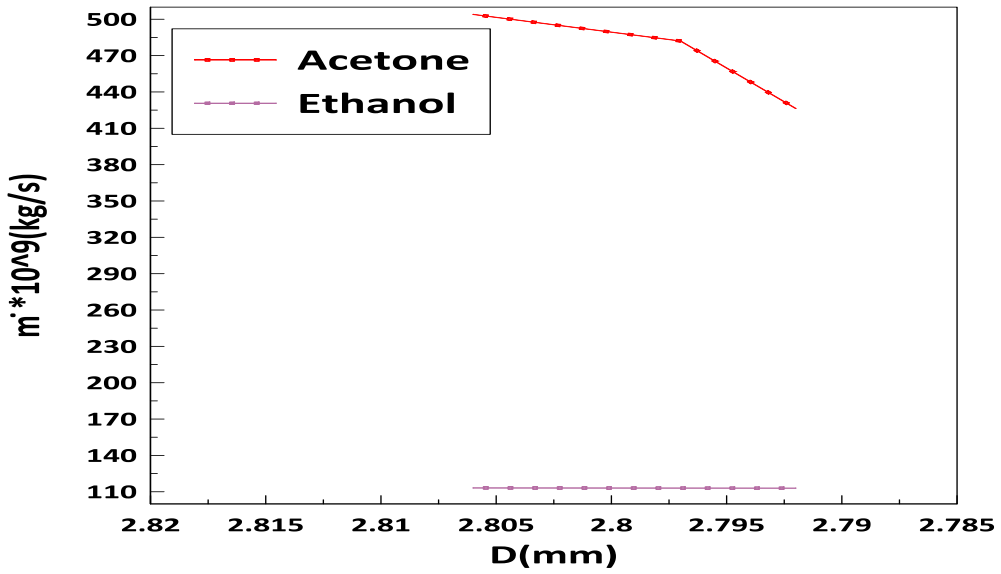

Figure(4.47)Variation of Evaporation Rate with Diameter for Acetone and Ethanol at T=25°C

4.4. Histogram Droplet.

The histogram(4-48) show the decrease in diameter of liquid droplets used inside the evaporation chamber for three time. Stations after injection and at temperatures 25°C and 45°C . At 25°C, we notice a decrease in the initial droplet diameter of acetone 2.82mm to 2.815 mm after 0.27sec from injection and after 0.18sec decreases to 2.811mm for becomes 2.809mm in time 0.5625 sec from injection. That is, the rate of evaporation during this time is 190.282×10^{-9} kg/s.

As for ethanol at this temperature , it is 25°C, decreases the initial droplet diameter 2.807mm to 2.8059mm during 0.27 sec and after 0.18 sec decreasing to 2.8052 mm to becomes 2.8048mm in time 0.5625 from injection. And at 45°C, acetone droplet decreases from 2.82 mm to 2.806 mm during 0.27sec and 0.18 sec decreasing to 2.797 mm to becomes 2.792 mm in time 0.5625 sec from injection. Ethanol decreases at 45°C and during 0.27sec from 2.807 to 2.8038mm and after 0.18 sec decreasing to 2.8017mm to becomes 2.8004 mm in time 0.5625 sec from injection.

	
Acetone do=2.82mm T=25	Acetone d1=2.815mm T=25
	
Acetone d2=2.811mm T=25	Acetone d3=2.809mm T=25

	
Acetone do=2.82mm T=45	Acetone d1=2.806mm T=45
	
Acetone d2=2.797 mm T=45	Acetone d3=2.792mm T=45

Figure (4- 48) Histogram Droplet for Acetone

	
Ethanol do=2.807mm T=25	Ethanol d1=2.8059mm T=25
	
Ethanol d2=2.8052mm T=25	Ethanol d3=2.8048 T=25

	
Ethanol do=2.807mm T=45	Ethanol d1=2.8038mm T=45
	
Ethanol d2=2.8017mm T=45	Ethanol d3=2.8004mm T=45

Figure (4- 48) Histogram Droplet for Ethanol

Chapter Five

Conclusions and Suggestions for Future Work

Chapter Five: Conclusions and Suggestions for Future Work

5.1. Conclusions

The following conclusions are drawn from the results presented in chapter Four:

1- It can be observed that the evaporation rate increases logarithmically with the increase in the temperature of the evaporation chamber.

2- The percentage reduction of droplet diameter ($\frac{D_\circ - D}{D_\circ}$) at temperature 25°C and at time 0.5625 sec after injection equals 0.177% for acetone, 0.04%,0.037%, 0.015%,0.009% for gasoline, ethanol, water, kerosene, respectively, while when the temperature increases to 45°C at the same time , this percentage becomes for acetone 0.496% and 0.099% ,0.111%,0.051%,0.028% for gasoline, ethanol, water, kerosene, respectively.

3- Increasing the temperature reduces the lifetime of the droplet. The lifetime of the droplet depends on the initial size of the droplet and temperature. The lifetime of a droplet of acetone decreases by 63.66% when the temperature is raised from 25^{o}C to 45°C. Lifetime at raises temperature from 25°C to 45°C of gasoline decreases by 59.1% and decreases by 66.76% for ethanol and percentage 70.58 for water and by 67.74% for kerosene . Increasing the temperature leads to an increase in the rate of evaporation and thus decreases the lifetime of the droplet.

4- The evaporation constant for a droplet increased by increasing the chamber temperature.

5- The evaporation constant curve the slope angle is 29.05° for acetone, 7.123° for ethanol,4.76° for gasoline, 1.96° for water, and 1.37° for kerosene.

6- It can be seen that acetone has the highest evaporation constant, and then it comes after ethanol, then gasoline, then water, and then kerosene. At room temperature (25ºC), the evaporation constant for gasoline, and ethanol are close.

5.2. Suggestion for future research

The following suggestion are recommended for future work

1- Using additives to the fuel, such as adding nanoparticles, and studying their effect on the droplet evaporation rate and lifetime.

2- Studying the process of evaporation of other types of liquids.

3- Study the effect of evaporation chamber pressure on droplet evaporation process.

4- Study the effect of evaporation chamber humidity on droplet evaporation process.

5-Study the effect of evaporation mechanism on droplet lifetime and evaporation rate.

REFERENCES

References

[1] H. Grosshans *et al.*, "Numerical and experimental study of the drying of bi-component droplets under various drying conditions," *International Journal of Heat and Mass Transfer,* vol. 96, pp. 97-109, 2016.

[2] K. Hasegawa, A. Watanabe, A. Kaneko, and Y .Abe, "Coalescence dynamics of acoustically levitated droplets," *Micromachines,* vol. 11, no. 4, p. 343, 2020.

[3] R. Mondragon *et al.*, "Study of the drying behavior of high load multiphase droplets in an acoustic levitator at high temperature conditions "،*Chemical engineering science,* vol. 66, no. 12, pp. 2734-2744, 2011.

[4] R. Mondragon, J. C. Jarque, J. E. Julia, L. Hernandez, and A. Barba, "Effect of slurry properties and operational conditions on the structure and properties of porcelain tile granules dried in an acoustic levitator," *Journal of the European Ceramic Society,* vol. 32, no. 1, pp. 59-70, 2012.

[5] C. Groenewold, C. Möser, H. Groenewold, and E. Tsotsas, "Determination of single-particle drying kinetics in an acoustic levitator," *Chemical Engineering Journal*, vol. 86, no. 1-2, pp. 217-222, 2002.

[6] H. Schiffter and G. Lee, "Single-droplet evaporation kinetics and particle formation in an acoustic levitator. Part 1: Evaporation of water microdroplets assessed using boundary-layer and acoustic levitation theories," *Journal of pharmaceutical sciences,* vol. 96, no. 9, pp. 2274-2283, 2007.

[7] B. A. Al Zaitone and C. Tropea, "Evaporation of pure liquid droplets: Comparison of droplet evaporation in an acoustic field versus glass-filament," *Chemical Engineering Science,* vol. 66, no. 17, pp. 3914-3921, 2011.

[8] K. Hasegawa, Y. Abe, A. Fujiwara, Y. Yamamoto, and K. Aoki, "External flow of an acoustically levitated droplet," *Microgravity Science and Technology,* vol. 20, no. 3, pp. 261-264, 2008.

[9] M. Junk, J. Hinrichs, F. Polt, J. Fechner, and W. Pauer, "Quantitative experimental determination of evaporation influencing factors in single droplet levitation," *International Journal of Heat and Mass Transfer*, vol. 149, p. 119057, 2020.

[10] Y. Fang, S. Rogers, C. Selomulya, and X. D. Chen, "Functionality of milk protein concentrate: Effect of spray drying temperature," *Biochemical Engineering Journal,* vol. 62, pp. 101-105, 2012.

[11] S. Rogers, W. D. Wu, S. X. Q. Lin, and X. D. Chen, "Particle shrinkage and morphology of milk powder made with a

monodisperse spray dryer," *Biochemical Engineering Journal,* vol. 62, pp. 92-100, 2012.

[12] J. Tröndle, A. Ernst, W. Streule, R. Zengerle, and P. Koltay, "Non-contact optical sensor to detect free flying droplets in the nanolitre range," *Sensors and Actuators A: Physical,* vol. 158, no. 2, pp. 254-262, 2010.

[13] J. Bae and C. Avedisian, "Experimental study of the combustion dynamics of jet fuel droplets with additives in the absence of convection," *Combustion and flame,* vol. 137, no. 1-2, pp. 148-162, 2004.

[14] Z. Wang, B. Yuan, Y. Huang, J. Cao, Y. Wang, and X. Cheng, "Progress in experimental investigations on evaporation characteristics of a fuel droplet," *Fuel Processing Technology,* vol. 231, p. 107243.2022 ،

[15] Y. Zhang *et al.,* "Effect of ambient temperature on the puffing characteristics of single butanol-hexadecane droplet," *Energy,* vol. 145, pp. 430-441, 2018.

[16] J. Wang, X. Wang, H. Chen, Z. Jin, and K. Xiang, "Experimental study on puffing and evaporation characteristics of jatropha straight vegetable oil (SVO) droplets," *International Journal of Heat and Mass Transfer,* vol. 119, pp. 392-399, 2018.

[17] Y. Zhang *et al.,* "The effect of different n-butanol-fatty acid methyl esters (FAME) blends on puffing characteristics," *Fuel,* vol. 208, pp. 30-40, 2017.

[18] M. Al Qubeissi *et al.,* "Heating and Evaporation of Droplets of Multicomponent and Blended Fuels: A Review of Recent Modeling Approaches," *Energy & Fuels,* vol. 35, no. 22, pp. 18220-18256 ، .2021

[19] X. Ma, F. Zhang, K. Han, B. Yang, and G. Song, "Evaporation characteristics of acetone–butanol–ethanol and diesel blends droplets at high ambient temperatures," *Fuel,* vol. 160, pp. 43-49, 2015.

[20] H. Ghassemi, S. W. Baek, and Q. S. Khan, "Experimental study on binary droplet evaporation at elevated pressures and temperatures," *Combustion science and technology,* vol. 178, no. 6, pp. 1031-1053, 2006.

[21] R. Volkov and P. Strizhak, "Using Planar Laser Induced Fluorescence and Micro Particle Image Velocimetry to study the heating of a droplet with different tracers and schemes of attaching it on a holder," *International Journal of Thermal Sciences,* vol. 159, p. 106603, 2021.

[22] J. Wang, X. Huang, X. Qiao, D. Ju, and C. Sun, "Experimental study on effect of support fiber on fuel droplet vaporization at high temperatures," *Fuel,* vol. 268, p. 117407, 2020.

[23] W. Xu and C.-H. Choi, "Effects of surface topography and colloid particles on the evaporation kinetics of sessile droplets on superhydrophobic surfaces," *Journal of heat transfer,* vol. 134, no. 5, 2012.

[24] Y.-S. Yu, Z. Wang, and Y.-P. Zhao, "Experimental and theoretical investigations of evaporation of sessile water droplet on hydrophobic surfaces," *Journal of colloid and interface science,* vol. 365, no. 1, pp. 254-259, 2012.

[25] S. Manukyan *et al.*, "Imaging internal flows in a drying sessile polymer dispersion drop using Spectral Radar Optical Coherence Tomography (SR-OCT)," *Journal of colloid and interface science,* vol. 395, pp. 287.2013 ،293-

[26] Á. G. Marín *et al.*, "Building microscopic soccer balls with evaporating colloidal fakir drops," *Proceedings of the National Academy of Sciences,* vol. 109, no. 41, pp. 16455-16458, 2012.

[27] N. Kovalchuk, A. Trybala, and V. Starov, "Evaporation of sessile droplets," *Current Opinion in Colloid & Interface Science,* vol. 19, no. 4, pp. 336-342, 2014.

[28] O. Soboleva and B. Summ, "The kinetics of dewetting of hydrophobic surfaces during the evaporation of surfactant solution drops," *Colloid Journal,* vol. 65, no. 1, pp. 89-93, 2003.

[29] E. Bormashenko *et al.*, "Contact angle hysteresis on polymer substrates established with various experimental techniques, its interpretation, and quantitative characterization," *Langmuir,* vol. 24, no. 8, pp. 40.2008 ،4025-20

[30] J. K. Park, J. Ryu, B. C. Koo, S. Lee, and K. H. Kang, "How the change of contact angle occurs for an evaporating droplet: effect of impurity and attached water films," *Soft Matter,* vol. 8, no. 47, pp. 11889-11896, 2012.

[31] P. Gurrala, S. Balusamy, S. Banerjee, and K. C. Sahu, "A review on the evaporation dynamics of sessile drops of binary mixtures: Challenges and opportunities," *Fluid Dyn. Mater. Process,* vol. 17, no. 2, pp. 253-284, 2021.

[32] M. A. Hampton, T. A. Nguyen, A. V. Nguyen, Z. P. Xu, L. Huang, and V. Rudolph, "Influence of surface orientation on the organization of nanoparticles in drying nanofluid droplets," *Journal of colloid and interface science,* vol. 377, no. 1, pp. 456-462, 2012.

[33] N. Fu, M. W. Woo, and X. D .Chen, "Single droplet drying technique to study drying kinetics measurement and particle functionality: A review," *Drying Technology,* vol. 30, no. 15, pp. 1771-1785, 2012.

[34] Z. Ma, Y. Li, Z. Li, W. Du, Z. Yin, and S. Xu, "Evaporation and combustion characteristics of hydrocarbon fuel droplet in sub-and super-critical environments," *Fuel*, vol. 220, pp. 763-768, 2018.

[35] U. Patel and S. Sahu, "Effect of air turbulence and fuel composition on bi-component droplet evaporation," *International Journal of Heat and Mass Transfer*, vol. 141, pp. 757-768, 2019.

[36] M. Dai, J. Wang, N. Wei, X. Wang, and C. Xu, "Experimental study on evaporation characteristics of diesel/cerium oxide nanofluid fuel droplets," *Fuel*, vol. 254, p. 115633, 2019.

[37] X. Wang, M. Dai ،J. Wang, Y. Xie, G. Ren, and G. Jiang, "Effect of ceria concentration on the evaporation characteristics of diesel fuel droplets," *Fuel*, vol. 236, pp. 1577-1585, 2019.

[38] J. Hinrichs, V. Shastry, M. Junk, Y. Hemberger, and H. Pitsch, "An experimental and computational study on multicomponent evaporation of diesel fuel droplets," *Fuel*, vol. 275, p. 117727, 2020.

[39] S. P. R. Yadav, C. Saravanan, S. Karthick, K. Senthilnathan, and A. Gnanaprakash, "Fundamental droplet evaporation and engine application studies of an alternate fuel produced from waste transformer oil," *Fuel*, vol. 259, p. 116253, 2020.

[40] T. Valiullin, K. Y. Vershinina, G. Kuznetsov, and P. Strizhak, "An experimental investigation into ignition and combustion of groups of slurry fuel droplets containing high concentrations of water," *Fuel Processing Technology*, vol. 210, p. 106553, 2020.

[41] Y. Luo, Z. Jiang, Y. Gan, J. Liang, and W. Ao, "Evaporation and combustion characteristics of an ethanol fuel droplet in a DC electric field," *Journal of the Energy Institute*, vol. 98, pp. 216-222, 2021.

[42] M. A. Rosli, A. R. A. Aziz, M. A. Ismael, N. O. Elbashir, M. Baharom, and S. E. Mohammed, "Experimental study of micro-explosion and puffing of gas-to-liquid (GTL) fuel blends by suspended droplet method," *Energy*, vol. 218, p. 119462, 2021.

[43] O. Kastner, G. Brenn, D. Rensink, and C. Tropea, "The acoustic tube levitator–a novel device for determining the drying kinetics of single droplets," *Chemical Engineering & Technology: Industrial Chemistry- Plant Equipment- Process Engineering- Biotechnology*, vol. 24, no. 4, pp. 335-339, 2001.

[44] G. Brenn, D. Rensink, C. Tropea, and A. L. Yarin, "Investigation of droplet drying characteristics using an acoustic-aerodynamic levitator," *International Journal of Fluid Mechanics Research*, vol. 24, no. 4-6, 1997.

[45] R. Vehring, "Pharmaceutical particle engineering via spray drying," *Pharmaceutical research*, vol. 25, no. 5, pp. 999-1022, 2008.

[46] L. Hennet *et al.*, "Aerodynamic levitation and laser heating," *The European Physical Journal Special Topics*, vol. 196, no. 1, pp. 151-165, 2011.

[47] S. S. Sazhin, "Advanced models of fuel droplet heating and evaporation," *Progress in energy and combustion science*, vol. 32, no. 2, pp. 162-214, 2006.

[48] Y. Ra and R. D. Reitz, "A vaporization model for discrete multi-component fuel sprays," *International Journal of Multiphase Flow*, vol. 35, no. 2, pp. 101-117, 2009.

[49] S. Tonini and G. Cossali, "A multi-component drop evaporation model based on analytical solution of Stefan–Maxwell equations," *International Journal of Heat and Mass Transfer*, vol. 92, pp. 184-189, 2016.

[50] M. Al Qubeissi and S. S. Sazhin, "Models for droplet heating and evaporation: an application to biodiesel, diesel and gasoline fuels," *Int. J. Eng. Syst. Model. Simul*, vol. 9, pp. 32-40, 2017.

[51] A. Arabkhalaj, A. Azimi, H. Ghassemi, and R. S. Markadeh, "A fully transient approach on evaporation of multi-component droplets," *Applied Thermal Engineering*, vol. 125, pp. 584-595, 2017.

[52] M .Al Qubeissi, S. Sazhin, and A. Elwardany, "Modelling of blended Diesel and biodiesel fuel droplet heating and evaporation," *Fuel*, vol. 187, pp. 349-355, 2017.

[53] S. S. Sazhin *et al.*, "A multi-dimensional quasi-discrete model for the analysis of Diesel fuel droplet heating and evaporation," *Fuel*, vol. 129, pp. 238-266, 2014.

[54] O. Rybdylova *et al.*, "A model for multi-component droplet heating and evaporation and its implementation into ANSYS Fluent," *International Communications in Heat and Mass Transfer*, vol. 90, pp. 29-33, 2018.

[55] S. Sazhin, M. Al Qubeissi, R. Kolodnytska, A. Elwardany, R. Nasiri, and M. Heikal, "Modelling of biodiesel fuel droplet heating and evaporation," *Fuel*, vol. 115, pp. 559-572, 2014.

[56] S. Sazhin, A. Elwardany, E. Sazhina, and M. Heikal, "A quasi-discrete model for heating and evaporation of complex multicomponent hydrocarbon fuel droplets," *International Journal of Heat and Mass Transfer*, vol. 54, no. 19-20, pp. 4325-4332, 2011.

[57] A. Elwardany and S. Sazhin, "A quasi-discrete model for droplet heating and evaporation: application to Diesel and gasoline fuels," *Fuel*, vol. 97, pp. 685-694, 2012.

[58] J. Dgheim, M. Abdallah, and N. Nasr, "Evaporation phenomenon past a rotating hydrocarbon droplet of ternary components "، *International journal of heat and fluid flow*, vol. 42, pp. 224-235, 2013.

[59] G. Xiao, K. H. Luo, X. Ma, and S. Shuai, "A molecular dynamics study of fuel droplet evaporation in sub-and supercritical conditions," *Proceedings of the Combustion Institute* ،vol. 37, no. 3, pp. 3219-3227, 2019.

[60] A. Azimi, A. Arabkhalaj, R. S. Markadeh, and H. Ghassemi, "Fully transient modeling of the heavy fuel oil droplets evaporation," *Fuel,* vol. 230, pp. 52-63, 2018.

[61] M. Al Qubeissi, "Predictions of droplet heating and evaporation: An application to biodiesel, diesel, gasoline and blended fuels," *Applied Thermal Engineering*, vol. 136, pp. 260-267, 2018.

[62] A. P. Pinheiro, J. M. Vedovoto, A. da Silveira Neto, and B. G. van Wachem, "Ethanol droplet evaporation :effects of ambient temperature, pressure and fuel vapor concentration," *International Journal of Heat and Mass Transfer,* vol. 143, p. 118472, 2019.

[63] H. Nomura, Y. Ujiie, H. J. Rath, J. i. Sato, and M. Kono, "Experimental study on high-pressure droplet evaporation using microgravity conditions," in *Symposium (International) on Combustion*, 1996, vol. 26, no. 1: Elsevier, pp. 1267-1273 .

[64] K. Harstad and J. Bellan, "An all-pressure fluid drop model applied to a binary mixture: heptane in nitrogen," *International Journal of Multiphase Flow*, vol. 26, no. 10, pp. 1675-1706, 2000.

[65] T. Kitano, J. Nishio, R. Kurose, and S. Komori, "Effects of ambient pressure, gas temperature and combustion reaction on droplet evaporation," *Combustion and Flame,* vol. 1 ،61no. 2, pp. 551-564, 2014.

[66] G. Lupo, M. N. Ardekani, L. Brandt, and C. Duwig, "An immersed boundary method for flows with evaporating droplets," *International Journal of Heat and Mass Transfer,* vol. 143, p. 118563, 2019.

[67] R. S. Markadeh, A. Arabkhalaj, H. Ghassemi, and A. Azimi, "Droplet evaporation under spray-like conditions," *International journal of heat and mass transfer,* vol. 148, p. 119049, 2020.

[68] V. V. Tyurenkova, M. N. Smirnova, and V. F. Nikitin, "Two-phase fuel droplet burning in weightlessness," *Acta Astronautica,* vol. 176, pp. 672-681, 2020.

[69] Y. Gong, G. Xiao, X. Ma, K. H. Luo, S. Shuai, and H. Xu, "Phase transitions of multi-component fuel droplets under sub-and supercritical conditions," *Fuel,* vol. 287, p. 119516, 2021.

[70] A. E. Saufi, A. Frassoldati, T. Faravelli, and A. Cuoci, "Interface-resolved simulation of the evaporation and combustion of a fuel droplet suspended in normal gravity," *Fuel,* vol. 287, p. 119413, 2021.

[71] H. Ruitian, Y. Ping, and L. Tie, "Evaporation and condensation characteristics of n-heptane and multi-component diesel droplets

under typical spray relevant conditions," *International Journal of Heat and Mass Transfer*, vol. 163, p. 120162, 2020.

[72] S. Gavhane, S. Pati, and S. Som, "Evaporation of multicomponent liquid fuel droplets: Influences of component composition in droplet and vapor concentration in free stream ambience," *International Journal of Thermal Sciences,* vol. 105, pp. 83-95, 2016.

[73] G. Hubbard, V. Denny, and A. Mills, "Droplet evaporation: effects of transients and variable properties," *International journal of heat and mass transfer*, vol. 18, no. 9, pp. 1003-1008, 1975.

[74] Y. Gong, K. H. Luo, X. Ma, S. Shuai, and H. Xu, "Atomic-level insights into transition mechanism of dominant mixing modes of multi-component fuel droplets: From evaporation to diffusion," *Fuel*, vol. 304, p. 121464, 2021.

[75] S. D. Givler and J. Abraham, "Supercritical droplet vaporization and combustion studies," *Progress in Energy and combustion Science* ، vol. 22, no. 1, pp. 1-28, 1996.

[76] H.-H. Chiu, "Advances and challenges in droplet and spray combustion. I. Toward a unified theory of droplet aerothermochemistry," *Progress in Energy and Combustion Science,* vol. 26, no. 4-6, pp. 381-416, 2000.

[77] V .Yang, "Modeling of supercritical vaporization, mixing, and combustion processes in liquid-fueled propulsion systems," *Proceedings of the Combustion Institute,* vol. 28, no. 1, pp. 925-942, 2000.

[78] S. Chakraborty and L. Qiao, "Molecular investigation of sub-to-supercritical transition of hydrocarbon mixtures: Multi-component effect," *International Journal of Heat and Mass Transfer,* vol. 145, p. 118629, 2019.

[79] M. S. Dodd, D. Mohaddes, A. Ferrante, and M. Ihme, "Analysis of droplet evaporation in isotropic turbulence through droplet-resolved dns," *International Journal of Heat and Mass Transfer*, vol. 172, p. 121157, 2021.

[80] J.-S. Wu, K.-H. Hsu, P.-M. Kuo, and H.-J. Sheen, "Evaporation model of a single hydrocarbon fuel droplet due to ambient turbulence at intermediate Reynolds numbers," *International journal of heat and mass transfer*, vol. 46, no. 24, pp. 4741-4745, 2003.

[81] S. Mouvanal *et al.*, "Evaporation of thin liquid film of single and multi-component hydrocarbon fuel from a hot plate," *International Journal of Heat and Mass Transfer*, vol. 141, pp. 379-389, 2019.

[82] L. Poulton *et al.*, "Modelling of multi-component kerosene and surrogate fuel droplet heating and evaporation characteristics: A comparative analysis," *Fuel*, vol. 269, p. 11711.2020 ،5

[83] M. Ochowiak *et al.*, "The D 2-Law of Droplet Evaporation When Calculating the Droplet Evaporation Process of Liquid Containing Solid State Catalyst Particles," *Energies*, vol. 15, no. 20, p. 7642, 2022.
[84] S. R. Turns, *Introduction to combustion*. McGraw-Hill Companies New York, NY, USA, 2012.
[85] S. A. Bell, "A beginner's guide to uncertainty of measurement," 2001.

APPENDICES

Appendix A

Uncertainty analysis example

Uncertainty of diameter measurements (mm)

$$Su = \frac{S.D}{\sqrt{N}} \tag{3.14}$$

$$S.D = \sqrt{\frac{\sum_{i=1}^{N}(X_i - X_{average})^2}{(N-1)}} \tag{3.15}$$

$$X_{average} = \frac{1}{N}\sum_{i=1}^{N} X_i \ \ldots\ldots \tag{3.16}$$

$$X_{average} = \frac{2.816 + 2.863 + 2.863 + 2.823 + 2.829 + 2.840 + 2.826 + 2.836 + 2.818 + 2.817}{10}$$

$X_{average} = 2.8331$

$\sum_{i=1}^{N}(X_i - X_{average})^2 = (2.816 - 2.8331)^2 + (2.863 - 2.8331)^2 + (2.863 - 2.8331)^2 + (2.823 - 2.8331)^2 + (2.829 - 2.8331)^2 + (2.840 - 2.8331)^2 + (2.826 - 2.8331)^2 + (2.836 - 2.8331)^2 + (2.818 - 2.8331)^2 + (2.817 - 2.8331)^2 = 0.00279$

$$S.D = \sqrt{\frac{0.00279}{(9)}} = 0.01762$$

$$Su = \frac{0.01762}{\sqrt{10}} = 0.00557$$

To calculate the relative uncertainty of evaporation constant is

$$K = \frac{1 + \frac{d_2^{\,2}}{d_1^{\,2}}}{\left(\frac{t}{d_1^{\,2}}\right)}$$

$$\frac{\Delta K}{K} = \left[\left(\frac{\partial K}{\partial d_1}\frac{\Delta d_1}{d_1}\right)^2 + \left(\frac{\partial K}{\partial d_2}\frac{\Delta d_2}{d_2}\right)^2\right]^{0.5} \tag{3.18}$$

Where $\Delta d_1 = \Delta d_2 = 0.00557$

$$\frac{\partial K}{\partial d_1} = 0.02122$$

$$\frac{\partial K}{\partial d_2} = -0.02113$$

$$K \pm \Delta K = 2.753 * 10^{-7} \pm 0.00016668$$

Appendix B

- **State of the Art of Fuel Droplet Evaporation .This paper is accepted and published in International Journal of Heat and Technology, Vol.40,No.5, October,pp.1327-1339.**

IIETA International Information and Engineering Technology Association

International Journal of Heat and Technology
Vol. 40, No. 5, October, 2022, pp. 1327-1339
Journal homepage: http://iieta.org/journals/ijht

State of the Art of Fuel Droplet Evaporation

Wissam Yassin Jabr Giyad*, Haroun A.K. Shahad

College of Engineering, Mechanical Engineering Department, University of Babylon, Babylon City 51001, Hilla, Iraq

Corresponding Author Email: wissam.giyad.engh418@student.uobabylon.edu.iq

https://doi.org/10.18280/ijht.400528

Received: 23 September 2022
Accepted: 20 October 2022

Keywords:
evaporation, hydrocarbon fuel, droplet, sessile droplet, levitated droplet, free-flying droplet

ABSTRACT

The process of fuel droplet evaporating is one of the most important factors that directly affect the efficiency of the combustion process. Therefore, the current study reviews previous studies that focused on the process of evaporation of a drop of fuel. The review is divided into points. The first part is concerned with modeling of the evaporation process under different initial condition and temperature of the droplet. The second part present the experimental studies concerned with measuring the evaporation time of the droplet, as well as the shape of the droplet during the evaporation process. Most of the studies related to this subject can be divided into three categories: The first category is the studies that are concerned with the process of heating the droplet and studying the evaporation time for different types of fuels or by adding nanomaterials to the fuel and studying their effect on the evaporation process. The second category is the studies concerned with the mechanics of droplet evaporation and the study of droplet shape. The third category is the studies that focus on studying the effect of initial conditions, such as temperature and pressure, as well as the concentration of gasses surrounding the drop and their types. There are other studies concerned with projecting the electric field onto the drop during the evaporation process and studying its effect.

1. INTRODUCTION

The studying of fuel evaporation helps to better understanding of combustion process and to reduce the emission. Al Qubeissi [1] studied and analyzed the fuel droplet evaporation by using Discrete Component Model (DCM). They used diesel, biodiesel, gasoline, and blended fuels. The results showed that increasing the fraction of biodiesel in the diesel-biodiesel mixture on the droplet evaporation and surface temperature of droplet was noticeable. So that its needs more than 5% fraction of biodiesel to effected on the droplet evaporation time.

Sazhin et al. [2] introduce novel method for simulating the evaporation of fuel droplet. They used gasoline fuel with specific condition as in real condition in internal combustion engine. The numerical model used to simulate the number of components of gasoline with identical chemical formulae and similar thermodynamic and transport properties. The modeling process used to replace the 83 components of original composition of gasoline fuel with 20 components only. In a subsequent study by the same researcher Al Qubeissi et al. [3] the blended Diesel and biodiesel fuel was used .They found that Multi-component model gives longer evaporation time and higher surface temperature than single component model for both gasoline and diesel fuel droplet.

Poulton et al. [4] studied the evaporation process theoretically by using A Discrete Component Model (DCM). The used kerosene droplet with suspended technique. They focused on the effect of natural convection and wire material on the evaporation process. The simulation results showed that the supporting wire material very affect the evaporation time.

They used droplet diameter ranges from 0.9 mm to 1.1 mm with ambient gas temperature range from 400°C to 800°C. The SiC fiber with 100μm diameter used to suppurated the droplet. The results showed that at gas temperature 400°C. The droplet diameter reaches 0.127mm after 6.540 s, and reached to 0.199mm after 1.3085 for 800°C gas temperature. Many studied analyzed the discrete component model or individual component to simulate fuel droplet heating and evaporation such as [5-9]. They found that discrete component model gives highest accuracy. A multi-dimensional quasi-discrete model was utilized in several investigations [3, 10]. A modest number of representative components were used in place of a huge number of other components in this modeling.

Rybdylova et al. [11] modeled the analytical approximations to the heat conduction and species diffusion equations in the liquid phase, the multi-component droplet heating and evaporation was using ANSYS Fluent software. They used three droplets (25% ethanol/75% acetone), (50% ethanol/50% acetone), (75% ethanol/25% acetone). The results indicated that the highest variation between estimated temperatures did not exceed 0.16% for t = 4 ms, 0.14% for t = 5 ms, and 0.13% for t = 6 ms. This indicates that the consistency between ANSYS Fluent's predictions and the in-house code is reasonably excellent. In practically all practical applications, this disparity between the findings can be disregarded.

Dai et al. [12] investigated the evaporation of characteristics of Nano fuel with different dose 0.05% ,0.25% ,1.25% and 5% by weight Diesel/cerium oxide nanofluid fuel. The nanoparticle used is ceria nanoparticles at temperature 673K and 873K under normal gravity. The results showed that the

الخلاصة

عملية تبخير قطرات هي واحدة من العناصر المهمة جدا وذلك لتأثيرها المباشر على كفاءة او فعالية عملية الاحتراق. العمل الحالي هو دراسة تجريبية على عملية الاحتراق لخمس أنواع مختلفة من الوقود ، وهي الكيروسين والبنزين والإيثانول والأسيتون ، بالإضافة إلى الماء. درجة حرارة غرفة التبخر تتراوح من 25 الى 100 درجة مئوية. تأثير درجة الحرارة ونوع الوقود على معدل التبخر وثابت التبخر وكذلك عمر القطرة سيتم بحثه ودراسته. الجهاز التجريبي بني لدراسة عملية التبخير على قطرة حرة طائرة في داخل غرفة تبخر أسطوانية. التحكم بانتشار وضع التبخر هو الوضع الأكثر أهمية فقط في هذه الدراسة. القطرة صورت خلال عملية التبخر باستخدام كاميرا عالية السرعة لغرض حساب معدل تبخر القطرة. الصورة المستخرجة من الكاميرا تحلل او تدرس باستخدام ماتلاب . النتائج اثبتت معدل التبخر يزداد لوغاريتميًا مع زيادة درجة الحرارة لغرفة التبخر. يعتمد معدل التبخر بشكل أساسي على ضغط تبخر السائل ، لأن الزيادة في درجة الحرارة تعني زيادة في ضغط التبخر ، ومن ثم يرتفع معدل التبخر. عمر قطرة الاسيتون ينقص بنسبة 63٪ عندما ترتفع درجة الحرارة إلى 45 درجة مئوية. عمر قطرة الايثانول ينقص بنسبة 66.7٪ عندما ترتفع درجة الحرارة من 25 درجة مئوية إلى 45 درجة مئوية. عمر قطرة الكازولين ينقص بنسبة59.1٪ عندما ترتفع درجة الحرارة من 25 درجة مئوية إلى 45 درجة مئوية. عمر قطرة الماء ينقص بنسبة 70.5٪. عمر قطرة الكيروسين ينقص بنسبة 67.7٪ عندما ترتفع درجة الحرارة من 25 درجة مئوية إلى 45 درجة مئوية . تؤدي زيادة درجة الحرارة إلى زيادة معدل التبخر وبالتالي تقليل عمر القطرة. يرتفع ثابت التبخر بمقدار 0.007 ،0.021 ، 0.006 ، 0.02 ، 0.015 مم^2 / ثانية لكل درجة حرارة مئوية واحدة للكيروسين والأسيتون والماء والإيثانول والبنزين على التوالي.

جمهورية العراق
وزارة التعليم العالي والبحث العلمي
جامعة بابل / كلية الهندسة
قسم الهندسة الميكانيكية

دراسة تجريبية لتبخر القطرة لأنواع مختلفة من الوقود الهيدروكاربوني السائل و الماء

رسالة

مقدمة إلى قسم الهندسة الميكانيكية / كلية الهندسة / جامعة بابل وهي جزء من متطلبات نيل درجة الماجستير في الهندسة/ الهندسة الميكانيكية/ قدرة

أعدت من قبل

وسام ياسين جبر جياد

بأشراف

أ. د. هارون عبد الكاظم شهد

1445هـ *2023 م*